MASSACHUSETTS INSTITUTE OF TECHNOLOGY
DEPARTMENT OF NAVAL ARCHITECTURE AND MARINE ENGINEERING

# THE SOLUTION OF PROPELLER LIFTING SURFACE PROBLEMS BY VORTEX LATTICE METHODS

by
JUSTIN E. KERWIN

JUNE 1961



Prepared Under
Contract No. Nonr-1841(63)
Bureau of Ships
U.S. Department of the Navy
administered by the
David Taylor Model Basin



Cambridge 39, Massachusetts

June, 1961

Department of Naval Architecture and Marine Engineering
Massachusetts Institute of Technology

# THE SOLUTION OF PROPELLER LIFTING SURFACE PROBLEMS BY VORTEX LATTICE METHODS

by

Justin E. Kerwin

June 1961

Prepared Under
Contract No. Nonr - 1841(63)
Bureau of Ships
U. S. Department of the Navy
administered by the
David Taylor Model Basin

## ABSTRACT

The basis for current propeller design methods is lifting line theory supplemented by an approximate correction for lifting surface effect. Recent studies have indicated that this correction is not entirely satisfactory, and that a more exact lifting surface theory for marine propellers is needed.

In the present work, methods are developed to determine pitch and camber corrections for propellers with arbitrary blade outline and radial load distribution. The pitch and camber is determined by the requirement that the desired load distribution be obtained with the sections operating at their ideal angle of attack. The method may be used both for homogeneous-flow and wake-adapted propellers.

The method is an adaptation of the vortex lattice method developed for wings of arbitrary shape by Falkner. By replacing the continuous vortex distribution by a lattice of discrete vortex elements, the singular integral equation occurring in lifting surface theory is replaced by a set of linear algebraic equations.

From the form of these equations, it is shown that a propeller with symmetrical blades and with mean lines which are symmetrical about the mid-chord has no pitch correction due to lifting surface effect.

To obtain a preliminary check on the accuracy of vortex lattice theory, methods of approximating propeller lifting line theory are developed, and numerical results obtained with an IBM 709 Computer are given. These results agree substantially with existing lifting line data.

Lifting surface results obtained with an IBM 709 and an IBM 7090 computer are discussed. From these results it is tentatively concluded that an accuracy of $\pm$ 2% in the camber correction may be achieved with reasonable computation times. The sample results indicate that lifting surface corrections are dependent on such variables as blade shape and circulation distribution, which are not taken into account in current design methods.

## ACKNOWLEDGEMENT

The author wishes to express his appreciation to the following individuals and organizations:

Professor Martin A. Abkowitz for valuable assistance provided during his supervision of this project.

Mr. John A. Mercier for his assistance in data preparation and analysis and for his most helpful suggestions.

The M. I. T. Computation Center, where most of the program testing was performed.

The M. I. T. Civil Engineering Computer Laboratory, where some of the preliminary work on the numerical integration was done.

The Applied Mathematics Laboratory at the David Taylor Model Basin, and Mr. Lou Mueller, in particular, for their cooperation in running many of the final results.

The content of this report is essentially the same as the Ph.D. thesis submitted by Justin E. Kerwin to the Department of Naval Architecture and Marine Engineering.

TABLE OF CONTENTS

# LIST OF FIGURES

## NOMENCLATURE

$C_L$ - lift coefficient = $L/1/2\rho V^2 \ell$

$c_{ij}$ - Fourier coefficients of circulation distribution

$D$ - propeller diameter

$F_n$ - function defined in (2.19)

$f$ - maximum camber of mean line

$\bar{f}$ - non-dimensional camber = $(f/\ell)/C_L$

$G$ - non-dimensional circulation = $\Gamma/2\pi Ru^*$

$G'$ - non-dimensional circulation = $\Gamma/2\pi R\ V_a$

$g$ - number of blades

$h_q$ - slope of mean line with unit camber at point q

$k$ - camber factor = camber in 3-dimensional flow/camber in 2-dimensional flow

$I$ - radial terms in Fourier series for G distribution

$J$ - chordwise terms in Fourier series for G distribution

$K$ - index in coefficient matrix of equation (5.33) and (6.18)

$L$ - index in coefficient matrix of equation (5.33) and (6.18)

$\ell$ - chord length of expanded section

$M$ - number of radial lattice elements

$N$ - number of chordwise lattice elements

$P$ - number of radial control points

$Q$ - number of chordwise control points

$R$ - propeller radius

$r$ - radius, radius to a control point

$r_o$ - radius of a helical vortex element

$S$ - non-dimensional vortex sheet strength = $\gamma/u^*$

$u$ - induced velocity

$u_a$, $u_t$, $u_r$, $u_n$ - axial, tangential, radial, and normal induced velocity components

$\bar{u}$ = non-dimensional induced velocity = $4\pi ru/\Gamma$

$u^*$ = displacement velocity defined in Fig. 4.1

$V_a$ = axial inflow velocity

$V^*$ = resultant relative velocity at a blade from lifting line theory

$W_k$ - integration rule weights

$\alpha$ - angle of attack of section relative to $\beta_i$

$\bar{\alpha}$ - non-dimensional pitch correction = $\alpha/C_L$

$\beta$ - geometrical pitch angle

$\beta_i$ - hydrodynamic pitch angle from lifting line theory

$\beta_{io}$ - hydrodynamic pitch angle from lifting line theory at radius $r_o$

$\gamma$ - vortex sheet strength

$\zeta_{mp}$ - relative load factor defined in (4.19)

$\zeta_1$, $\zeta_2$ - chordwise lattice constants defined in (5.14)

$\eta$ - non-dimensional radius $r_o/r$

$\varkappa$ - Goldstein factor

$\lambda_i$ - hydrodynamic advance coefficient = $\chi \tan \beta_i$

$\mu_{nj}$ - chord-load factor defined in (5.20)

$\xi$ - $x/r$ = non-dimensional axial distance

$\rho$ - transformed radial coordinate according to (4.3) or (5.1), fluid mass density

$\sigma$ - transformed chordwise coordinate according to (5.1)

$\omega$ - propeller rotational speed

# CHAPTER I

# INTRODUCTION

## Propeller Design Methods

The basis for current propeller design methods is lifting line theory supplemented by an approximate correction for lifting surface effect. A description of such methods may be found in recent publications by Lerbs[1], [2], Van Manen[3], [4], and Eckhardt and Morgan[5]. Since the historical development of propeller theory is treated extensively in these references, we will be concerned primarily with a brief summary of the assumptions and general methods of solution involved in propeller theory as it is applied at the present time.

In lifting line theory, the propeller blades are replaced by straight radial vortex lines. A free vortex sheet extends downstream from each of the lifting lines forming an approximately helical surface. The propeller is assumed to be rotating with constant angular velocity in an axially directed stream whose velocity may be a function of radius only. The flow will then be steady relative to a coordinate system rotating with the propeller. The flow in the neighborhood of the propeller is assumed to be unaffected by the free surface or by extraneous solid boundaries.

Even this idealized model cannot be solved exactly since the velocity induced by the vortex sheets and the position of the sheets are mutually dependent. It is therefore assumed that the induced velocities are small compared with the resultant relative velocities

at the lifting lines. The elements of the free vortex sheet can then be assumed to be helical lines of constant radius and pitch, where the pitch is determined by the angle of the resultant flow at the lifting line including induced velocities. This latter refinement complicates matters somewhat since the pitch of the free vortex lines and the velocities induced at the lifting line are still interdependent, however, a solution may readily be obtained by iteration.

The justification for neglecting the axial deformation of the vortex sheet is that the velocity induced at the lifting line by an element of the sheet decreases rapidly with distance so that an error in the assumed position of the sheet becomes less critical as the distance downstream increases.

The relationship between the bound vortex strength and the induced velocities at the lifting line may be determined by the Lerbs induction factor method[1], [4]. In the special case when the inflow velocity is constant and the pitch of the free vortex sheet is independent of radius, the circulation distribution may also be determined by means of the Goldstein factors[6]. These methods will be discussed further in Chapter 4.

Due to the low aspect ratio of most marine propeller blades, the use of lifting line theory results in unacceptably large errors unless supplemented by a lifting surface correction of some kind. Some early attempts to explain this discrepancy were based on the application of two-dimensional cascade theory, however, as pointed out by Lerbs[7], this application was not justified. The lifting surface correction which is presently used was first developed by Ludwieg and Ginzel in 1944[8] and later refined by Ginzel[9], [10]. Their approach was to find the

induced flow curvature at the mid-chord and to use this to determine the camber of the blade sections. The pitch was still to be determined from lifting line theory by the requirement that the sections be at zero angle of attack relative to the induced flow.

Their theory is linearized to the extent that the blade surface is assumed to lie in the neighborhood of a true helical surface, the vortex system and the point where the induced velocity is to be determined is on the helical surface rather than on the blade itself. The curvature of the flow is related to the derivative of the normal component of induced velocity in the chordwise direction, or, more briefly, the "downwash derivative". They assume a constant circulation distribution over the chord, and with this simplification it is easy to show that the downwash derivative is equal to the downwash produced by a "remainder" vortex system consisting of a line vortex representing the blade outline and a set of chordwise vortices connecting the leading and trailing edge.

Their results can be expressed in terms of a camber correction factor k which is defined as the ratio of the camber required in three-dimensional flow to the camber in two-dimensional propeller flow for the same lift coefficient. While the theory can take into account the contribution of the other blades to the downwash derivative, this effect was neglected to simplify the computations. Their results show that the camber correction factor depends principally on blade area (aspect ratio) and on the radial circulation distribution.

In order to apply their results to propeller sections which do not have a constant chordwise circulation distribution, the chord

lengths are modified in such a way that the actual section and the constant-load section would have the same total lift and downwash derivative in two-dimensional flow.

After the pitch has been determined from lifting line theory and the camber of the sections from the Ludweig and Ginzel theory, the design is completed by superimposing the velocities induced by a symmetrical thickness form to those due to the cambered mean line. As in linearized thin airfoil theory, the velocities due to the thickness form contribute to the local pressure, but not to the lift. Finally, an allowance is made for viscous effects by adding a profile drag force and by adding a small angle of attack or camber increment (or both) to allow for the loss of lift attributed to the presence of the boundary layer. Both these corrections and the velocity increments due to thickness are determined by a two-dimensional strip theory based on the resultant inflow velocity from lifting line theory.

It has been observed that propellers designed in this way do not have the correct pitch in many cases. To explain this Lerbs[7] considered the possibility that the induced curvature may not be constant over the chord and that a pitch correction might be necessary to take this into account. To do this the Weissinger[34] lifting surface theory was applied approximately at one point on the blade. In this theory the bound circulation is concentrated at the 1/4 chord line and the downwash is determined at the 3/4 chord line. The pitch is then adjusted so that the boundary condition at the 3/4 chord line is satisfied.

This correction is used in the design method described by Eckhardt and Morgan[5]. However, Van Manen and Crowley[11] found that this correction did not seem to help in bringing their theoretical and experimental results into agreement. The author is also of the opinion that the approximations involved in applying this correction are such that it is questionable whether it can serve to improve the accuracy of the Ludweig - Ginzel theory. This was illustrated in the present author's discussion to a paper given by Morgan in 1959[12].

Another form of correction which has been used principally at the Netherlands Ship Model Basin is an empirical modification in the ideal efficiency of the propeller, which results in a change in pitch. This is applied principally to wake-adapted propellers and includes the effects of unsteady flow[3]. It is not possible to say how much of this correction is due to errors in steady-state propeller theory.

Current Research in Steady-State Propeller Theory

The fact that current design methods are not entirely reliable has resulted in a recent interest in propeller lifting surface theory. There are many possible approaches, some of which will be discussed briefly in this section.

While the Ludwieg-Ginzel theory has a number of inherent simplifying assumptions, it is still by no means being applied to its full advantage at the present time. For example, their results show a very strong dependence of the camber correction on the radial load distribution, yet this fact is ignored in current design methods. It appears that the design curves given by Van Manen[3] are for an optimum

radial load distribution, while those appearing in Eckhardt and Morgan[5] are for a reduced circulation at the outer part of the blade. However, the latter is applied to propellers with both optimum and non-optimum circulation distribution. Furthermore, the modification in effective chord length due to changes in the chord-load distribution is not taken into account. Finally, the effect of the other blades which was originally neglected to save numerical work could easily be taken into account now due to the availability of high-speed digital computers. A reanalysis of the Ludweig and Ginzel theory has just been completed by Cox[13], and it is possible that these new numerical results will result in better agreement between theory and experiment.

Following another approach, Alef [14] has been working on the exact application of the Weissinger theory to propellers, although to the author's knowledge, no numerical results are available as yet. While this should be a distinct improvement over the approximate application of the Weissinger theory, it is still subject to question whether or not this will offer any improvement over the Ludweig and Ginzel theory.

Work is also in progress at the Netherlands Ship Model Basin by Sparenberg[15] on a more rigorous lifting surface theory. In that reference, the basic integral equation is derived. It is understood that work is in progress to solve the integral equation for the special case of elliptic blade outlines with constant circulation over the blade surface.

General Method of Approach

In the present work we consider the solution of the lifting surface problem for a propeller with arbitrary blade outline, pitch distribution and circulation distribution operating in an axially directed velocity field. It is assumed that the radial circulation distribution is given and that the blade surface is to be formed from a known mean-line type by determining the camber and pitch at each radius. These two parameters are to be determined by the requirement that the desired radial circulation distribution is obtained with the sections operating at their ideal angle of attack.* The chordwise circulation distribution will then be determined by these two conditions; by the boundary condition that the flow be tangent to the blade surface, and by the Kutta condition.

This approach differs from any of the theories discussed in the preceding sections in that no restrictive assumptions need be made as to the circulation distribution or blade outline, and the results may be applied both to open water or to wake-adapted propellers.

The procedure is similar to a method developed by Falkner[16], [17], [ to determine the lift distribution of wings of arbitrary shape. The continuous distribution of radial and helical vortices is replaced by a lattice of discrete vortex lines. The lattice can be considered as formed from a number of "horshoe" vortex elements of constant strength as shown schematically in Fig. 5.1. The velocity induced at an arbitrary point in space by each lattice element can be determined by integration

*The ideal angle of attack, or condition of "shock -free entrance" is defined as the angle of attack for which the infinite suction at the leading edge given by thin airfoil theory vanishes.

according to the law of Biot-Savart[19], [20]. By determining the velocity at a number of control points on the blade surface at the mid-points of the lattice a set of linear equations may be formed relating the strengths of the lattice elements to the shape of the blade surface.

The singular integral equation encountered in lifting surface theory is therefore replaced by a set of simultaneous linear equations. Since the process is very largely numerical, it is not necessary to make the usual simplifying assumptions as to the blade outline and circulation distribution.

The question naturally arises as to whether the lattice method will converge to the solution of the integral equation as the spacing is made smaller. Obviously, if the spacing is made very small, the coefficients in the equations will become large, due to the proximity of the control points to the vortex lines. Consequently, from a computational point of view there will be a point of diminishing returns after which the set of linear equations will be too nearly singular to be solved. The question of whether a sufficiently accurate solution can be obtained before this takes place can be settled by computing special cases for which the solution of the integral equation is known and observing how the error depends on lattice spacing.

This was done by Falkner[18] in the case of wings of various shapes and it was observed that errors of less than one percent could be achieved with lattices of reasonable size.* Since the convergence

*The finest spacing used twenty vortices over the semi-span and eight over the chord.

properties of the lattice should not be altered drastically by going from a plane to a helical surface, the method should be expected to work in the case of a propeller.

It should be mentioned that this approach has been studied to some extent by Guilloton[21] and Strscheletzky[22]. However, since their work was done in the pre-digital computer era, it is somewhat questionable whether a numerical solution on a small enough scale to be done by hand would offer any advantage in accuracy over existing results. This conclusion is based on the results of the present work in which it was found that the necessary computations were far from trivial even for a large-scale digital computer and definitely beyond the capacity of small machines, not to mention humans.

Basic Assumptions

The assumptions will be similar in part to those made in lifting line theory as described in the beginning of this chapter. The fluid is assumed to be frictionless and incompressible and the flow in the neighborhood of the propeller is assumed to be unaffected by a free surface, extraneous solid boundaries, or cavitation. The inflow velocity, as in lifting line theory, is assumed to be axial and a function of radius only.

The free vortex system is assumed to lie on a helical surface whose pitch is determined from lifting line theory with the same radial load distribution. The pitch of this helical reference surface may be a function of radius. The blade surface is assumed to be approximately on the helical reference surface. The problem is linearized to the extent that the boundary condition is applied on the helical

surface rather than on the blade itself and the induced velocities are assumed to be small relative to the resultant inflow. As in lifting line theory, the flow is assumed to lie on cylindrical surfaces concentric with the propeller axis of rotation. This assumption is obviously not very realistic near the tip of the blades, but should be reasonable elsewhere for moderate propeller loadings.

It is assumed that the Kutta-condition holds, i.e., that the bound circulation is zero at the trailing edge. It is also assumed that the bound circulation is zero at the blade tip and at the hub radius, and that the boundary condition of zero radial velocity at the hub cylinder can be disregarded. These last two assumptions concerning the hub are by no means essential to the vortex lattice method, and it is believed that a more accurate representation of the hub effect can be added at a later time.

Outline of Results

In order to apply the vortex lattice method, the velocity induced at an arbitrary point in space by a set of helical or radial vortices is needed. Expressions for these are derived in Chapters 2 and 3 respectively, and methods of computation and error estimates are discussed. In Chapter 4 vortex lattice methods are applied to solve the lifting line problem, both for optimum propellers in homogeneous flow, and for non-optimum or wake-adapted propellers. This is included to indicate to some extent the convergence properties of the lattice method by comparison with known results. These results are also needed in the solution of the lifting surface problem for symmetrical blades.

In Chapter 5 a lattice solution is developed for propellers of generally arbitrary blade outline, section type, and radial circulation distribution, and in Chapter 6 these results are specialized in the case of propellers with symmetrical blades. In the latter case, the resulting symmetry greatly simplifies the computations.

Finally, in Chapter 7 numerical results for camber and pitch corrections are presented and compared with results according to the Ludwieg and Ginzel theory.

## CHAPTER 2

## THE VELOCITY INDUCED BY HELICAL VORTEX LINES

### Introduction

In this chapter the problem of determining the velocity induced at an arbitrary point in space by a set of helical vortices will be considered. It will be assumed that the vortices are of true helical shape, i.e., that their radius and pitch remains constant, and that there will be g vortices of equal strength symmetrically located around the circumference. The axial extent of the set of vortices may either be finite, as in the case of a vortex segment lying on the blade surface, or semi-infinite as in the case of the free vortex system extending downstream from the trailing edge of the blade.

The velocity induced by a vortex line of arbitrary shape may be expressed in terms of an integral taken along the vortex line by means of Biot-Savart's Law[19]. Expressions for these integrals in the case of helical vortices have been derived by Betz[23], Strscheletsky[22] and others. However, since the derivation is very short, it will be included here for convenience since these references are not widely available. This will also serve to establish the notation, which is by no means universal.

Since these integrals cannot be solved explicitly, other methods have generally been used in the past to obtain the induced velocity components. In lifting line theory, for example, the velocity induced on the lifting line by a set of semi-infinite helical vortices can be reduced to the two-dimensional problem of finding the velocity induced by a helical vortex of infinite axial extent, as was first shown by Betz[23].

This can be treated as a two-dimensional potential problem and solutions for the case of a set of helical vortex lines have been obtained by Lerbs[1] and in the case of a set of true helical surfaces by Goldstein[6].

However, in a vortex lattice approximation to the lifting-surface problem, the velocity induced at an arbitrary point in space by a segment of a helical vortex line must be determined. Since this is now a three-dimensional problem, the Biot-Savart integrals would appear to provide the best way of obtaining the induced velocities.

In the case of a finite interval, the integration may be performed by numerical methods as will be discussed later. In the semi-infinite case, numerical integration may be used up to a sufficiently large distance downstream at which point the remaining value of the integral to infinity can be estimated. Both of these steps introduce errors normally defined in numerical analysis as "truncation errors". However, in this application the term "integration error" will mean the error introduced by the numerical integration formula, while "truncation error" will refer to the estimate of the integral to infinity. Both of these errors will be considered in detail later in the chapter.

The Induced Velocity Components Determined by Biot-Savart's Law

As shown in Fig. (2.1), a right-handed cartesian coordinate system is located with the x axis along the propeller axis of rotation with positive direction downstream. The y axis passes through the control point, i.e., the point in space where the velocity is to be determined. A cylindrical system $(x, r, \theta)$ is oriented so that the line $x = 0$, $\theta = 0$ in the cylindrical system corresponds to the y axis in the cartesian system.

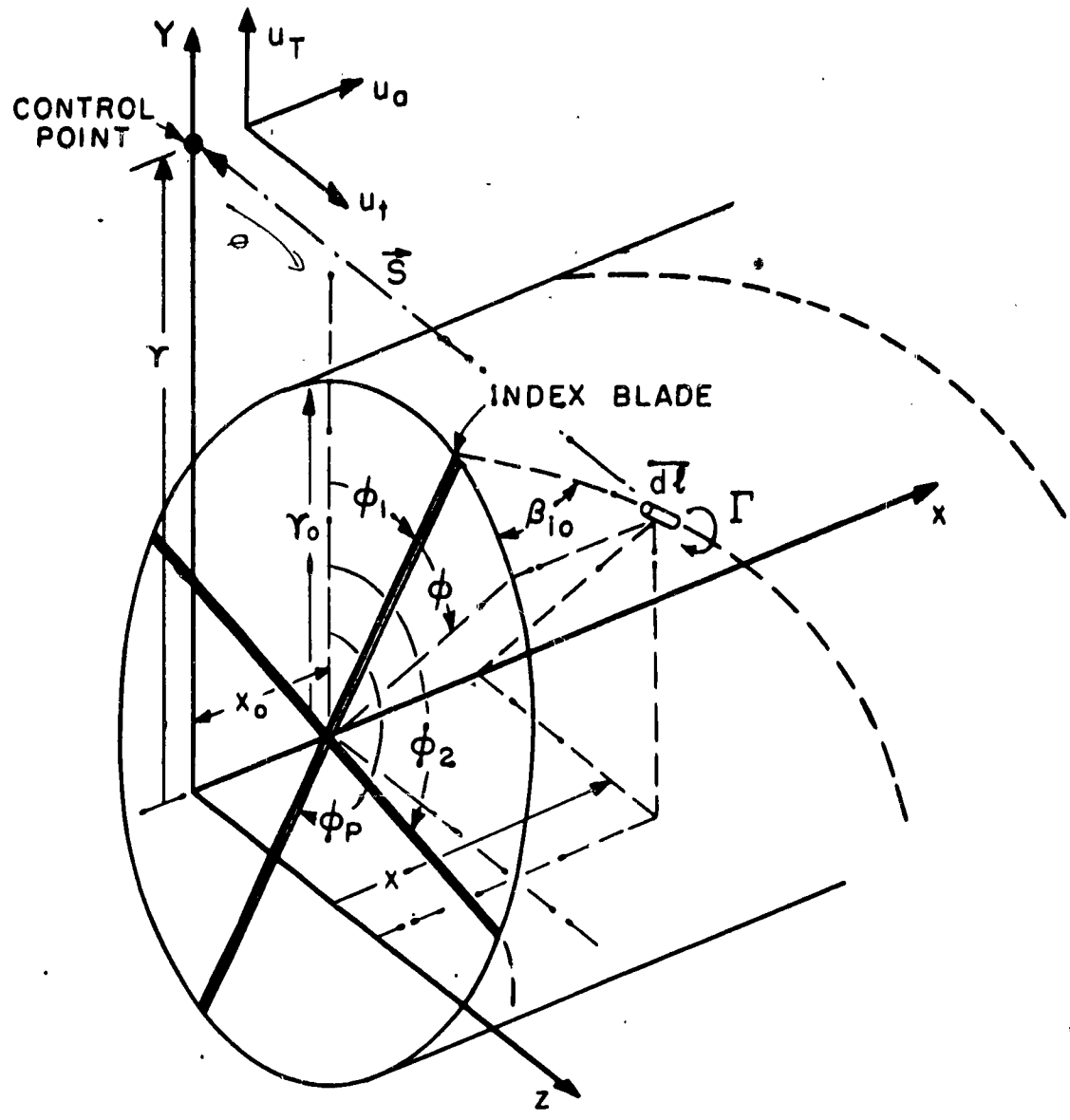


FIG. 2.1 COORDINATE SYSTEM AND NOTATION FOR HELICAL VORTICES

There will be g helical vortices (one from each blade) which have the following properties:

a) The vortices all start with the same axial coordinate $x_o$, radial coordinate $r_o$, but with different angular coordinates $\theta = \varphi_p$, $p = 1, 2, \ldots g$.

b) The vortices are of constant radius $r_o$, and constant pitch angle $\beta_{io}$.

Biot-Savart's Law may be written

$$\vec{u} = \frac{\Gamma}{4\pi} \int \frac{\vec{d\ell} \times \vec{S}}{S^3} \tag{2.1}$$

where $\Gamma$ = vortex strength ($ft^2/sec$)

$\vec{S}$ = vector distance from vortex element to control point (ft)

$\vec{d\ell}$ = vector element of distance along the vortex (ft)

$\vec{u}$ = vector induced velocity. (ft/sec)

The distance S has the following x, y, and z components:

$$\vec{S} = \left[-x_o - r_o\varphi \tan \beta_{io},\ r - r_o \cos(\varphi + \varphi_p),\ -r_o \sin(\varphi + \varphi_p)\right] \tag{2.2}$$

where $\varphi$ is the angular coordinate measured from $\varphi_p$ as shown in Fig. (2.1).

The vortex element $d\ell$ is

$$\vec{d\ell} = \left[\tan \beta_{io},\ -\sin(\varphi + \varphi_p),\ \cos(\varphi + \varphi_p)\right] r_o\, d\varphi \tag{2.3}$$

The cross-product $\vec{d\ell} \times \vec{S}$ is as follows

$$\vec{d\ell} \times \vec{S} = r_o\, d\varphi \begin{vmatrix} \vec{i} & \vec{j} & \vec{k} \\ \tan\beta & -\sin(\varphi+\varphi_p) & \cos(\varphi+\varphi_p) \\ -x_o - r_o\varphi\tan\beta & r - r_o\cos(\varphi+\varphi_p) & -r_o\sin(\varphi+\varphi_p) \end{vmatrix}$$

$$= r_o \, d\varphi \begin{cases} r_o - r \cos(\varphi + \varphi_p), \\ r_o \tan \beta_{io} \left[ \sin(\varphi + \varphi_p) - \varphi \cos(\varphi + \varphi_p) \right] \\ \quad - x_o \cos(\varphi + \varphi_p), \\ \tan \beta_{io} \left[ r - r_o \cos(\varphi + \varphi_p) - r_o \varphi \sin(\varphi + \varphi_p) \right] \\ \quad - x_o \sin(\varphi + \varphi_p) \end{cases} \tag{2.4}$$

and the scalar quantity $S^3$ is

$$S^3 = \left[ (x_o + r_o \varphi \tan \beta_{io})^2 + r^2 + r_o^2 - 2r \, r_o \cos(\varphi + \varphi_p) \right]^{3/2} \tag{2.5}$$

Substituting (2.2) through (2.5) in (2.1) and summing over the g blades gives the following expressions for the axial, tangential, and radial velocity components

$$u_a = \frac{\Gamma \, r_o}{4\pi} \int \sum_{p=1}^{g} \frac{1}{S^3} \left[ r_o - r \cos(\varphi + \varphi_p) \right] d\varphi \tag{2.6}$$

$$u_t = \frac{\Gamma r_o}{4\pi} \int \sum_{p=1}^{g} \frac{1}{S^3} \left[ \tan \beta_{io} \{ r - r_o \cos(\varphi + \varphi_p) \} \right.$$
$$\left. - \sin(\varphi + \varphi_p) (x_o + r_o \varphi \tan \beta_{io}) \right] d\varphi \tag{2.7}$$

$$u_r = \frac{\Gamma r_o}{4\pi} \int \sum_{p=1}^{g} \frac{1}{S^3} \left[ - (r_o \varphi \tan \beta_{io} + x_o) \cos(\varphi + \varphi_p) \right.$$
$$\left. + \tan \beta_{io} \, r_o \sin(\varphi + \varphi_p) \right] d\varphi \tag{2.8}$$

The above equations, after due changes in nomenclature, are in agreement with Strzheletsky's[22] formula 35. Furthermore, in the special case when one of the helix starting angles, $\varphi_p$, as well as the axial starting points, $x_o$, are zero, these expressions agree with those given by Betz[23] and Lerbs[1]. This latter case corresponds to the

the velocity components at a blade in propeller lifting line theory.

Equations (2.6) - (2.8) can be made non-dimensional in terms of the following variables

$$\eta = r_o/r$$
$$\xi = x_o/r \qquad (2.9)$$
$$\bar{u} = \frac{4\pi r u}{\Gamma}$$

The non-dimensional induced velocity components $\bar{u}$ can then be written

$$\bar{u}_a = \eta \int \sum_{p=1}^{\infty} \frac{1}{D^{3/2}} \left[\eta - \cos(\varphi + \varphi_p)\right] d\varphi \qquad (2.10)$$

$$\bar{u}_t = \eta \int \sum_{p=1}^{\infty} \frac{1}{D^{3/2}} \left[\tan\beta_{io} \{1 - \eta \cos(\varphi + \varphi_p)\} - \sin(\varphi + \varphi_p)\{\xi + \eta \tan\beta_{io}\,\varphi\}\right] d\varphi \qquad (2.11)$$

$$\bar{u}_r = \eta^2 \int \sum_{p=1}^{\infty} \frac{1}{D^{3/2}} \left[\tan\beta_{io} \sin(\varphi + \varphi_p) - \{\varphi \tan\beta_{io} + \xi/\eta\}\cos(\varphi + \varphi_p)\right] d\varphi \qquad (2.12)$$

where the denominator in each of the integrals above is

$$D^{3/2} = \left[(\xi + \eta\,\varphi \tan\beta_{io})^2 + 1 + \eta^2 - 2\eta\cos(\varphi + \varphi_p)\right]^{3/2} \qquad (2.13)$$

The non-dimensional velocity $\bar{u}$ is related to the Lerbs[1] induction factors i by the relation

$$\bar{u} = \frac{i}{1 - \eta} \qquad (2.14)$$

The reason for selecting a different non-dimensional form is based on a consideration of numerical accuracy. The total velocity at a control point is to be obtained by summing the velocities induced

by the elements of a lattice system. The velocity induced by the nearby elements will become very large as the lattice spacing becomes small, so that these must be computed to an increasingly large number of significant figures for a prescribed accuracy in the resultant velocity. The quantity $\bar{u}$ will tend to infinity as $(1 - \eta)^{-1}$ as $\eta \to 1$, hence requiring a fixed accuracy in $\bar{u}$, (say three decimal places correct) is equivalent to requiring a higher percentage accuracy as the magnitude of $\bar{u}$ increases.

On the other hand, the induction factors remain finite due to the factor $(1 - \eta)$, so that if the number of decimal places in the computation of the induction factors is sufficient for the nearby elements of the lattice, the induction factors for the distant elements will be unnecessarily accurate.

In general, the velocity component normal to a particular boundary is to be determined. Let $(\ell, m, n)$ be the $(x, y, z)$ components of a unit vector normal to the surface. The non-dimensional normal velocity is then given by

$$\bar{u}_n = \ell\, \bar{u}_a + m\, \bar{u}_r + n\, \bar{u}_t \qquad (2.15)$$

For purposes of computation, it is convenient to express the integral in the following form

$$\bar{u}_n = \int_{p=1}^{\#\,8} \frac{(c_3 + c_4 \cos\varphi + c_5 \sin\varphi + c_6\, \varphi \cos\varphi + c_7\, \varphi \sin\varphi)\, d\varphi}{(d_1 \varphi^2 + d_2 \varphi + d_3 + d_4 \cos\varphi + d_5 \sin\varphi)^{3/2}} \qquad (2.16)$$

where the c's and d's are constants in the integration, but depend on the blade index p. From (2.5) these constants can be written as

$$c_3 = \ell c_{3a} + m\, c_{3r} + n\, c_{3t}$$

$$c_4 = \ell c_{4a} + m\, c_{4r} + n\, c_{4t}$$

etc. (2.17)

By expanding $\sin(\varphi + \varphi_p)$ and $\cos(\varphi + \varphi_p)$ in (2.10) - (2.12) and collecting coefficients, the following expressions are obtained

$$\left.\begin{aligned} c_{3a} &= \eta^2 \\ c_{4a} &= -\eta \cos\varphi_p \\ c_{5a} &= \eta \sin\varphi_p \\ c_{6a} &= c_{7a} = 0 \end{aligned}\right\} \text{axial component}$$

$$\left.\begin{aligned} c_{3r} &= 0 \\ c_{4r} &= \eta^2 \tan\beta_{io} \sin\varphi_p - \eta\xi\cos\varphi_p \\ c_{5r} &= \eta^2 \tan\beta_{io} \cos\varphi_p + \eta\xi\sin\varphi_p \\ c_{6r} &= \eta^2 \tan\beta_{io} \cos\varphi_p \\ c_{7r} &= \eta^2 \tan\beta_{io} \sin\varphi_p \end{aligned}\right\} \text{radial component}$$

$$\left.\begin{aligned} c_{3t} &= \eta \tan\beta_{io} \\ c_{4t} &= -\eta^2 \tan\beta_{io} \cos\varphi_p - \eta\xi\sin\varphi_p \\ c_{5t} &= \eta^2 \tan\beta_{io} \sin\varphi_p - \eta\xi\cos\varphi_p \\ c_{6t} &= \eta^2 \tan\beta_{io} \sin\varphi_p \\ c_{7t} &= -\eta^2 \tan\beta_{io} \cos\varphi_p \end{aligned}\right\} \text{tangential component}$$

The coefficients of the denominator, which are the same for all three components, are

$$d_1 = \eta^2 \tan^2\beta_{io}$$

$$d_2 = 2\varphi_1 \eta^2 \tan^2\beta_{io}$$

$$d_3 = \varphi_1^2 \eta^2 \tan^2 \beta_{io} + 1 + \eta^2$$

$$d_4 = -2 \eta \cos \varphi_p$$

$$d_5 = 2 \eta \sin \varphi_p \qquad (2.18)$$

By considering the non-existent constants $c_1$, $c_2$, $d_6$, and $d_7$ to be zero, and by defining a function $F_n(\varphi)$ as follows

$$F_1 = \varphi^2 \quad F_2 = \varphi \quad F_3 = 1 \quad F_4 = \cos \varphi$$

$$F_5 = \sin \varphi \quad F_6 = \varphi \cos \varphi \quad F_7 = \varphi \sin \varphi \qquad (2.19)$$

a more compact expression for $\bar{u}_n$ is obtained

$$\bar{u}_n = \int \sum_{p=1}^{g} \frac{\left[\sum_{n=1}^{7} c_n F_n(\varphi)\right]}{\left[\sum_{n=1}^{7} d_n F_n(\varphi)\right]^{3/2}} d\varphi \qquad (2.20)$$

If the integral is to be evaluated by an I point integration formula with weights $W_i$, (2.20) may be written

$$\bar{u}_n = \sum_{i=1}^{I} W_i \sum_{p=1}^{g} \frac{\left[\sum_{n=1}^{7} C_n F_{ni}\right]}{\left[\sum_{n=1}^{7} d_n F_{ni}\right]^{3/2}} \qquad (2.21)$$

where $F_{ni}$ means $F_n(\varphi_i)$. This is a convenient form for use with a digital computer. As is described in Appendix ( A ), values of $F_{ni}$ may be computed and stored in a table so that only the constants $c_n$ and $d_n$ need be computed for each integration. This results in a large saving in computation time, which is important since the evaluation of these integrals represents the major part of the numerical work in obtaining lifting surface solutions by a lattice method.

The velocity component normal to a true helical surface can be determined by substituting the components of the unit normal in (2.15).

Choosing the positive direction for the normal to be directed upstream, i.e., in the direction in which a propeller would normally be developing thrust, there follows

$$\ell = -\cos\beta_i \quad m = 0 \quad n = +\sin\beta_i$$
$$\bar{u}_n = -\bar{u}_a \cos\beta_i + \bar{u}_t \sin\beta_i \qquad (2.23)$$

where $\beta_i$ is the pitch angle of the helix at the control point radius r.

Integration Error

In the case of a semi-infinite vortex, equations (2.10) - (2.12) or (2.22) may be solved by numerical integration up to some angle $\varphi_t$, and the remaining contribution from $\varphi_t$ to $\infty$ estimated. In this section the error introduced in the numerical integration from 0 to $\varphi_t$ will be considered. These results may be applied equally well to the integration of vortex segments of finite length on the blades.

To get some idea of the spacing required, the error in the axial component will be derived in the case of numerical integration by Simpson's Rule. The expression for Simpson's Rule[24], including the error term, is

$$\int_{x_o}^{x_2} f(x)\,dx = \frac{h}{3}(f_o + 4f_1 + f_2) - \frac{4h^5}{90} f^{IV}(\xi) \qquad (2.23)$$

where the total length of the interval $x_2 - x_o = 2h$, and $x_o \leq \xi \leq x_2$. Note that x and $\xi$ refer to the variable of integration in general, not to the coordinates defined in Fig. (2.1).

If the magnitude of the maximum allowable error in one revolution of the integration is $\epsilon$, the number of Simpson's Rule elements per revolution is

$$\frac{2\pi}{2h} = \pi/h \qquad (2.24)$$

and the maximum error per element is

$$\epsilon h/\pi = \frac{h^5}{90} \quad f^{IV}(\xi) \tag{2.25}$$

so that the maximum integration spacing is:

$$h = \left( \frac{90\,\epsilon}{\pi \quad f^{IV}(\xi)} \right)^{1/4} \tag{2.26}$$

If $f^{IV}(\xi)$ is interpreted as the maximum value in the interval, $\epsilon$ will be an upper bound on the error for a spacing h.

The fourth derivative of the integrand of (2.10) after an elementary, but lengthy calculation, may be expressed as follows in terms of the notation of Fig. (2.1).

$$f^{IV}(\varphi) = \sum_{p=1}^{g} \left[ r_o D_1 - r \cos \varphi_p D_2 + r \sin \varphi_p D_3 \right] \tag{2.27}$$

where: $D_1 = C_1$

$D_2 = (C_1 + C_2) \cos \varphi + C_3 \sin \varphi$

$D_3 + (C_1 + C_2) \sin \varphi - C_3 \cos \varphi$

$$C_1 = 59.0625\, s^{-11/2} s'^4 - 78.75\, s^{-9/2} s'^2 s'' + 11.25\, s^{-7/2} s''^2 + 15.0\, s^{-7/2} s' s''' - 1.5\, s^{-5/2} s^{IV}$$

$$C_2 = -22.5\, s^{-7/2} s'^2 + 9.0\, s^{-5/2} s'' + s^{-3/2}$$

$$C_3 = 52.5\, s^{-9/2} s'^3 - 45.0\, s^{-7/2} s' s'' + 65^{-5/2} s''' - 6\, s^{-5/2} s'$$

$$s = d + e\varphi\, f\, \varphi^2 + g \cos \varphi + h \sin \varphi$$

$$s' = e + 2f\varphi - g \sin \varphi + h \cos \varphi$$

$$s'' = 2f = g \cos \varphi = h \sin \varphi$$

$$s''' = g \sin \varphi - h \cos \varphi$$

$$s^{IV} = g \cos \varphi + h \sin \varphi$$

$$d = x_o^2 + r^2 r_o^2$$

$$e = 2 x_o r_o \tan \beta_{io}$$

$$f = r_o^2 \tan^2 \beta_{io}$$

$$g = -2r r_o \cos \varphi_p$$

$$h = 2r r_o \sin \varphi_p$$

Unfortunately, many of the terms in the above expression are of the same magnitude, so that it does not seem possible to obtain a simple upper bound for $f^{IV}(\varphi)$ without being unreasonably conservative.

The above equations were therefore programmed for an IBM 650 and a few sample curves of $f^{IV}(\varphi)$ were computed.

Fig. (2.2) shows a sample plot of $\left[f^{IV}(\varphi)\right]^{1/4}$ for a three and five-bladed propeller with $\eta = 2$ and $\beta_{io} = 20^\circ$. From (2.26) this is seen to be inversely proportional to the spacing required. This indicates that the spacing after one revolution can be about ten times the initial spacing for constant error.

When $\eta$ is close to one, the fourth derivative is initially very large. The following values are for $\eta = .95$, $\beta_{io} = 20^\circ$, and $g = 3$

| $\varphi^\circ$ | $f^{IV}(\varphi)$ | $\left[f^{IV}(\varphi)\right]^{1/4}$ |
|---|---|---|
| 0 | $3.31 \times 10^9$ | 240 |
| 3 | $8.99 \times 10^7$ | 97 |
| 6 | $2.74 \times 10^7$ | 72 |

In order to guarantee an error of less than .0001 per revolution in this case, an initial spacing of about .05 degrees would be required, while for $\eta = 2$ the initial spacing could be 2.8 degrees. After one revolution, a spacing of around 30 degrees would be sufficient, regardless of the value of $\eta$.

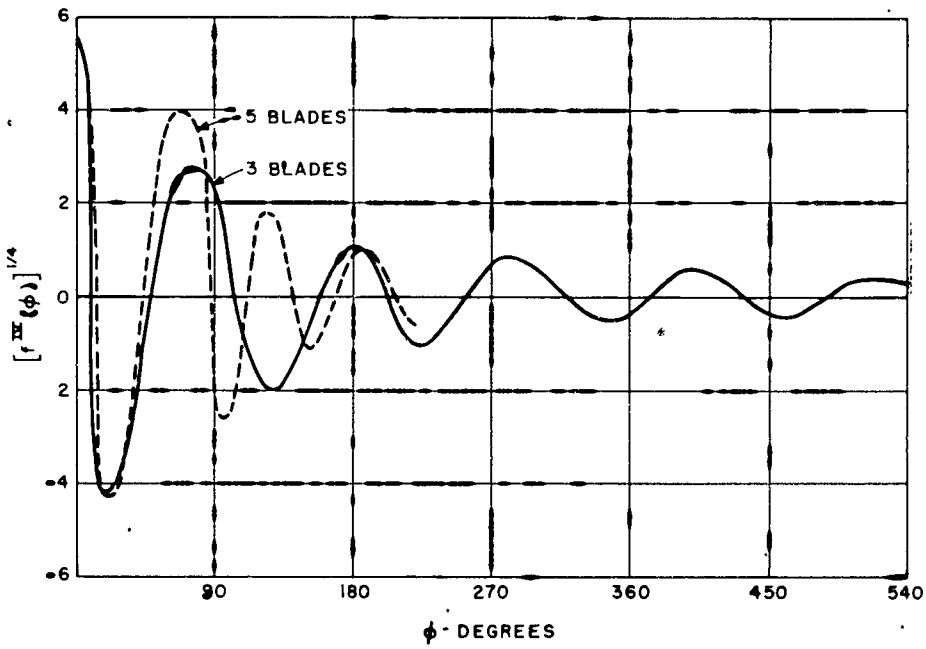


FIG. 2.2 PLOT OF $[f^{III}(\phi)]^{1/4}$ FOR AXIAL INDUCED VELOCITY FOR $\nu = 2$ $\beta_{1_0} = 20°$

$$\int_0^1 f(x)\,dx = \sum_{k=1}^{5} W_k\, f(x_k) + (\text{const})\, f^{IV}(\xi) \qquad (2.28)$$

where the weights and ordinates are given in Table A-2 in the Appendix. While this formula would be very cumbersome for a hand calculation due to the irrational weights and unevenly spaced ordinates, on a digital computer this would take the same length of time per point as Simpson's Rule and would have a much higher degree of precision.

As a result of calculating a large number of induced velocity integrals, it was observed that in all cases a larger spacing between points could be used with the 5 point Gauss Rule than with Simpson's Rule. The advantage was greatest for values of $\eta$ near unity where the Gauss rule spacing could be five times as large as the Simpson's rule spacing for equal accuracy.

As a result of these sample calculations, it was also noted that when $|1 - \eta|$ was small it was not necessary to decrease the spacing when integrating the blades other than the index blade. By using a wide spacing for the non-index blades, a significant reduction in computation time could be achieved, particularly for five or six-bladed propellers.

Although the spacing required for a particular accuracy depends on $g$, $\eta$, $\tan \beta_{io}$, and $x_o$, there is very little to be gained in including a parameter which has a relatively small effect on the required spacing since the time spent selecting and manipulating blocks of stored tables may affect any time savings in the actual integration process. It appears as though the critical parameter is $|1 - \eta|$ and that the effect of $g$, $\tan \beta_{io}$ and $x_o$ on the required spacing can be ignored. It also appears reasonable to divide $|1 - \eta|$ into the following three regions:

$$.02 \leq |1 - \eta| \leq .10 \qquad \text{Fine Spacing}$$

$$.10 < |1 - \eta| \leq .25 \qquad \text{Medium Spacing}$$

$$.25 < |1 - \eta| \qquad \text{Coarse Spacing} \qquad (2.29)$$

Values of $|1 - \eta| < .02$ were not considered, since this is the smallest value which would be obtained with the vortex lattice systems anticipated. Table (A-I) in the Appendix contains a list of angular intervals which when divided into 5-point Gauss ordinates will produce values of the integrals correct to 3 decimal places.

Truncation Error

An upper bound on the error introduced by truncating the integration at some angle $\varphi_t$ can be obtained as follows:

The integral to be estimated is:

$$\delta \bar{u}_a = \eta \int_{\varphi_t}^{\infty} \sum_{p=1}^{g} \frac{1}{D^{3/2}} \left[\eta - \cos(\varphi + \varphi_p)\right] d\varphi \qquad (2.30)$$

The denominator can be simplified as follows:

$$D^{3/2} = \left[(\xi + \eta\varphi \tan\beta_{io})^2 + 1 + \eta^2 - 2\eta\cos(\varphi + \varphi_p)\right]^{3/2}$$

$$\geq \eta^3 \varphi^3 \tan^3 \beta_{io} \qquad (2.31)$$

Subsituting (2.31) in (2.30) and replacing $-\cos(\varphi + \varphi_p)$ by 1,

$$|\delta \bar{u}_a| \leq \left| \frac{\eta + 1}{\eta^2 \tan^3 \beta_{io}} \sum_{p=1}^{g} \int_{\varphi_t}^{\infty} \frac{d\varphi}{\varphi^3} \right| = \left| \frac{g(\eta + 1)}{2\eta^2 \tan^3 \beta_{io} \varphi_t^2} \right| \qquad (2.32)$$

Similarly from (2.11) the tangential velocity estimate is

$$\left| \delta \bar{u}_t \right| \leq \left| \frac{1}{\eta^2 \tan^3 \beta_{io}} \sum_{p=1}^{g} \int_{\varphi_t}^{\infty} \frac{(1+\eta) \tan \beta_{io} + \xi + \eta \tan \beta_{io}\, \varphi}{\varphi^3} \, d\varphi \right|$$

$$= \left| \frac{g}{\eta \tan^2 \beta\, \varphi_t} \left[ 1 + \frac{(1+\eta) \tan \beta_{io} + \xi}{2\eta \tan \beta_{io}\, \varphi_t^2} \right] \right| \quad (2.33)$$

For example, if $\eta = 1$, $\tan \beta_{io} = 1$, $\xi = 0$ and $g = 3$, the maximum error introduced by truncating the integration after n revolutions ($\varphi_t = 2\pi n$) is shown in Table 2.1.

Table 2.1 Truncation Error Bound

| No. of Revolutions n | $\left\| \delta \bar{u}_a \right\|$ max. | $\left\| \delta \bar{u}_t \right\|$ max. |
|---|---|---|
| 1 | .0760 | .5500 |
| 2 | .0190 | .2570 |
| 3 | .0084 | .1650 |
| 4 | .0047 | .1240 |
| 5 | .0030 | .0985 |
| 6 | .0021 | .0815 |
| 13 | .0005 | |

While this estimate is very conservative, particularly in the case of the tangential velocity, it illustrates the fact that after 2 or 3 revolutions the error decreases very slowly. On the other hand, after a few revolutions, the value of the integral to infinity can be accurately estimated as follows:

For large values of $\varphi_t$:

$$\delta \bar{u}_a \approx \frac{1}{\eta^2 \tan^3 \beta_{io}} \int_{\varphi_t}^{\infty} \sum_{p=1}^{g} \frac{\eta - \cos(\varphi + \varphi_p)}{\varphi^3} \, d\varphi$$

$$= \frac{1}{\eta^2 \tan^3 \beta_{io}} \left[ \sum_{p=1}^{g} \eta \int_{\varphi_t}^{\infty} \frac{d\varphi}{\varphi^3} - \sum_{p=1}^{g} \cos \varphi_p \int_{\varphi_t}^{\infty} \frac{\cos \varphi \, d\varphi}{\varphi^3} \right.$$

$$\left. \sum_{p=1}^{g} \sin \varphi_p \int_{\varphi_t}^{\infty} \frac{\sin \varphi \, d\varphi}{\varphi^3} \right] \qquad (2.34)$$

The last two integrals in (2.34) can be reduced to the Sine Ingetral $\left[ Si\ (\varphi) \right]$ and Cosine Integral $\left[ Ci\ (\varphi) \right]$ which are tabulated functions. However, if the blades have equal angular spacing, the sums over $\cos \varphi_p$ and $\sin \varphi_p$ are zero so that only the first term remains. In this case the estimated value of the integral becomes:

$$\delta \bar{u}_a \approx \frac{g}{2\eta \tan^3 \beta_{io} \varphi_t^2} \qquad (2.35)$$

Similarly, the approximate value of the tangential velocity is:

$$\delta \bar{u}_t \approx \frac{g}{2\eta^2 \tan^2 \beta_{io} \varphi_t^2} \qquad (2.36)$$

An upper bound on the error introduced by using (2.35) can be obtained as follows:

Assume that the actual value of $D^{3/2}$ and the approximate value differ by the factor $\left[ 1 + \epsilon\ (\varphi) \right]$, where $\epsilon \ll 1$. Then

$$\eta \int_{\varphi_t}^{\infty} \frac{1}{D^{3/2}} \left[ \eta - \cos (\varphi + \varphi_p) \right] d\varphi = \eta \int_{\varphi_t}^{\infty} \frac{\eta - \cos (\varphi + \varphi_p) \, d\varphi}{(1 + \epsilon)(\eta^3 \varphi^3 \tan^3 \beta_{io})}$$

$$= \eta \int_{\varphi_t}^{\infty} \frac{\eta - \cos (\varphi + \varphi_p) \, d\varphi}{\eta^3 \tan^3 \beta_{io} \varphi^3} - \eta \int_{\varphi_t}^{\infty} \frac{\epsilon \, (\eta - \cos (\varphi + \varphi_p) \, d\varphi}{\eta^3 \tan^3 \beta_{io} \varphi^3} + \cdots\cdots$$

$$= \delta \bar{u}_a + \delta \qquad (2.37)$$

Where

$$\delta = - \frac{1}{\eta^2 \tan^3 \beta_{io}} \int_{\varphi_t}^{\infty} \frac{\epsilon \left[ \eta - \cos (\varphi + \varphi_p) \right]}{\varphi^3} \, d\varphi \qquad (2.38)$$

is the error in the approximation $\delta \bar{u}_a$. If $\epsilon_{max}$ is the maximum value of $\epsilon(\varphi)$ in the interval $\varphi_t \leq \varphi \leq \infty$, $\delta$ can be written:

$$|\delta| \leq \left| \frac{\epsilon_{max}(\eta + 1)}{2\eta^2 \tan^3 \beta_{io} \varphi_t^2} \right| \tag{2.39}$$

The quantity $\epsilon_{max}$ can be estimated as follows:

$$(1 + \epsilon)(\eta^3 \varphi^3 \tan^3 \beta_{io}) = \left[(\xi + \eta \varphi \tan \beta_{io})^2 + 1 + \eta^2 - 2\eta \cos(\varphi + \varphi_p)\right]^{3/2}$$

Solving for $\epsilon$:

$$\epsilon = \frac{\left[(\xi + \eta \varphi \tan \beta_{io})^2 + 1 + \eta^2 - 2\eta \cos(\varphi + \varphi_p)\right]^{3/2}}{\eta^3 \varphi^3 \tan^3 \beta_{io}} - 1$$

$$|\epsilon| \leq \left| \frac{\left[\xi^2 + 2\eta \xi \varphi \tan \beta_{io} + \eta^2 \varphi^2 \tan^2 \beta_{io} + 1 + \eta^2 + 2\eta\right]^{3/2}}{\eta^3 \varphi^3 \tan^3 \beta_{io} + 0} - 1 \right| \tag{2.40}$$

In the case when $\xi = 0$ and $\varphi^2 \gg 1$, the 3/2 power in the numerator can be expanded giving the approximate result:

$$|\epsilon| \leq \left| \frac{3}{2} \frac{(1 + \eta^2 + 2\eta)}{\eta^2 \varphi^2 \tan^2 \beta_{io}} \right| \tag{2.41}$$

The maximum value of $\epsilon$ is when $\varphi = \varphi_t$. Substituting this in (2.39) gives the result

$$|\delta| \leq \left| \frac{3}{4} \frac{(1 + \eta^2 + 2\eta)(\eta + 1)}{\eta^4 \tan^5 \beta_{io} \varphi_t^4} \right| \tag{2.42}$$

Solving for $\varphi_t$

$$\varphi_t = \left| \frac{3 (1 + \eta^2 + 2\eta)(\eta + 1)}{4 \delta \eta^4 \tan^5 \beta_{io}} \right|^{1/4} \tag{2.43}$$

Taking the same numerical example as before, if $\eta = 1$ $\tan \beta_{io} = 1$ $\xi = 0$ $g = 3$ and $\delta = .0005$, (2.43) gives the result:

$\varphi_t = 13.8$ radians $\approx 2$ revolutions.

According to Table (2.1), it would require 13 revolutions to obtain the same accuracy if the numerical integrations were used entirely. Since Table (2.1) represents a very conservative estimate, the actual saving in using the approximate value of the integral from $\varphi_t$ to $\infty$ is somewhat less.

Equation (2.43) and a similar one for the tangential velocity could be used to determine $\varphi_t$. However, this is also a little conservative, so that it is more efficient to use a more empirical way of deciding when to stop the numerical integration. This is done by estimating the value of the integrals to infinity from (2.35) and (2.36) after each revolution in the numerical integration has been completed. When two successive estimates agree to the desired tolerance, the approximation of the integral is assumed to have converged.

Numerical Results

In order to check the preceding results, induced velocity components were computed corresponding to three numerical examples given by Wrench[25]. The velocity components obtained by numerical integration converted to induction factors by (2.14) agreed to four decimal places with Wrench's values, which was the total number of places given. Checks against gross errors were made by comparing induction factors over a wider set of parameters with the tables given by Morgan[26], and in all cases the agreement was satisfactory.

In addition, large numbers of computations were made to determine the optimum integration spacing as was discussed previously, however, since these results are of limited usefulness once the spacing criterion has been established, this data will not be reported.

## CHAPTER 3

## THE VELOCITY INDUCED BY RADIAL VORTEX LINES

The velocity induced by a straight radial vortex segment of constant strength can be obtained by integration using Biot-Savart's Law. While the helical case was somewhat complicated due to the necessity of using numerical integration, the expressions obtained for the radial case are very simple and may easily be integrated explicitly.

The notation to be used is shown in Fig. 3.1, and is substantially the same as Fig. 2.1. A set of g radial vortex lines are located at angles $\varphi_p$ and extend from $r_1$ to $r_2$. The remaining notation is the same as in the helical case, except that the variable of integration is now $r_o$ instead of $\varphi$.

The components of the vector element of vortex line $d\vec{\ell}$ are

$$d\vec{\ell} = \left[ 0,\ dr_o \cos \varphi_p,\ dr_o \sin \varphi_p \right] \tag{3.1}$$

and the distance from the vortex element to the control point is

$$\vec{s} = \left[ -x_o,\ r - r_o \cos \varphi_p,\ - r_o \sin \varphi_p \right] \tag{3.2}$$

Substituting these quantities into the expression for Biot-Savart's Law (2.1), the following expressions for the velocity components are obtained

$$u_a = \frac{\Gamma}{4\pi} \int_{r_1}^{r_2} \sum_{p=1}^{g} \frac{-r \sin \varphi_p \, d r_o}{(x_o^2 + r^2 + r_o^2 - 2r r_o \cos \varphi_p)^{3/2}}$$

$$u_r = 0$$

$$u_t = \frac{\Gamma}{4\pi} \int_{r_1}^{r_2} \sum_{p=1}^{g} \frac{x_o \cos \varphi_p \, dr_o}{(x_o^2 + r^2 + r_o^2 - 2r r_o \cos \varphi_p)^{3/2}} \tag{3.3}$$

As in Chapter 2, these can be expressed in terms of the non-dimensional quantities

$$\eta = r_o/r \qquad \xi = x_o/r \qquad \bar{u} = u \frac{4\pi r}{\Gamma} \tag{3.4}$$

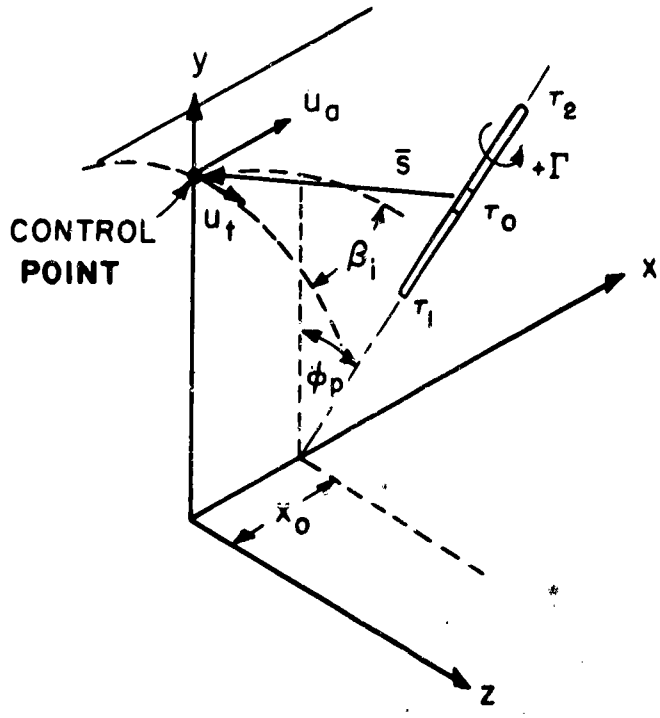


FIG. 3.1 COORDINATE SYSTEM FOR RADIAL VORTICES

resulting in the following expressions

$$\bar{u}_a = -\sum_{p=1}^{g} \sin\varphi_p \int_{\eta_1}^{\eta_2} \frac{d\eta}{E^{3/2}}$$

$$\bar{u}_t = \xi \sum_{p=1}^{g} \cos\varphi_p \int_{\eta_1}^{\eta_2} \frac{d\eta}{E^{3/2}} \qquad (3.5)$$

where the denominator is

$$E^{3/2} = \left[\xi^2 + 1 + \eta^2 - 2\eta\cos\varphi_p\right]^{3/2} \qquad (3.6)$$

Equations (3.5) can be integrated to give the following

$$\bar{u}_a = -\sum_{p=1}^{g} \sin\varphi_p \, I_p \qquad \bar{u}_t = \xi \sum_{p=1}^{g} \cos\varphi_p \, I_p \qquad (3.7)$$

where

$$I_p = \frac{\eta - \cos\varphi_p}{(\xi^2+\sin^2\varphi_p)E^{1/2}} \Bigg]_{\eta_1}^{\eta_2} \qquad \xi^2 + \sin^2\varphi_p \neq 0 \qquad (3.8)$$

$$I_p = \frac{-1}{2\,(\eta + \cos\varphi_p)^2} \Bigg]_{\eta_1}^{\eta_2} \qquad \xi^2 + \sin^2\varphi_p = 0 \qquad (3.9)$$

The latter form corresponds to the case when the vortex segment coincides with the y axis, at which point the velocity is zero as can be seen from (3.5)

As in Chapter 2, the velocity normal to a helical surface with pitch angle $\beta_i$ at a radius r is

$$\bar{u}_n = -\bar{u}_a \cos\beta_i + \bar{u}_t \sin\beta_i$$

which in this case can be written

$$\bar{u}_n = \sum_{p=1}^{g} \left[\sin\varphi_p \cos\beta_i + \xi \cos\varphi_p \sin\beta_i\right] I_p \qquad (3.10)$$

CHAPTER 4

# SOLUTION OF PROPELLER LIFTING-LINE PROBLEMS BY VORTEX LATTICE METHODS

## Introduction

Before applying vortex lattice methods to the solution of propeller lifting surface problems, it would seem advisable to apply similar methods to certain lifting line problems whose solutions are well known. In particular, this would provide some preliminary information on the spacing and arrangement of control points necessary to produce results with sufficient accuracy for design applications. As will be shown in Chapter 6, it is also necessary in the lifting surface case to have lifting-line results obtained with an identical radial lattice arrangement. The two problems which will be discussed are:

1. To find the radial distribution of circulation to produce a free vortex sheet of true helical shape in homogeneous flow, i.e., the optimum propeller.
2. To find the radial distribution of circulation to produce a free vortex sheet with a specified radial pitch distribution in an axially symmetric velocity field.

## Goldstein Factors

The solution of the first problem is expressed in terms of Goldstein Factors which are defined as follows:

$$\kappa\,(r, \lambda_i, g) = \frac{g\Gamma}{4\pi r\, u_t} \qquad (4.1)$$

where: $\kappa$ = Goldstein factor (non-dimensional)

$\Gamma$ = Strength of bound vortex at radius r - ($ft^2$/sec)

r = Radius of vortex element under consideration. (ft.)

$u_t$ = tangential component of induced velocity at the lifting line as shown in Fig. 4.1 (ft/sec)

$g$ = number of blades

$\lambda_i = r/R \tan \beta_i = \chi \tan \beta_i$

$\beta_i$ = angle of relative flow at the lifting line

$\chi$ = non-dimensional radius r/R, where R is the (ft) radius of the propeller.

This problem was first solved by Goldstein[6] in 1929. If the contraction and axial deformation of the free vortex system is neglected, the problem can be reduced to the two-dimensional problem of a rigid helical surface moving with a fictitious displacement velocity 2u* as shown on Fig. 4.1.* Goldstein's original paper included numerical results for two-bladed propellers for $2 \leq 1/\lambda_i \leq 10$ and for four-bladed propellers for $1/\lambda_i = 5$. Later Kramer[27] and Lock and Yeatman[28] obtained values for propellers with 2-5 blades over the same range of $\lambda_i$. These were recomputed in 1956 by Tachmindji and Milam[29] by a more accurate method. Goldstein Factors for g = 2-6 and $1.5 \leq 1/\lambda_i \leq 6$ were obtained using a Univac computer at David Taylor Model Basin, and those results showed that previous values could be off by as much as 6%. Tachmindji and Milam[30] and McCormick[31] extended Goldstein's theory to include a finite propeller hub, however, their initial assumptions regarding the value of the circulation at the hub are not the same.

*The velocities shown in the figure are at the lifting line. At a large distance downstream the induced velocities are doubled, hence, the displacement velocity is 2u*.

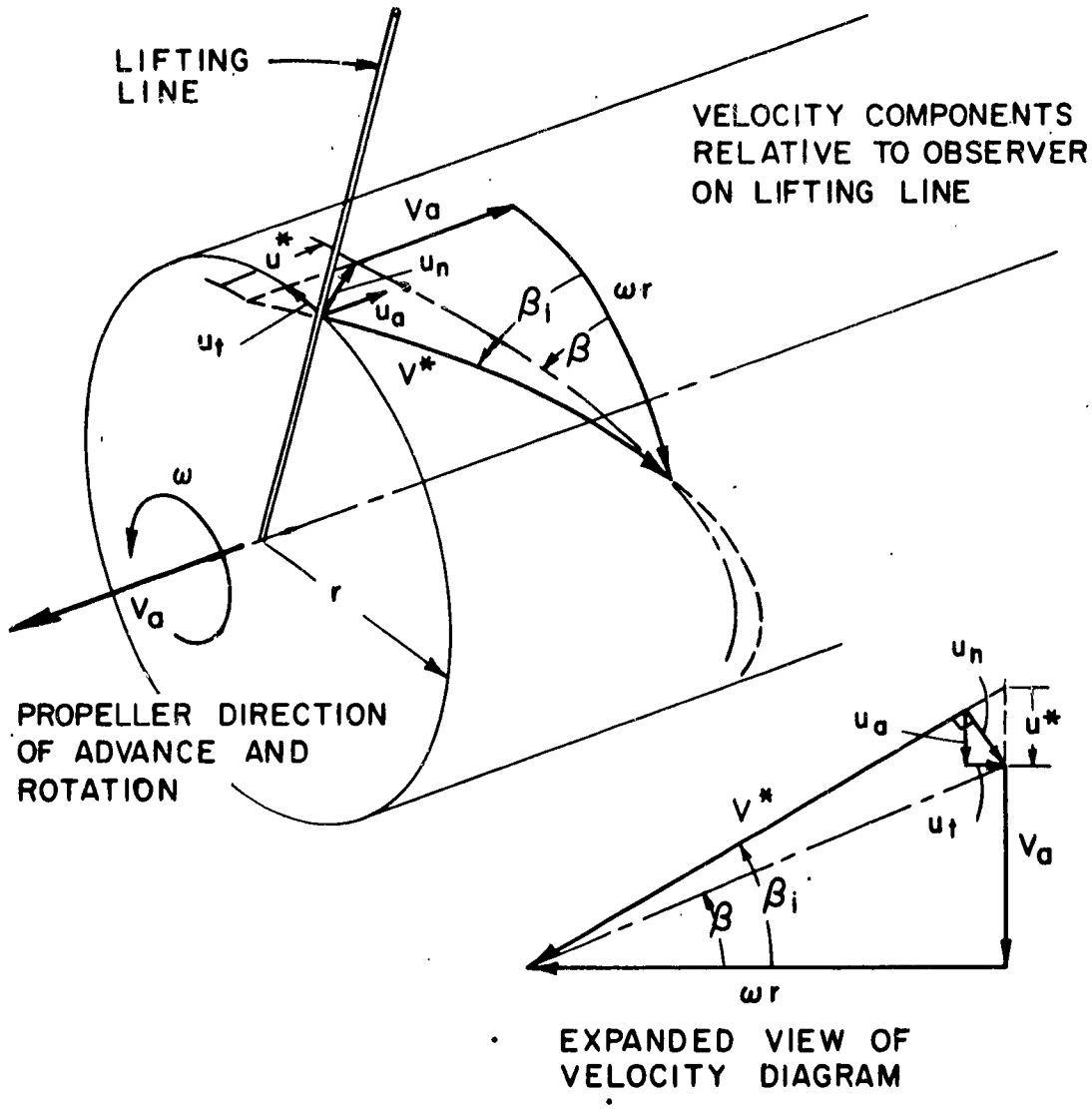


FIG. 4.1 VELOCITY DIAGRAM - OPTIMUM LIFTING-LINE PROPELLER

Another way of computing Goldstein Factors is the induction factor method developed by Lerbs[1]. In this method, the velocity induced by each helical vortex line forming the sheet can be computed from a potential as discussed in Chapter 2. The velocity induced at a point on the lifting line by the entire sheet can be obtained by integrating over the radius. The resulting singular integral can be solved by expanding both the circulation distribution and the induction factors in a Fourier series with a prescribed number of terms. The integral is then approximated by a series of singular integrals of the Glauert type whose value is known from wing lifting line theory[19].

To obtain Goldstein factors by a lattice method the free vortex sheet is replaced by a finite number of helical line vortices as shown schematically in Fig. 4.2. The velocity induced at a point on the lifting line by any of these vortex lines could be computed either from the potential given by Lerbs[7] or by numerical integration as described in Chapter 2. In this case numerical integration will be used since this can easily be extended to the lifting surface case, while the two-dimensional potential for the induction factors cannot.

By computing the velocity induced by each element of the lattice at a number of control points on the lifting line, a set of linear equations results relating the strength of the individual vortices to the resultant slope of the flow at the control points. This can be considered as another way of getting around the singular integral which occurs with the continuous vortex sheet. The equivalent step in the induction factor method is determining the Fourier coefficients of the induction factors which are obtained by one of the usual methods of harmonic analysis from the induction factors evaluated at a number of

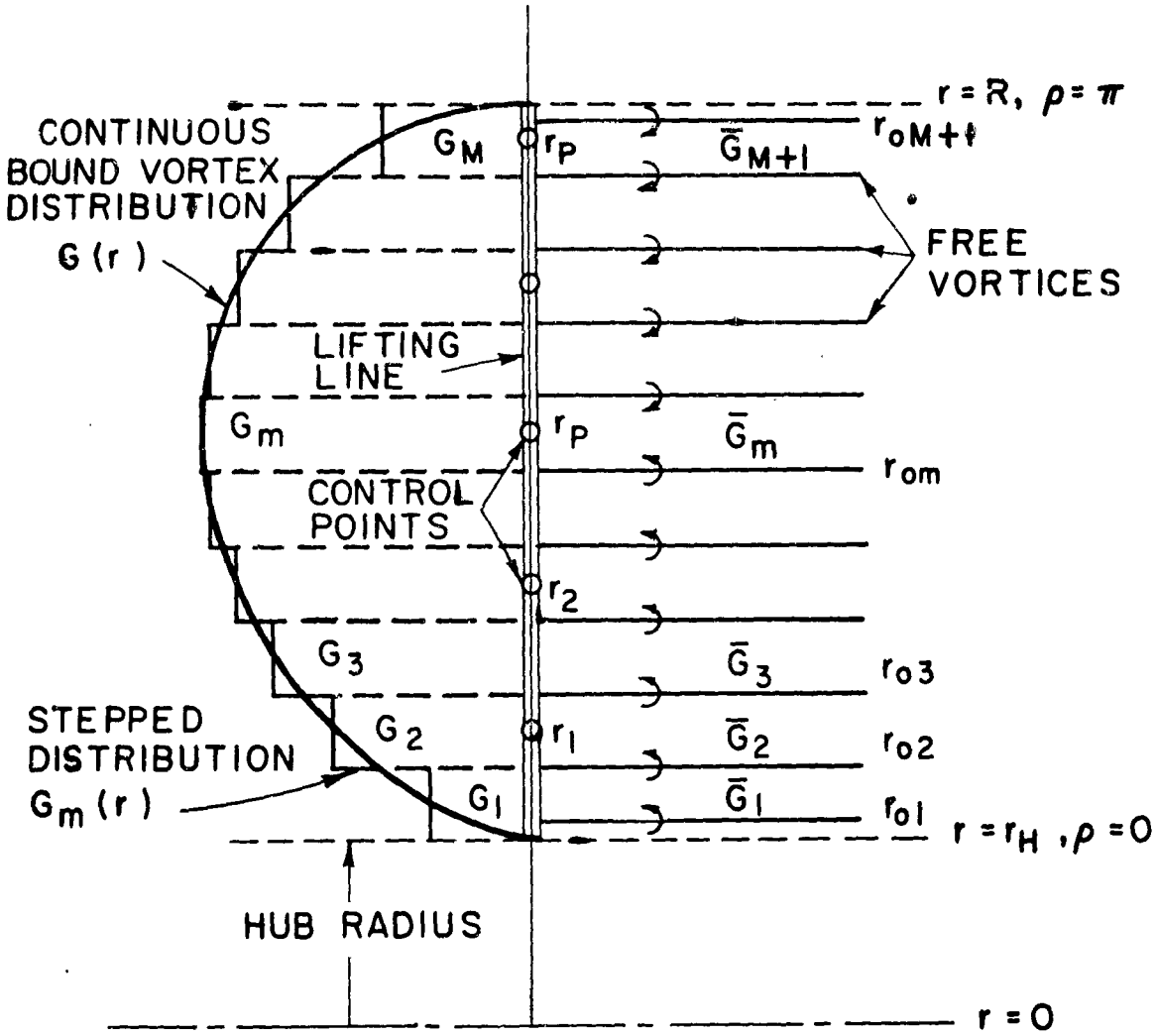


FIG. 4.2 SCHEMATIC ARRANGEMENT OF VORTEX LATTICE WITH M = 10, P = 5

distinct points. In general, the velocity induced at some point on a propeller blade will be due to both the free vortex system and the bound vortices. However, in lifting line theory where the blades have been replaced by straight, radial bound vortices only the free vortex system need be considered. This is because the resultant velocity induced anywhere on one lifting line by a symmetrically arranged set of lifting lines of equal strength is zero.

To proceed with the specific formulation of the problem, it is first assumed that the strength of the bound vortex representing each blade is given by an I term Fourier sine series

$$G(\rho) = \frac{\Gamma(\rho)}{2\pi R u^*} = \sum_{i=1}^{I} a_i \sin i\rho \qquad (4.2)$$

where G is the non-dimensional bound vortex strength and $\rho$ is a new variable which is zero at the hub radius $r_h$ and $\pi$ at the tip.* The variables $\rho$ and $\chi$ are related by

$$\chi = \frac{1}{2}(1 + \chi_h) - \frac{1}{2}(1 - \chi_h)\cos\rho$$

$$\rho = \cos^{-1}\left[\frac{1 + \chi_h - 2\chi}{1 - \chi_h}\right] \qquad (4.3)$$

The vortex distribution given by (4.2) is automatically zero at the hub and tip for any values of the coefficients $a_i$. This is in accordance with the assumption made by Lerbs[1] and Tachmindji and Milam[30] that the circulation falls continuously to zero at the hub. However, as indicated by McCormick[31] and a recent unpublished study by Tachmindji,

*This is not the usual non-dimensional circulation which is defined as $G' = \Gamma/2\pi R V_a$ when $V_a$ is the speed of advance. In the present work, it is more convenient to use u* as the non-dimensionalizing velocity so that G will be independent of loading.

the assumption of zero circulation at the hub does not appear to be valid, but rather that the value at the hub should follow from the solution of the boundary value problem.

In any event, to take the hub into account using vortex lattice methods, it would still be necessary to obtain a suitable series expansion for the hub potential whose coefficients along with those in (4.2) could be obtained by including control points on the hub cylinder as well as on the blade. However, since the effect of normal size hubs ($\chi_h < .2$) on overall propeller performance is small, the solution for the hub potential will be considered at a later time. In the meantime, the hub will be taken into account only by requiring that $G(\chi_h) = 0$ while the radial velocity boundary condition will be disregarded. As will be shown later in the numerical examples, the Goldstein Factors obtained under these fairly crude assumptions are in reasonable agreement with the values given by Tachmindji and Milam[30].

The vortex lattice arrangement is shown schematically in Fig. 4.2, while the actual arrangements used in the numerical examples are shown in Fig. 4.3. The interval from $r = r_h$ to $r = R$ is divided into M equal spaces and the radius to the inner end of the m'th space is called $r_{om}$. The continuous bound vortex distribution $G(r)$ is replaced by a stepped distribution whose value is equal to that of the continuous distribution at the mid-point of each interval.

$$
\begin{aligned}
G_m &= G\left[\tfrac{1}{2}\{(r_o)_{m+1} + (r_o)_m\}\right] \quad (1 \le m \le M-1) \\
G_1 &= G\left[\tfrac{1}{2}\{(r_o)_2 + r_h\}\right] \qquad (m = 1) \\
G_M &= G\left[\tfrac{1}{2}\{R + (r_o)_m\}\right] \qquad (m = M)
\end{aligned}
\tag{4.4}
$$

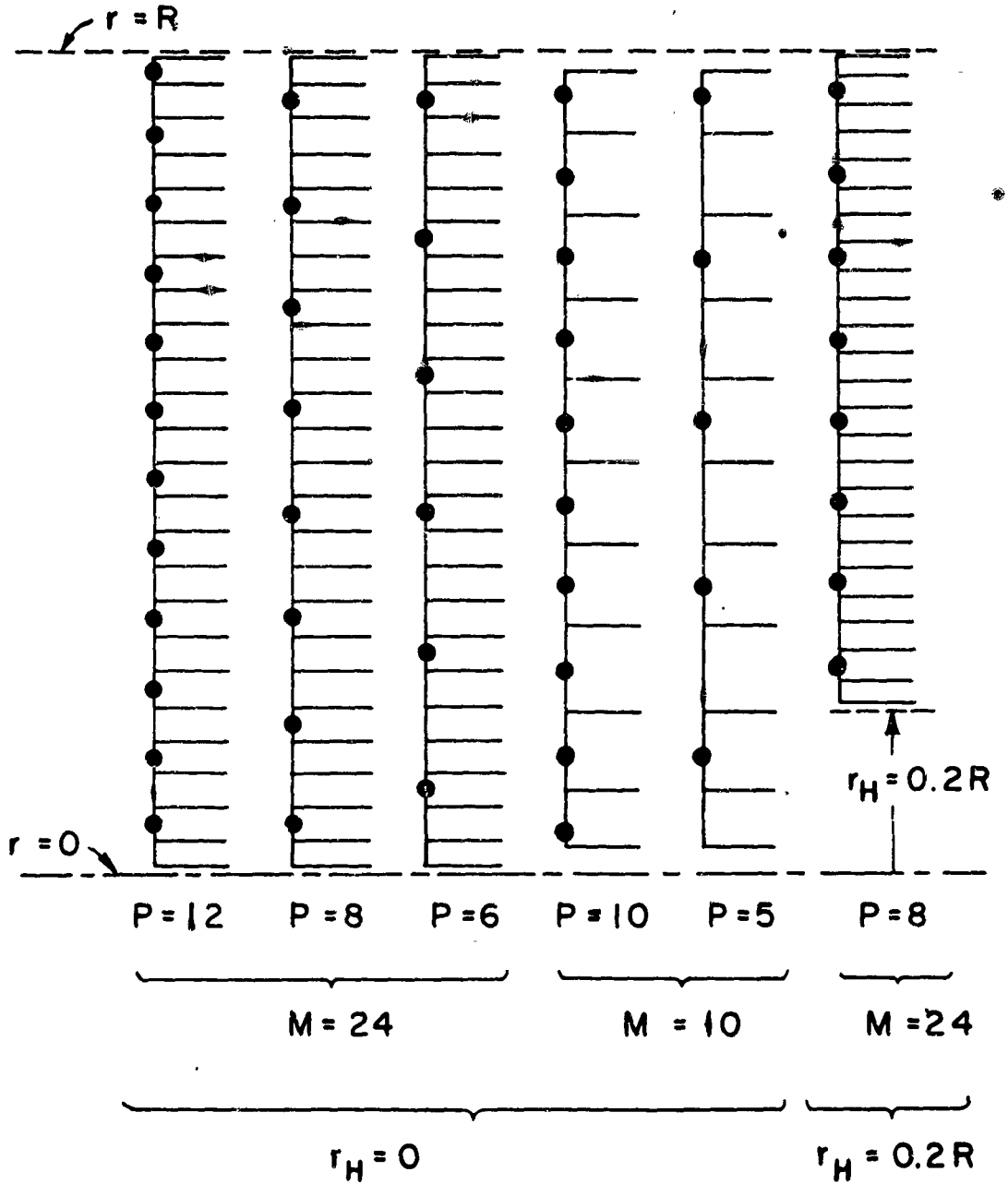


FIG. 4.3 LATTICE ARRANGEMENTS USED IN NUMERICAL EXAMPLES .

The free vortex lines originate at $(r_o)_m$ where the value of $G_m$ changes. Calling the free vortex at $(r_o)_m$ $\tilde{G}_m$ there follows

$$\tilde{G}_m = G_m - G_{m-1} \tag{4.5}$$

This can be made to hold for m = 1, 2, ..... M + 1 by defining the non-existent vortex segments

$$G_o = G_{M+1} = 0 \tag{4.6}$$

It should be noted that the same result could be obtained by noting that the strength of the continuous free vortex sheet at a radius r is dG/dr and replacing the derivative of G by the first order central difference.

The free vortex lines can be considered as replacing a continuous vortex sheet which extends 1/2 space on either side of the free vortex. The only exception is at both ends, where in the continuous case, the sheet must end at the hub and blade tip. It would therefore seem reasonable to move the end vortices in 1/8 space so that they would be located approximately in the region which would actually be occupied by the sheet. In this case, the free vortices are at the following radii:

$$(r_o)_m = r_h + \frac{(R - r_h)(m - 1)}{M} \qquad 2 \leq m \leq M$$

$$(r_o)_1 = r_h + 1/8 \frac{(R - r_h)}{M}$$

$$(r_o)_{M+1} = 1 - 1/8 \frac{(R - r_h)}{M} \tag{4.7}$$

The velocity is to be computed at P control points located at radii $r_1$, $r_2$ .....$r_p$ midway between free vortex elements. There is no restriction on how many of the available control point positions are to be used.

The non-dimensional velocity components induced at $r_p$ by a set of semi-infinite helical vortices originating from each blade with radius $r_{om}$ are

$$(\bar{u}_a)_{mp} = (u_a)_{mp} \frac{4\pi r_p}{\bar{\Gamma}_m} = \frac{2 \chi_p (u_a)_{mp}}{u^* \bar{G}_m}$$

$$(\bar{u}_t)_{mp} = (u_t)_{mp} \frac{4\pi r_p}{\bar{\Gamma}_m} = \frac{2\chi_p (u_t)_{mp}}{u^* \bar{G}_m}$$

$$(\bar{u}_n)_{mp} = (u_n)_{mp} \frac{4\pi r_p}{\bar{\Gamma}} = \frac{2 \chi_p (u_n)_{mp}}{u^* \bar{G}_m} \qquad (4.8)$$

where $\bar{u}$ is the non-dimensional velocity as defined in Chapter 2, u is the dimensional velocity and the subscripts a, t, and n denote axial, tangential and normal components.

The requirement that the relative flow at the lifting line be of constant pitch can be seen from Fig. 4.1 to be

$$u^* = \frac{u_t}{\sin \beta_i \cos \beta_i} = \frac{u_a}{\cos^2 \beta_i} = \frac{u_n}{\cos \beta_i} = \text{const} \qquad (4.9)$$

expressed in terms of either the tangential, axial, or normal components. These relations make use of the known result that the resultant induced velocity is normal to the helical surface formed by the free vortex system.

The tangential velocity induced at $\chi_p$ by the set of vortices $\bar{G}_m$ is

$$(u_t)_p = \frac{u^*}{2 \chi_p} \sum_{m=1}^{M+1} (\bar{u}_t)_{mp} \bar{G}_m$$

$$= \frac{u^*}{2 \chi_p} \sum_{m=1}^{M+1} (\bar{u}_t)_{mp} \sum_{i=1}^{I} a_i (\sin i\rho_m - \sin i \rho_{m-1})$$

$$= u^* \sin \beta_{ip} \cos \beta_{ip} \tag{4.10}$$

which follows from (4.2), (4.5), (4.8), and (4.9). The subscript i in $\beta_i$ following generally accepted propeller nomenclature stands for "induced angle" and is not to be confused with the index i in the Fourier series. Rearranging (4.10) and cancelling out u* gives

$$\sum_{i=1}^{I} a_i \sum_{m=1}^{M+1} (\bar{u}_t)_{mp} \quad (\sin i \rho_m - \sin i \rho_{m-1})$$

$$= 2\chi_p \sin \beta_{ip} \cos \beta_{ip} \tag{4.11}$$

Substituting the geometrical relations

$$\lambda_i = \chi_p \tan \beta_{ip} \qquad \sin \beta_{ip} = \frac{\lambda_i}{\sqrt{\chi_p^2 + \chi_i^2}}$$

$$\cos \beta_{ip} = \frac{\chi_p}{\sqrt{\chi_p^2 + \lambda_i^2}} \tag{4.12}$$

into (4.11) gives the set of linear equations for the unknown coefficients $a_i$

$$\sum_{i=1}^{I} a_i \sum_{m=1}^{M+1} (\bar{u}_t)_{mp} \quad (\sin i \rho_m - \sin i \rho_{m-1})$$

$$= \frac{2\chi_p^2 \lambda_i}{\chi^2 + \lambda_i^2} \tag{4.13}$$

$$p = 1, 2, \ldots\ldots I$$

By selecting I control points as indicated above a set of I equations for the unknown coefficients results. The Goldstein factor at any radius can then be determined in terms of the a's from (4.1) and (4.2)

$$\kappa = \frac{g\,(\chi^2 + \lambda_i^2)}{2\chi^2 \lambda_i} \sum_{i=1}^{I} a_i \sin i\rho \tag{4.14}$$

Since the induced velocity components are all related by (4.9), the set of equations for $a_i$ can be expressed in terms of the axial component

$$\sum_{i=1}^{I} a_i \sum_{m=1}^{M+1} (\bar{u}_a)_{mp} \quad (\sin i \rho_m - \sin i \rho_{m-1}) = \frac{2\chi_p^3}{\chi_p^2 + \lambda_i^2} \qquad (4.15)$$

or in terms of the normal component

$$\sum_{i=1}^{I} a_i \sum_{m=1}^{M+1} (\bar{u}_n)_{mp} \quad (\sin i \rho_m - \sin i \rho_{m-1}) = \frac{2\chi_p^2}{\sqrt{\chi_p^2 + \lambda_i^2}} \qquad (4.16)$$

Numerical Examples

Since the integral for the axial velocity is the easiest to compute, equation (4.15) would be the most efficient. However, to test the computation scheme for the normal component which would be needed later in the lifting surface case, a program using equation (4.16) was also prepared. The greatest discrepancy between the results using the axial and normal velocity was found to be .0001. The method of computation is discussed in Appendix (A ).

Figure 4.4 shows the Goldstein Factors for 3-bladed propellers with zero hub diameter by a lattice arrangement with M = 24 and P = 8 shown schematically in Fig. 4.3. The curves shown in solid lines are taken from Tachmindji and Milam[29] while the points and dotted lines (where necessary) are the values obtained from the lattice. Fig. 4.5 shows a comparison of five different lattice arrangements in the case where g = 3 and $\lambda_i$ = .5 which is the value of $\lambda_i$ which showed the greatest disagreement with existing data. Each of the lattice arrangements are shown in Fig. 4.3.

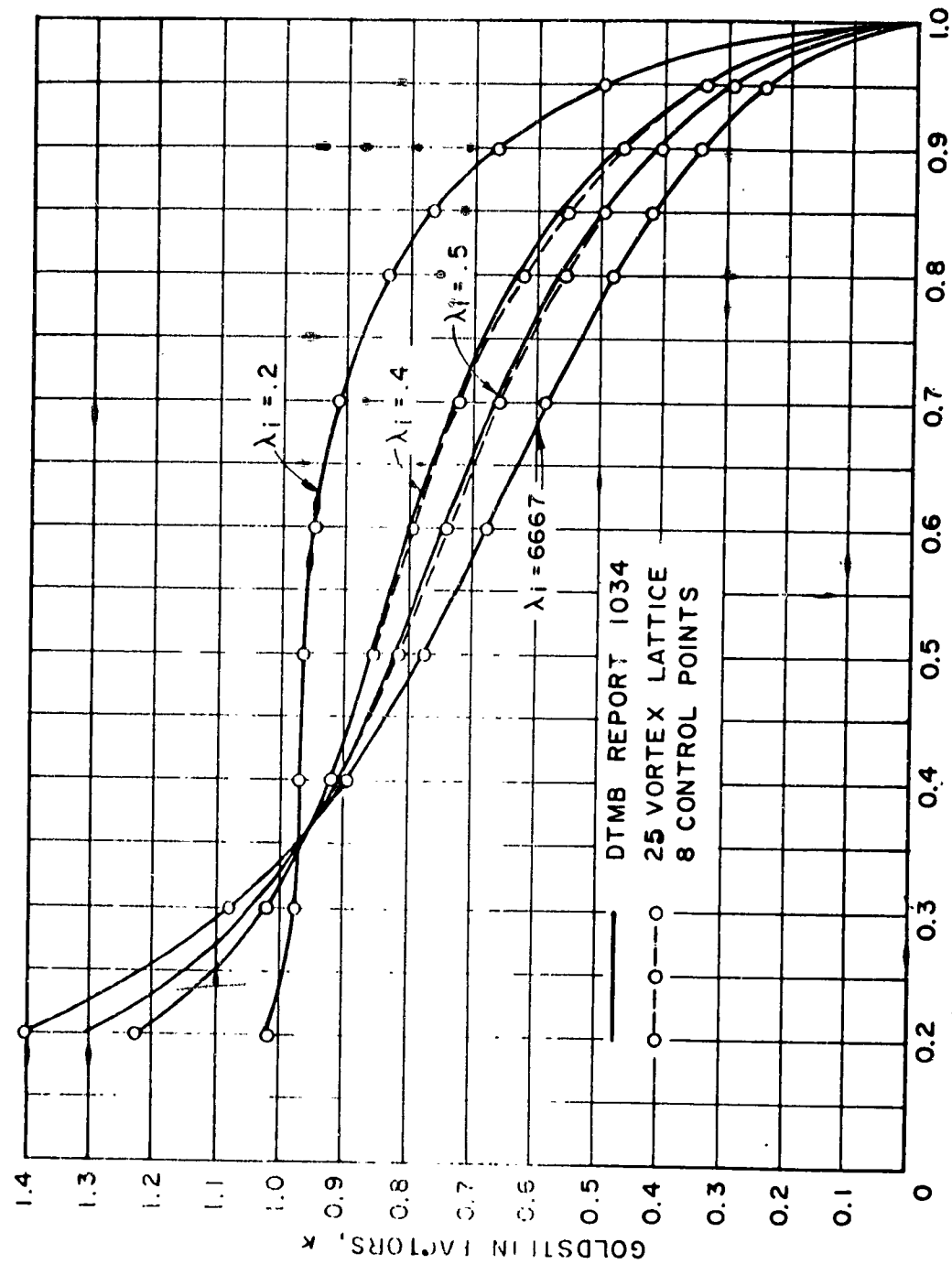


FIG. 4.4 GOLDSTEIN FACTORS 3 BLADED PROPELLER ZERO HUB

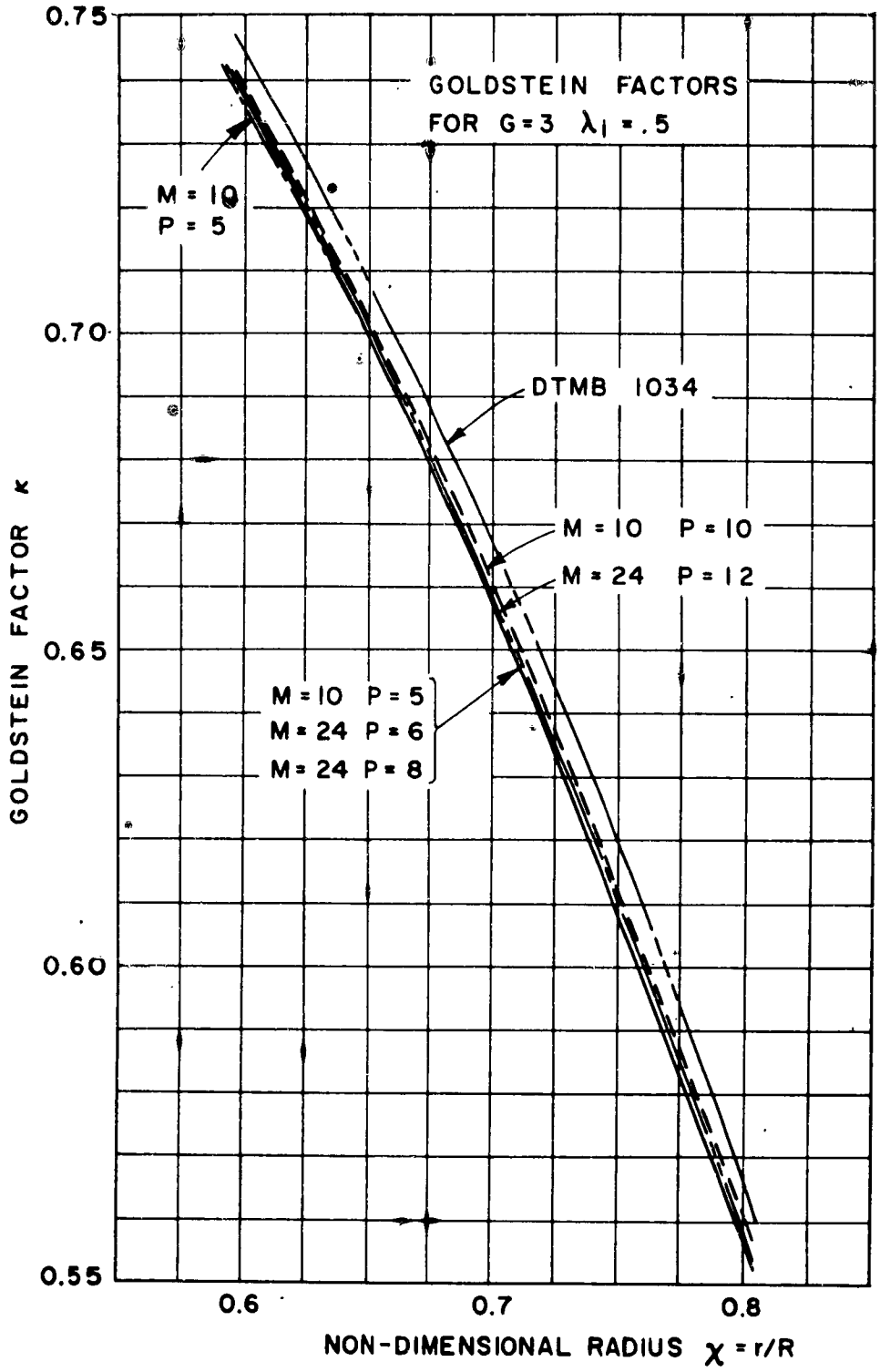


FIG. 4.5 COMPARISON OF GOLDSTEIN FACTORS OBTAINED BY SEVERAL LATTICE ARRANGEMENTS WITH VALUES FROM DTMB REPORT 1034

It is evident that the lattice results are in agreement with existing data both for low and high values of $\lambda_i$. In the region where the agreement is not as good, extreme variations in lattice arrangements produce changes of no more than .003, while the basic disagreement with (29) is about .010.

A possible explanation of the discrepancy may lie in the method of computation of the Goldstein Factors in (29). The solution of the potential problem involves the solution of an infinite system of linear equations relating the coefficients in the series expansions of the potential outside and inside the propeller radius. For small values of $\lambda_i$, an approximate solution to the set of equations may be expressed in closed form. For large values of $\lambda_i$, this approximation is not sufficiently accurate, and a more exact solution was developed by Tachmindji and Milam for values of $\lambda_i \geq .667$. For values of $\lambda_i \leq .4$ the approximate coefficients were used, and the range in between from $.4 < \lambda_i < .667$ were obtained by interpolation.

Since the only noticeable disagreement exists in the in-between region, it would seem likely that the lattice values are more accurate in that interval.

As an additional check, calculations were made for 6-bladed propellers where the approximate coefficients were known to be much more accurate than for 3-bladed propellers. The results are shown in Fig. 4.6 for $\lambda_i = .2, .4$, and .667 and it can be seen that the agreement is very satisfactory.

As was mentioned previously in the discussion of the hub boundary condition, Goldstein Factors were calculated for $g = 3$, $\lambda_i = .2$,

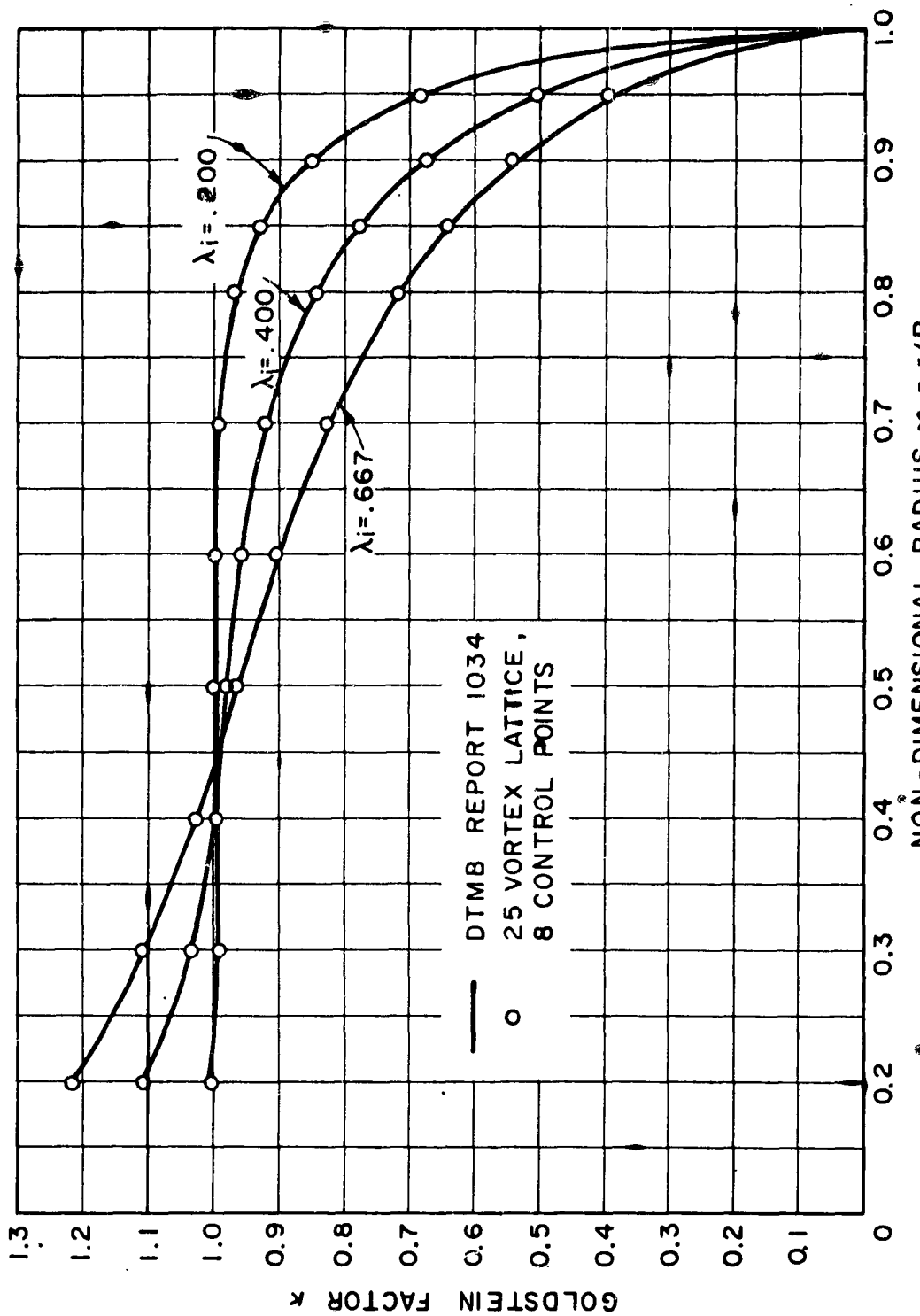


FIG. 4.6 GOLDSTEIN FACTORS 6 BLADED PROPELLER ZERO HUB

and $\chi_h = 0.2$. These are shown in Fig. 4.6 where it can be seen that the consequences of neglecting the boundary condition of zero radial velocity at the hub are not too serious.

Finally, since two-bladed propellers were not included in recent re-calculations of Goldstein Factors, a complete set was obtained by the lattice method and the results appear in Fig. 4.8. Shown on the same plot are some values taken from Lock and Yeatman[38] which seem to be in reasonably good agreement with the new data. These results also seem to agree very closely with results appearing in Goldstein's original paper[6].

Non-Optimum or Wake-Adapted Propellers

The preceding development can be extended very easily to the case where the pitch of the free vortex system is arbitrary, and the axial inflow velocity $V_a$ is a prescribed function of radius. It is assumed that the pitch angle of the free vortex system $\beta_i(r)$ and the geometrical inflow angle $\beta(r) = \tan^{-1}(V_a/\omega r)$ is known and that the non-dimensional circulation G is to be determined. In this case it will be necessary to compute the normal velocity component, since the resultant velocity is not necessarily normal to the free vortex sheets.

In this case the boundary condition may be written as follows.

$$(u_n)_p = \frac{1}{2\chi_p} \sum_{m=1}^{M+1} (\tilde{u}_n)_{mp} \sum_{i=1}^{I} a_i \left(u^*_m \sin i\rho_m - u^*_{m-1} \sin i\rho_{m-1}\right)$$

$$= u^*_p (\cos \beta_i)_p \qquad (4.17)$$

In this case u* is a function of radius

$$u^* = \omega r (\tan \beta_i - \tan \beta) \qquad (4.18)$$

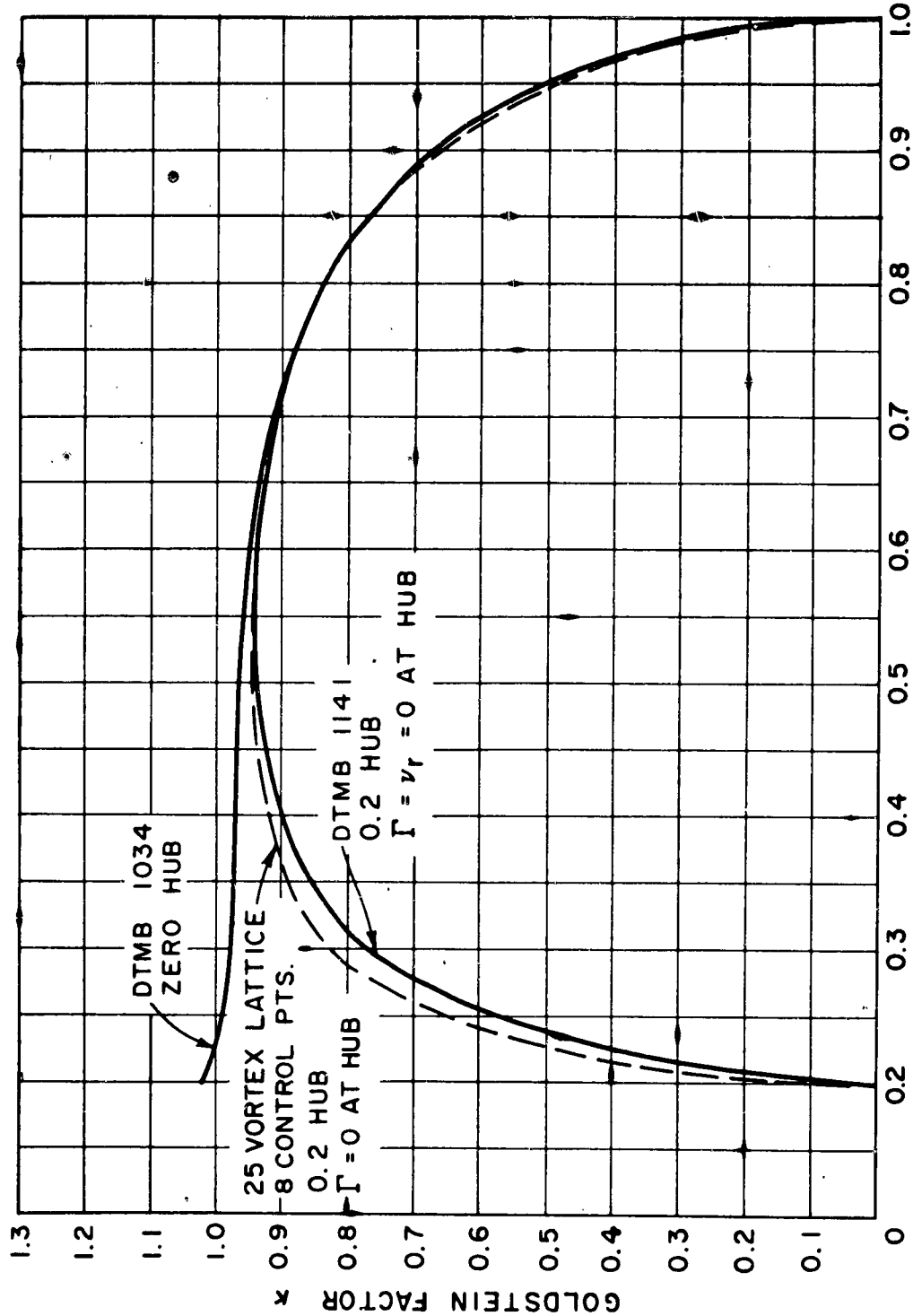


FIG. 4.7 GOLDSTEIN FACTORS 3 BLADED PROPELLER $\lambda_i = .200$

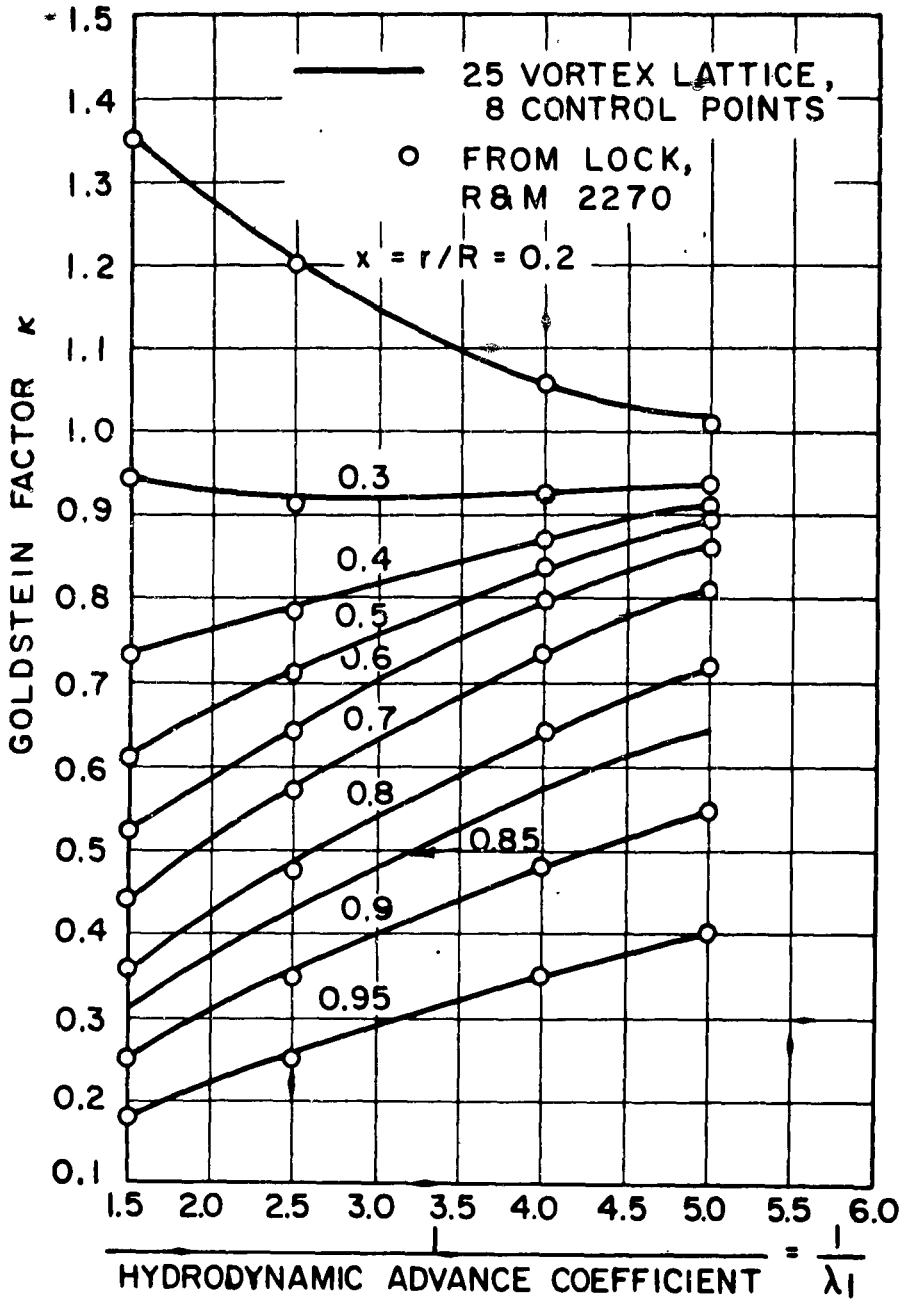


FIG. 4.8 GOLDSTEIN FACTORS
G = 2 BLADES
ZERO HUB

as can be seen from Fig. 4.1. Introducing the ratio

$$\zeta_{mp} = \frac{u^*_m}{u^*_p} = \left[\frac{(\tan \beta_i)_m - (\tan \beta)_m}{(\tan \beta_i)_p - (\tan \beta)_p}\right] \frac{r_m}{r_p} \tag{4.19}$$

into (4.17) gives the result

$$\sum_{i=1}^{I} a_i \sum_{m=1}^{M+1} (\bar{u}_n)_{mp} \left( \zeta_{mp} \sin i \rho_m - \zeta_{m-1,p} \sin i \rho_{m-1} \right)$$

$$= 2\chi_p \cos (\beta_i)_p \tag{4.20}$$

For an optimum propeller in homogeneous flow

$$\zeta_{mp} = 1$$

and $$(\cos \beta_i)_p = \chi_p / \chi_p^2 + \lambda_i^2$$

so that (4.20) reduces in that case to (4.16).

The program prepared for the computation of Goldstein Factors was modified to accept an aribtrary distribution of $\beta$ and $\beta_i$, and the results were found to be in agreement with the standard induction factor method in use at the David Taylor Model Basin[32], except near the hub where the hub boundary conditions are not the same.

# CHAPTER 5
# LIFTING-SURFACE SOLUTIONS FOR BLADES OF ARBITRARY SHAPE

## Introduction

In this chapter we consider the problem of determining the camber and pitch correction for a propeller with a prescribed blade outline, mean line type, and radial load distribution. As indicated in Chapter 1, the pitch and camber corrections are determined by the requirement that the prescribed radial load distribution be obtained with the sections operating at their ideal angle of attack. The chordwise load distribution is unknown initially and will be determined along with the pitch and camber.

The nomenclature used in this chapter is basically the same as in the lifting line case except that an extra dimension must be added due to the chordwise load distribution. As shown in Figures 5.1 and 5.2, an $(x', y', z')$ cartesian coordinate system is fixed on the propeller with the $x'$ axis axial and the $y'$ axis passing through the tip of the index blade. The $z'$ axis completes the right-handed system. A cylindrical system $(x', r', \theta)$ corresponds to the $(x', y', z')$ system with $\theta = 0$ on the $y'$ axis and positive $\theta$ clockwise when looking in the positive $x'$ direction.

A movable cartesian system $(x, y, z)$ and a corresponding cylindrical system $(x, r, \varphi)$ is oriented with the $x$ axis axial and the $y$ axis (or $\varphi = 0$ line) passing through a particular control point on the index blade.

There are $P \times Q$ control points on the index blade where $p = 1, 2, \ldots P$ indicates the radial position and $q = 1, 2, \ldots Q$ indicates the chordwise position. It should be mentioned that all pairs

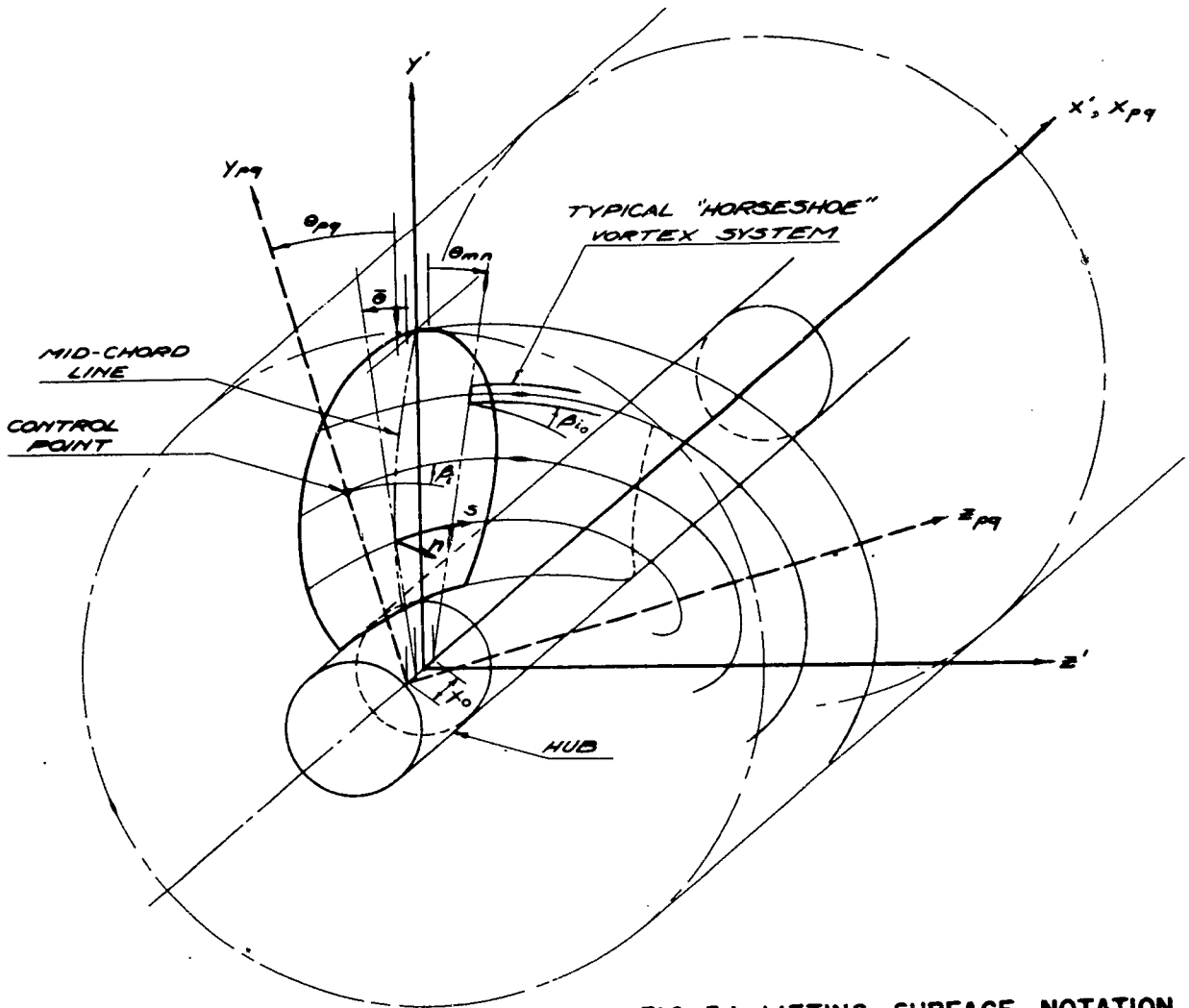


FIG. 5.1 LIFTING SURFACE NOTATION

of coordinates or subscripts referring to radial and chordwise directions are given adjacent alphabetic symbols with the higher symbol (alphabetically) referring to the chordwise direction.

There will be P x Q possible positions for the movable system and the notation $y_{pq}$, for example, means the y axis of the movable system corresponding to the pq'th control point. Following this notation, the quantities $\theta_{pq}$ and $(x_o^*)_{pq}$ are the displacements of the movable system measured from the fixed system.

A non-dimensional radius is defined as $\chi = r/R$ where R is the radius of the propeller. To distinguish the radius of a control point from that of a helical vortex line (on the end of a bound vortex segment) the latter is given a zero subscript. The non-dimensional quantities $\eta = r_o/r$ and $\xi = x/r$ as defined in Chapter 2, will also be used.

Finally, a curvilinear system is defined at any radius by the intersection of an axial cylinder with the reference helical surface. The origin is taken at the mid-chord line of the blade whose angular coordinate in the (x', r', $\theta$) system is $\bar{\theta}$. The s axis is along the helix with the positive direction towards the trailing edge. The n axis is perpendicular to s and lies on the cylindrical surface with positive direction upstream as shown in Fig. 5.2. If the cylindrical surface is expanded and viewed from the propeller axis out towards the tip, a blade section results as shown in Fig. 5.3. The chord length of the expanded section is $\ell(r)$, consequently, $s = -\ell/2$ corresponds to the leading edge and $s = +\ell/2$, the trailing edge. The angle of attack of the section relative to the reference helix is $\alpha$ and the maximum camber measured from the nose-tail line is given the symbol f.

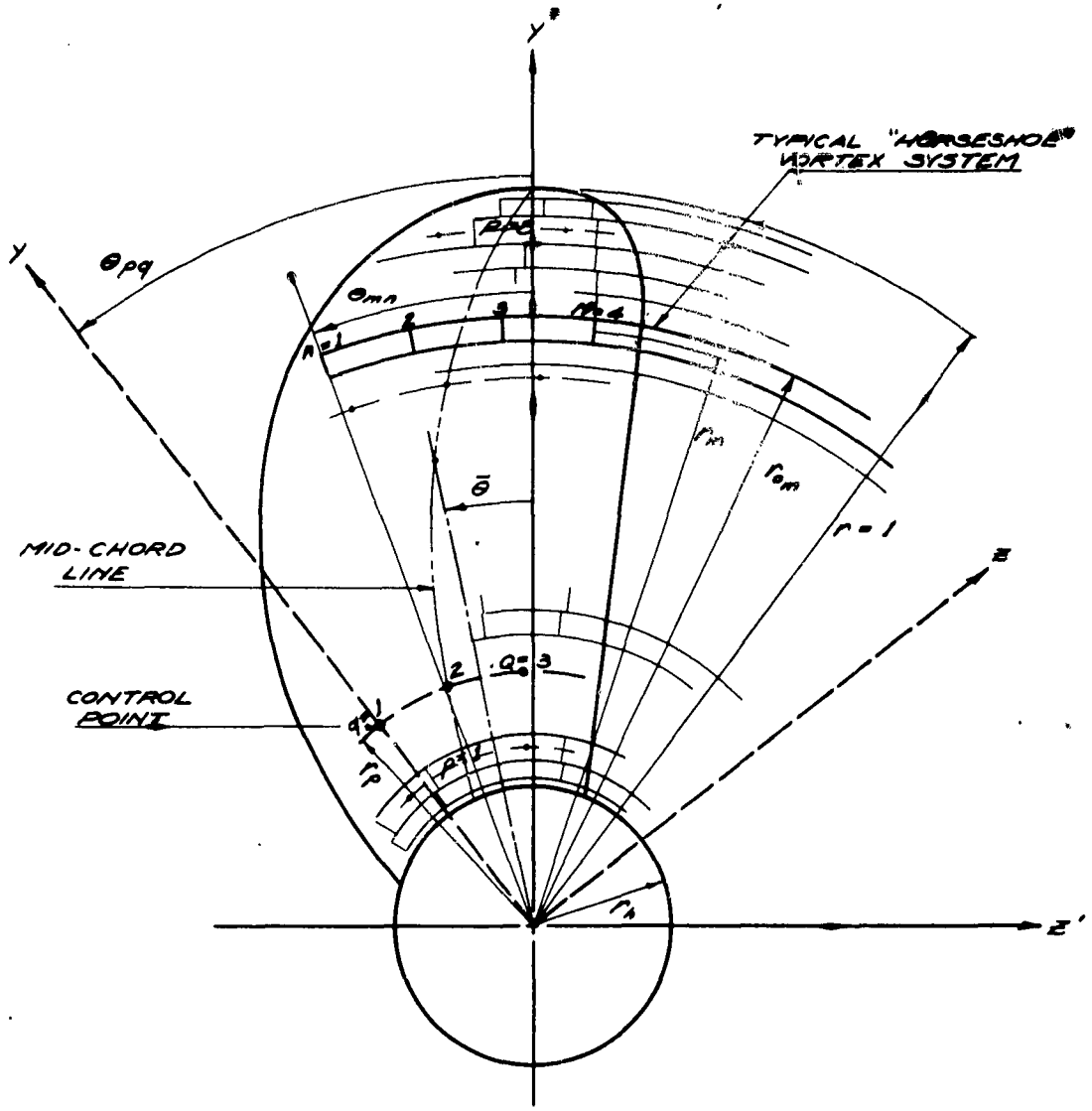


FIG. 5.2 COORDINATE SYSTEMS

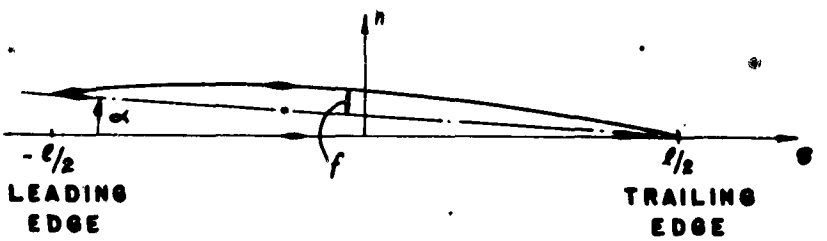


FIG. 5.3 EXPANDED BLADE SECTION

The Reference Helix

As stated in Chapter 1, the blade surface is assumed to be approximately on a helical surface whose pitch at any given radius is determined by the angle of relative flow according to lifting line theory with the same radial load distribution. However, this does not define the surface completely since so far nothing has been said about the relative orientation of the helical lines forming the surface. Since actual propellers may have both rake and skew, an accurate definition of the blade surface is a fairly disagreeable geometrical problem. It is also possible that the effects of some geometrical variations are of the same order as the errors introduced by the basic assumptions, such as the neglect of the deformation of the vortex sheets. Consequently, in the present work it will be assumed that the reference helix passes through the y' axis. If the helix is of constant pitch, any radial line will be contained in the surface, however, this will obviously not be so if the pitch is a function of radius. In the latter case it is further assumed that the bound vortex segments are radial, and that the axial distance between a control point and a vortex element is the same as if the helical surface were of constant pitch corresponding to the pitch at the control point radius. While these simplifying assumptions are not essential to the application of the vortex lattice method, it would seem that a more exact geometrical treatment could not be justified until the effect of the principal variables have been determined.

Bound Vortex Distribution

The bound circulation distributed over the blade surface will be expressed by a trigonometric series in the variables $\rho$ and $\sigma$ which

are related to r and s by

$$r = \frac{1}{2}(R + r_h) - \frac{1}{2}(R - r_h)\cos\rho$$

$$s = -\ell/2 \cos\sigma \qquad (5.1)$$

from which there follows

$$r = r_h \text{ when } \rho = 0,\ r = R \text{ when } \rho = \pi$$

$$s = -\ell/2 \text{ when } \sigma = 0,\quad s = \ell/2 \text{ when } \sigma = \pi \qquad (5.2)$$

The vortex sheet strength $\gamma$ can be converted to a non-dimensional quantity S by dividing by the displacement velocity u* as defined in the preceding chapter. It is assumed that S can be represented by a series of the form

$$S(\rho, \sigma) = \frac{4}{\ell/D}\left[\sum_{i=1}^{I} c_{io} \sin i\rho \cot\frac{\sigma}{2} + \sum_{i=1}^{I}\sum_{j=1}^{J} c_{ij} \sin i\rho \sin j\sigma\right] \qquad (5.3)$$

The second part is a Fourier sine series which has the property that S = 0 along the edge of the blade for any values of the constants $c_{ij}$. The first term goes to zero all along the trailing edge, but tends to infinity at the leading edge. For a fixed value of $\rho$ this is the chordwise circulation distribution of a flat plate at a small angle of attack in two-dimensional flow. According to linearized two-dimensional thin airfoil theory[33] the chordwise circulation distribution of any mean-line can be obtained by superimposing the flat plate distribution and a general distribution which is zero at both the leading and trailing edge. The angle of attack for which the coefficient of the "flat plate" term is zero is called the ideal angle of attack.

The radial circulation distribution is obtained by integrating $\gamma$ over the chord at a particular radius

$$\Gamma(\rho) = \int_0^{\pi} \gamma(\rho,\sigma) \frac{ds}{d\sigma} d\sigma \tag{5.4}$$

or in terms of non-dimensional quantities

$$G(\rho) = \frac{1}{\pi D} \int_0^{\pi} s(\rho, \sigma) \frac{ds}{d\sigma} d\sigma \tag{5.5}$$

where G is the non-dimensional circulation defined in the preceding chapter as

$$G = \frac{\Gamma}{\pi D u^*} \tag{5.6}$$

Substituting (5.3) for s in (5.5) and integrating gives the result*

$$G(\rho) = \sum_{i=1}^{I} (2 c_{io} + c_{i1}) \sin i\rho \tag{5.7}$$

If we now require that a particular radial load distribution $G(\rho)$ is to be obtained in the sections operating at their ideal angle of attack, there follows that $c_{io} = 0$ and that $c_{i1}$ are the known Fourier coefficients of the radial circulation distribution. The remaining coefficients

$$c_{ij} \qquad \begin{bmatrix} i = 1, 2, \ldots. I \\ j = 2, 3, \ldots. J \end{bmatrix}$$

which do not contribute to the radial load distribution are to be determined by the boundary conditions on the blade surface. For later use, it will be convenient to define

$$b_j(\rho) = \sum_{i=1}^{I} c_{ij} \sin i\rho \tag{5.8}$$

*The details appear in several aerodynamics texts such as "Theory of Wing Sections" (33).

so that (5.3) becomes

$$S(\rho, \sigma) = \frac{4}{\ell/D} \sum_{j=1}^{J} b_j(\rho) \sin j\sigma \qquad (5.9)$$

provided the angle of attack at each radius is ideal.

Vortex Lattice

The continuous bound vortex sheet is to be approximated by a finite number of radial bound vortex segments each with constant strength. At the ends of each segment a free vortex of the same strength must be shed forming a "horseshoe" vortex system as shown in Figs. 5.1 and 5.2. Naturally, parts of the free vortex system originating from bound vortices at the same and immediately adjacent radii coincide. Although this fact will be useful for computational purposes, each horseshoe system will be considered logically to be an independent unit.

The lattice arrangement is obtained by dividing the interval between the hub and blade tip into M equal spaces. Free vortices are shed at radii

$$(r_o)_m = \frac{(R - r_h)(m - 1)}{M} + r_h \qquad (5.10)$$

except at the ends, where they are moved in 1/8 space towards the interior of the blade (as in the lifting line case). There are N radial vortex elements between any two adjacent values of $r_o$. These will be centered at

$$r_m = \frac{1}{2}\left[(r_o)_m + (r_o)_{m+1}\right] \qquad (5.11)$$

and will be located by dividing the chord length at $r_m$ into N equal panels with the bound vortex at the mid-point of each panel. The

chordwise position relative to the mid-chord line is given by

$$s_{mn} = \frac{\ell_m}{2N} ( 2n - N - 1) \tag{5.12}$$

and the angular coordinate measured clockwise from the y' axis is

$$\theta_{mn} = \bar{\theta}_m + \frac{\ell_m}{ND} \frac{(\cos \beta_1)_m}{\chi_m} (2n - N - 1) \tag{5.13}$$

Control points are located at the midpoints of the panels formed by the horseshoe elements. In general, there will be many more horseshoe elements than control points, and it is completely arbitrary which of the possible control point arrangements are to be used. However, to simplify the computations somewhat, it will be assumed that the chordwise arrangement of control points will be the same at each radial position used. The number of chordwise control points is given by the expression

$$Q = \frac{N - 2 + \zeta_1 - \zeta_2}{\zeta_1} \tag{5.14}$$

where $\zeta_1$ is the number of radial vortex elements between each control point and $\zeta_2$ is the number of unused control point positions between the leading edge and the first control point. If (5.14) is a fraction, only the integer part is to be retained. Fig. (5.4) shows a number of chordwise lattice arrangements corresponding to various values of N, $\zeta_1$ and $\zeta_2$. The control point angles are then given by

$$\theta_{pq} = \bar{\theta}_p + \frac{\ell_p (\cos \beta_1)_p}{ND \chi_p} \left[ 2\{\zeta_1 (q - 1) + \zeta_2 + 1\} - N \right] \tag{5.15}$$

There are a total of P radial positions used, and are subject only to the restriction that $P \leq M$. The total number of control points is P x Q.

Relating Continuous and Lattice Distributions

Let $G_{mn}$ be the non-dimensional strength of the bound vortex located at $\theta_{mn}$ and centered at $r_m$. The strengths of the individual

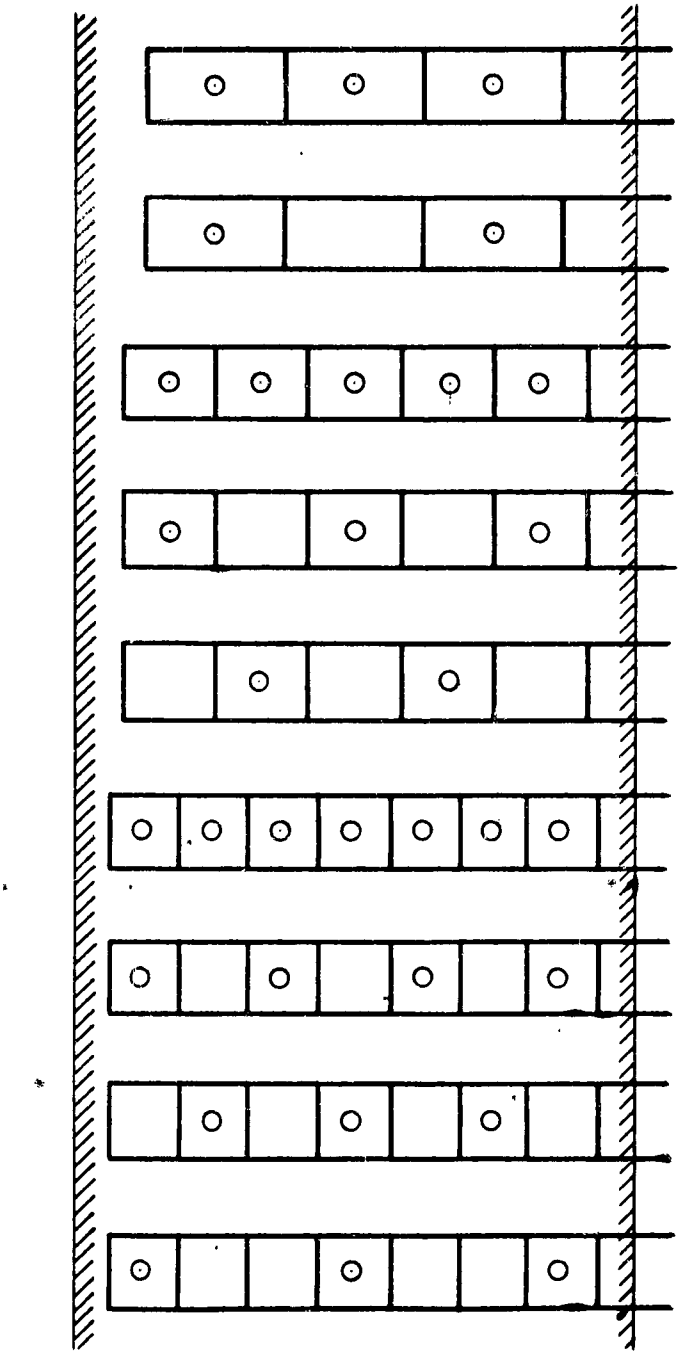


| N | Q | $y_1$ | $y_2$ |
|---|---|---|---|
| 4 | 3 | 1 | 0 |
| 4 | 2 | 2 | 0 |
| 6 | 5 | 1 | 0 |
| 6 | 3 | 2 | 0 |
| 6 | 2 | 2 | 1 |
| 8 | 7 | 1 | 0 |
| 8 | 4 | 2 | 0 |
| 8 | 3 | 2 | 1 |
| 8 | 3 | 3 | 0 |

FIG 5.4 EXAMPLES OF CHORDWISE LATTICE ARRANGEMENTS

elements are first of all subject to the requirement that the radial load distribution be the same as in the continuous case

$$\sum_{n=1}^{N} G_{mn} = [\text{illegible}] \quad (b_1)_m \tag{5.16}$$

The remaining N - 1 requirements will be that the lattice and continuous distributions induce the same velocity at each of the N - 1 possible control point positions in 2-dimensional flow. From thin-airfoil theory the non-dimensional velocity induced at the q'th control point by the N vortices at a particular radius $r_m$ is

$$\frac{(u_n)_{mq}}{u^*} = \frac{ND}{\ell_m} \sum_{n=1}^{N} \frac{G_{mn}}{2(n-q)-1} \tag{5.17}$$

where $u_n$ is the dimensional velocity normal to the vortex sheet. The velocity induced at the same point by the continuous distribution can be shown to be

$$\frac{(u_n)_{mq}}{u^*} = \frac{2D}{\ell_m} \sum_{j=0}^{J} b_j \cos(j+1)\sigma_q$$

$$\text{where } \sigma_q = \cos^{-1}\left[\frac{N-2q}{N}\right] \quad 0 \le \sigma_q \le \pi \tag{5.18}$$

Equating (5.16) and (5.17) for each value of q the following equation is obtained

$$\sum_{n=1}^{N} \frac{G_{mn}}{2(n-q)-1} = \frac{2}{N} \sum_{j=0}^{J} b_j \cos(j+1)\sigma_q$$

$$q = 1, 2, \ldots N-1 \tag{5.19}$$

which combined with (5.16) results in a set of N linear equations for the unknown $G_{mn}$.

Let the solution of this set of equations be expressed in the form:

$$G_{mn} = \sum_{j=1}^{J} \mu_{nj}\, b_{jm} \tag{5.20}$$

The chord load factors $\mu_{nj}$ are constants which can be computed once and for all. Values of $\mu$ are given by Falkner[17] and by Van Dorn and deYoung[34]. The latter values are slightly different, the authors stating that the former values are incorrect. However, on re-calculating the chord load factors, it would appear that Falkner's original values are correct. Values of $\mu_{nj}$ correct to 6 decimal places, were re-computed for N = 2, 4, 6, 8 and J = 0, 1, 2, .... N-1 using an IBM 650 and these results appear in Appendix ( C).

Velocity Induced by the Lattice in 3-Dimensional Flow

Let $\bar{u}_{mnpq}$ be the normal component of the non-dimensional velocity induced by the complete horseshoe system $G_{mn}$ at the control point at $r_p$, $\theta_{pq}$. The subscript n for "normal" will be omitted in this section since only the normal component will be considered. As in Chapter 2, $\bar{u}$ is related to the dimensional velocity u by

$$\bar{u}_{mnpq} = \frac{u_{mnpq}\, 4\pi\, r_p}{\Gamma_{mn}} \tag{5.21}$$

which can also be expressed in terms of the non-dimensional circulation

$$\bar{u}_{mnpq} = \frac{u_{mnpq}\, 2\, \chi_p}{u^*\, G_{mn}} \tag{5.22}$$

This velocity can be computed by a procedure which is outlined in Appendix ( A) using the results of Chapters 2 and 3.

Determining the Camber and Angle of Attack

As was mentioned previously, it is assumed that the blade surface is to be formed such that its expanded sections may all be derived from a single mean-line by suitably selecting the camber/length ratio $f/\ell$ and angle of attack $\alpha$ at each radius. The angle of attack is to be measured from the induced inflow angle $\beta_i$ determined from lifting line theory. It is also assumed that the magnitude of the resultant inflow velocity is the same as in the lifting line case, namely, V*. The value of $f/\ell$ and $\alpha$ at each radius are determined by the boundary condition that the flow be tangent to the mean line at each control point. The slope of the mean line relative to $\beta_i$ at a particular chordwise station is

$$\alpha_p - h_q (f/\ell)_p \tag{5.23}$$

where $h_q$ is the slope of the mean line with unit camber ratio. As can be seen from Fig. 5.5, the boundary condition can be written

$$\alpha_p - h_q (f/\ell)_p = \frac{-1}{V_p^*} \left[ \sum_{m=1}^{M} \sum_{n=1}^{N} u_{mnpq} \right] - (\beta_i - \beta)_p \tag{5.24}$$

assuming that the induced angles are small. Introducing (5.22) and noting that $\beta_i - \beta \approx u^* \cos \beta_i / V^*$, there follows

$$\alpha_p - h_q (f/\ell)_p = \frac{-1}{V_p^*} \left[ u_p^* (\cos \beta_i)_p + \frac{1}{2 \pi_p} \sum_{m=1}^{M} u^*_m \sum_{n=1}^{N} \bar{u}_{mnpq} G_{mn} \right] \tag{5.25}$$

It is now convenient to express $u^*/V^*$ in terms of the lift coefficient

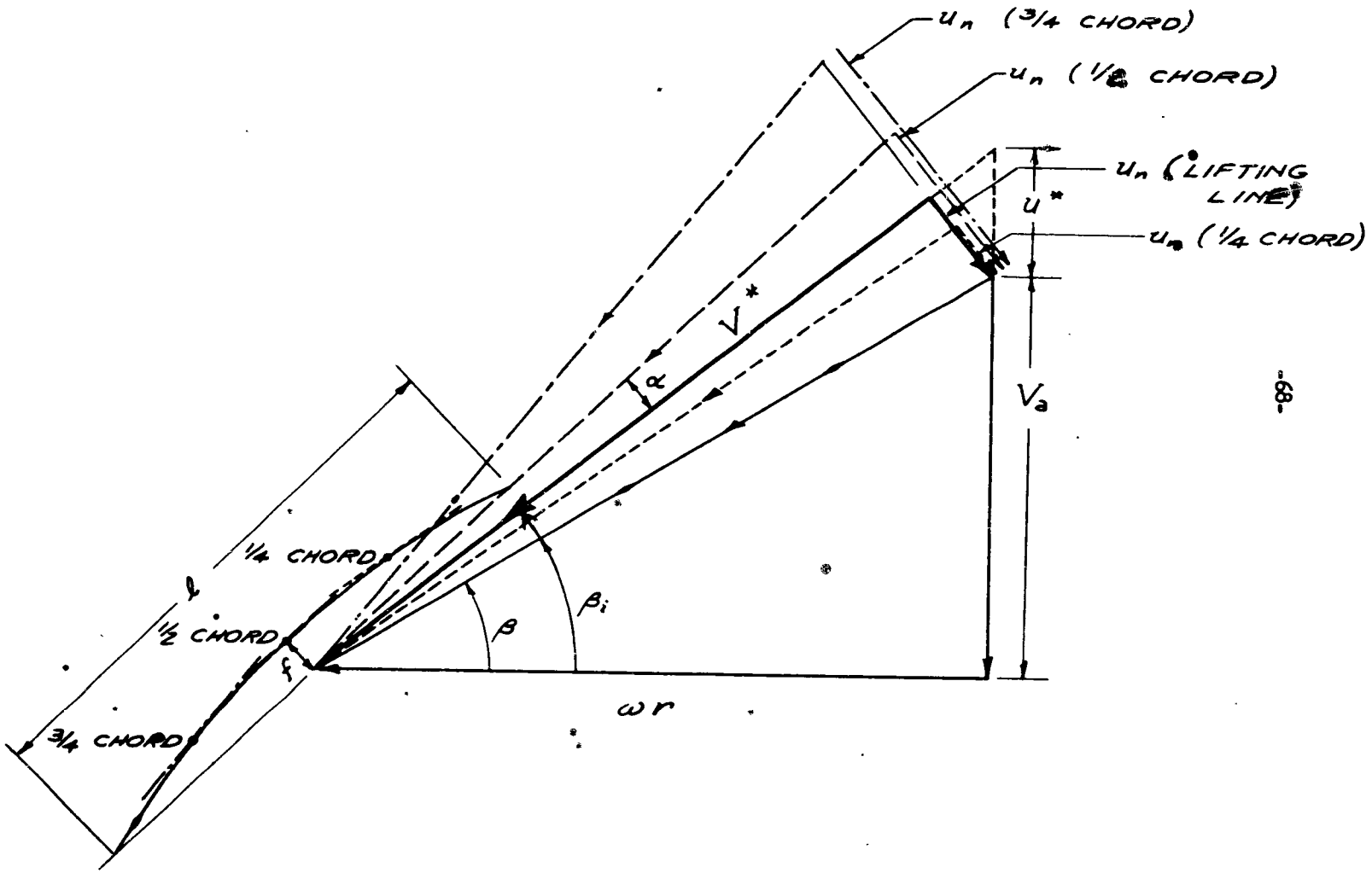


FIG. 5.5 VELOCITY DIAGRAM AT 3 CONTROL POINTS

of the section. From Kutta-Joukowski's law[19]

$$dL = \rho V^* \Gamma \, dr \tag{5.26}$$

where dL is the lift force acting on an element of bound vortex of radius dr and $\rho$ is the fluid mass density*. The lift coefficient is

$$C_L = \frac{dL}{\frac{1}{2}\rho V^{*2} \ell dr} = \frac{2\Gamma}{\ell V^*} = \left(\frac{2\pi G}{\ell/D}\right)\left(\frac{u^*}{V^*}\right) \tag{5.27}$$

Replacing G by $b_{s_i}$ in (5.27) and combining with (5.25) and (5.20), there follows

$$\frac{\alpha_p}{C_L} - h_q \frac{(f/\ell)_p}{C_L} = \frac{-(\ell/D)_p}{2\pi (b_o)_p}\left[(\cos \beta_i)_p + \frac{1}{2 \chi_p} \sum_{m=1}^{M} \zeta_{mp} \sum_{n=1}^{M} \bar{u}_{mnpq} \sum_{j=1}^{J} \mu_{nj} \, b_{jm}\right] \tag{5.28}$$

where $\zeta_{mp}$ is a factor which takes into account that u* may be a function of radius and is defined by

$$\zeta_{mp} = \frac{u^*_m}{u^*_p} = \frac{(\tan \beta_i)_m - (\tan \beta)_m}{(\tan \beta_i)_p - (\tan \beta)_p} \qquad \left[\frac{r_m}{r_p}\right] \tag{5.29}$$

For optimum, open water propellers, u* is independent of radius so that $\zeta_{mp} = 1$ and may be omitted in (5.28).

The quantities on the left in (5.28) are the angle of attack and camber ratio per unit lift coefficient and are given the symbols

$$\bar{\alpha} = \alpha/C_L \qquad \bar{f} = (f/\ell)/C_L \tag{5.30}$$

In two-dimensional flow, these are constants which depend only on the type of mean line. The ratio of the camber required in three-dimensional

*In all equations except (5.26) and (5.27) the symbol $\rho$ is the transformed radial coordinate.

to that required for an equal lift coefficient in two-dimensional flow is the camber correction factor as defined in current propeller design methods (3), (5). However, a similar definition cannot be used for the pitch correction since the ideal angle of attack of many mean lines in two-dimensional flow is zero.

Equation (5.28) written for each control point represents a set of linear equations for $\bar{\alpha}$, $\bar{f}$ and the coefficients of the non-lift-producing part of the circulation distribution. Rearranging (5.28) to put the unknowns on the left and introducing (5.8)

$$\left[\frac{4\pi (b_1)_p \chi_p}{(\ell/D)_p}\right] \bar{\alpha} - \left[\frac{4\pi (b_1)_p \chi_p h_q}{(\ell/D)_p}\right] \bar{f} + \sum_{m=1}^{M} \zeta_{mp} \sum_{n=1}^{N} \bar{u}_{mnpq} \sum_{j=2}^{J} \mu_{nj} \sum_{i=1}^{I} c_{ij} \sin i\rho_m = -2\chi_p (\cos \beta_1)_p - \sum_{m=1}^{M} \zeta_{mp} \sum_{n=1}^{N} \bar{u}_{mnpq} \mu_{n1} \sum_{i=1}^{I} c_{i1} \sin i\rho_m$$

$$p = 1, 2, \ldots P$$

$$q = 1, 2, \ldots Q \qquad (5.31)$$

If the number of radial terms I in the Fourier series for the circulation distribution is equal to the number of radial control point positions P, and if the number of chordwise terms J is one less than Q, the number of unknowns will be

$$2P + I(J - 1) = 2P + P(Q - 2) = PQ \qquad (5.32)$$

which equals the number of equations. The reason that $J = Q - 1$ is that the first term of the series is determined in advance by specifying the radial load distribution. Consequently, there must be at least two chordwise control points in order to determine a pitch and camber correction.

The set of equations represented by (5.31) can be written in matrix notation

$$A_{k\ell} \; X_\ell = B_k$$

where

$$A_{k\ell} = \begin{cases} \dfrac{4\pi (b_1)_p \chi_p}{(\ell/D)_p} & \begin{bmatrix} k = (p-1)Q + q \\ \ell = 2p-1 \end{bmatrix} \\ \dfrac{4\pi (b_1)_p \chi_p h_q}{(\ell/D)_p} & \begin{bmatrix} k = (p-1)Q + q \\ \ell = 2p \end{bmatrix} \\ \sum_{m=1}^{M} \zeta_{mp} \sum_{n=1}^{N} \bar{u}_{mnpq} \mu_{nj} & \begin{bmatrix} k = (p-1)Q + q \\ \ell = 2P + (i-1)(J-1) + j - 1 \end{bmatrix} \end{cases}$$

$$B_k = \left\{ -2\chi_p (\cos \beta_i)_p - \sum_{m=1}^{M} \zeta_{mp} \sum_{n=1}^{N} \bar{u}_{mnpq} \mu_{n1} \sum_{I=1}^{I} c_{i1} \sin i \rho_m \right. \qquad k = (p-1)Q + q$$

$$X_\ell \left\{ \begin{array}{l} \alpha_p \ldots \ell = 2p - 1 \le 2P - 1 \\ \bar{f}_p \ldots \ell = 2p \le 2P \\ c_{ij} \ldots \ell = 2p + (i-1)(J-1) + j - 1 \end{array} \right. \qquad (5.33)$$

# CHAPTER 6

## A LIFTING SURFACE SOLUTION FOR PROPELLERS WITH SYMMETRICAL BLADES

### The Symmetry of the Velocity Field

In the special case when both the blade outline and the mean line are symmetrical about the y' axis, an important simplification results from the symmetry of the integrals determining $\tilde{u}_{mnpq}$. As a result, it can be shown that within the limitations of the assumptions outlined in Chapter 1, a propeller with symmetrical blades has no pitch correction due to lifting surface effect.

First of all, defining $\varphi$ as the angle between a control point and a radial bound vortex or an element of a helical vortex, it is evident that the non-dimensional normal velocity induced by a bound vortex $u_b$ is an odd function of $\varphi$, while the normal velocity induced by an element of helical vortex $\delta u_h$ is an even function of $\varphi$. This can be seen from (3.9) and (3.10) for the bound vortices, since both $\sin\varphi$ and $\xi$ are odd functions of $\varphi$. The fact that $\delta u_h$ is an even function of $\varphi$ can be deduced from (2.10) and (2.11).

We now consider the velocity induced at three symmetrically oriented control points (labeled L, M and R) as sketched in Fig. 6.1. For simplicity, portions of three horseshoe vortex elements are shown and are numbered 1, 2, and 3 with 2 on the y' axis and 1 and 3 symmetrically arranged with respect to the y' axis.

The relative strength of the n'th bound vortex corresponding to the j'th term in the Fourier sine series is given by $\mu_{nj}$ as defined in (5.19). However, it is sufficient to note that $\mu_{nj}$ is an even function of n and $\theta$ when j is odd, and an odd function of n and $\theta$ when j is even.

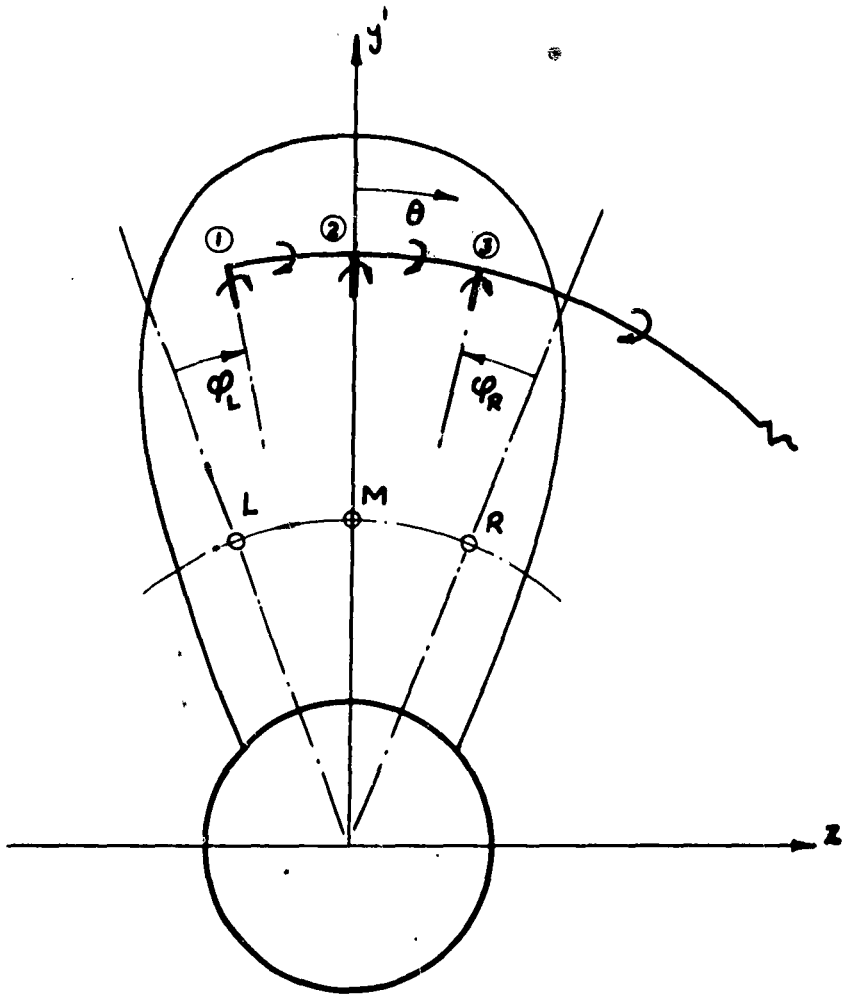


FIG: 6.1 ILLUSTRATION OF SAMPLE CONTROL POINTS & VORTEX LATTICE ELEMENTS ON A SYMMETRICAL BLADE

We first determine the velocities induced at M by the vortices located at 1 and 3 with strengths corresponding to the first term in the Fourier series, which is the only term contributing to the radial load distribution. Since the strengths of 1 and 3 are equal in this case, the velocity induced by the bound vortices cancels, while the two helical vortices starting at 1 and 3 are equivalent to a single vortex of twice the strength starting at 2. Consequently, the velocity at M due to the first term in the series is the same as in lifting line theory. It is also evident that the difference between the velocity according to lifting line theory and the velocity induced at L and R is an odd function of $\theta$. Therefore, as far as the first term in the series is concerned, the mean line should be symmetrical about the mid-chord.

Next consider the even terms in the series, $j = 2, 4, 6 \ldots$ in which case the strengths of 1 and 3 will be equal and opposite. The velocity induced at M by 1 and 3 will be non-zero since the effects of 1 and 3 will add. Furthermore, the velocity induced at L and R will be equal.

Finally, we consider the case when $j = 3, 5, 7 \ldots$ so that 1 and 3 again have equal strengths. Using the same symmetry arguments as in the case of $j = 1$, we conclude that the velocity at M is the same as if 1 and 3 were combined and located at 2, and that the difference between the velocity according to lifting line theory and the velocity induced at L and R is an odd function of $\theta$. However, for $j > 1$ the total strength of the chordwise lattice elements must be zero according to (5.16), so that the induced velocity obtained by combining all the vortex elements at 2 must be zero. Hence, the velocity induced

at M is zero, and the velocities induced at L and R are equal and opposite.

Simplifying the Simultaneous Equations

We next consider the effect of this symmetry on the set of equations given in (5.32). For simplicity it will be assumed that P = 1 and Q = 5, however, the conclusions will be valid in the general case. When written out, the equations would look as follows:

$$a_{11}\,\bar{\alpha} + a_{12}\,\bar{f} + a_{13}\,c_{12} + a_{14}\,c_{13} + a_{15}\,c_{14} = b_1 \qquad (6.1)$$

$$a_{11}\,\bar{\alpha} + a_{22}\,\bar{f} + a_{23}\,c_{12} + a_{24}\,c_{13} + a_{25}\,c_{14} = b_2 \qquad (6.2)$$

$$a_{11}\,\bar{\alpha} + 0 + a_{33}\,c_{12} + 0 + a_{35}\,c_{14} = 0 \qquad (6.3)$$

$$a_{11}\,\bar{\alpha} - a_{22}\,\bar{f} + a_{23}\,c_{12} - a_{24}\,c_{13} + a_{25}\,c_{14} = -b_2 \qquad (6.4)$$

$$a_{11}\,\bar{\alpha} - a_{12}\,\bar{f} + a_{13}\,c_{12} - a_{14}\,c_{13} + a_{15}\,c_{14} = -b_1 \qquad (6.5)$$

where the a's and b's are elements of the A and B matrices respectively as defined in (5.32). The unknowns $\bar{\alpha}$ and $\bar{f}$ are the pitch and camber factors defined in (5.29) and the c's are the unknown coefficients in the circulation distribution defined in (5.3). The symmetry of the coefficients has already been incorporated; for example, $a_{53}$ has been replaced by $a_{13}$.

Eliminating $c_{14}$ between (6.1) and (6.2) as well as between (6.4) and (6.5), a reduced set of equations is obtained

$$d_{11}\,\bar{\alpha} + d_{12}\,\bar{f} + d_{13}\,c_{12} + d_{14}\,c_{13} = e_1 \qquad (6.6)$$

$$a_{11}\,\bar{\alpha} + 0 + a_{33}\,c_{12} + 0 = 0 \qquad (6.7)$$

$$d_{11}\,\bar{\alpha} - d_{12}\,\bar{f} + d_{13}\,c_{12} - d_{14}\,c_{13} = -e_1 \qquad (6.8)$$

where the d's and e's are related to the a's and b's as follows

$$d_{11} = a_{11} - a_{11}\,a_{15}/a_{25}$$

$$e_1 = b_1 - b_2\,a_{15}/a_{25} \qquad (6.9)$$

The unknowns $\bar{\alpha}$, $\bar{f}$ and $d_{14}$ can be eliminated between (6.6), (6.7) and (6.8) to give the following

$$(d_{13} - a_{33}\, d_{11}/a_{11})\, c_{12} = 0 \tag{6.10}$$

from which we conclude that $c_{12}$ must be zero, provided the constant in parentheses is non-zero. However, since the constant is made up of independently variable geometrical inputs, it will not be zero in general.

Consequently, it can be seen from (6.7) that $\bar{\alpha}$ must also be zero, hence, there is no pitch correction. Furthermore, it is evident in this case that (6.6) and (6.8) are redundant.

Equations (6.1) and (6.5) may now be re-written as follows

$$a_{12}\, \bar{f} + a_{14}\, c_{13} + a_{15}\, c_{14} = b_1 \tag{6.11}$$

$$-a_{12}\, \bar{f} - a_{14}\, c_{13} + a_{15}\, c_{14} = -b_1 \tag{6.12}$$

showing that $c_{14} = 0$. Following the same procedure, it can be concluded that $c_{ij}$ must be zero for all even values of j, so that the circulation distribution must be an even function of $\theta$.

By removing all the zero terms and redundant equations from the original equations (6.1) - (6.5), the following equivalent set of equations is obtained

$$\begin{aligned} a_{12}\, \bar{f} + a_{14}\, c_{13} &= b_1 \\ a_{22}\, \bar{f} + a_{24}\, c_{13} &= b_2 \end{aligned} \tag{6.13}$$

which is a fairly drastic simplification.

Modification of Preceding Results for Symmetrical Blades

The development in Chapter 5 will now be modified to take advantage of these results. The continuous vortex sheet strength (5.3) is re-written as follows:

$$S(\rho, \sigma) = \frac{4}{\ell/D} \sum_{i=1}^{I} \sum_{j=1}^{J} c_{ij} \sin i\rho \sin (2j - 1)\sigma \qquad (6.14)$$

which is symmetrical about the mid-chord. Control points will be distributed only over the downstream half of the chord, and in particular cannot be located at the mid-chord, since this will result in A being singular. It is also convenient to define N as the number of chordwise lattice elements on each side of the mid-chord, so that the total number is 2N.

The angular coordinates of the bound vortex elements are given by the expression

$$\theta_{mn} = \frac{\ell_m}{2ND} \frac{(\cos \beta_i)_m}{\chi_m} \qquad (2n - 2N - 1) \qquad (6.15)$$

which replaces (5.13). The number of chordwise control points Q is still given by (5.14) since N has been re-defined. However, the expression for the control point angles (5.15) is now as follows

$$\theta_{pq} = \frac{\ell_p}{ND} \frac{(\cos \beta_i)}{\chi_p} \left[\zeta_1 (q - 1) + \zeta_2 + 1\right] \qquad (6.16)$$

The final set of equations is practically the same as in (5.30), except that the terms containing the pitch correction $\bar{\alpha}$ are no longer present.

$$\frac{4\pi (b_1)_p \chi_p h_q}{(\ell/D)_p} \bar{f} - \sum_{m=1}^{M} \zeta_{mp} \sum_{n=1}^{2N} \bar{u}_{mnpq} \sum_{j=2}^{J} \mu_{nj} \sum_{i=1}^{I} c_{ij} \sin i\rho_m$$

$$= 2\chi_p (\cos \beta_i)_p + \sum_{m=1}^{M} \zeta_{mp} \sum_{n=1}^{2N} \bar{u}_{mnpq} \mu_{n1} \sum_{i=1}^{I} c_{i1} \sin i\rho_m \qquad (6.17)$$

Finally, the location of the matrix elements corresponding to (5.32) is as follows:

$$A_{KL} = \begin{cases} \dfrac{4\pi (b_1)_p \chi_p h_q}{(\ell/D)_p} & \cdots \begin{cases} k = (p-1)Q + q \\ \ell = p \end{cases} \\ -\sum_{m=1}^{M} \zeta_{mp} \sum_{n=1}^{2N} \bar{u}_{mnpq} \mu_{nj} \sin i\rho_m & \cdots \begin{cases} k = (p-1)Q + q \\ \ell = P + (i-1)(J-1) + j-1 \end{cases} \end{cases}$$

$$B_K = 2\chi_p (\cos \beta_i)_p + \sum_{m=1}^{M} \zeta_{mp} \sum_{n=1}^{2N} \bar{u}_{mnpq} \mu_{nj} \sum_{i=1}^{I} c_{il} \sin i\rho_m$$

$$\cdots \quad k = (p-1)Q + q$$

$$X_L \quad \begin{cases} \bar{\Gamma} \cdots \quad \ell = p \le P \\ c_{ij} \cdots \ell = P + (i-1)(J-1) + j-1 \end{cases} \qquad (6.18)$$

There is one important consideration in using the simplified set of equations given in (6.17). In the case of Chapter 5, the pitch angle of the free vortex system $\beta_i$ for a prescribed radial circulation distribution did not have to be given exactly, since small errors in $\beta_i$ could be absorbed in the pitch correction. However, in this case any discrepancy between G and $\beta_i$ will come out as an error in the camber correction, since the assumed symmetry will not actually be present.

A simple way to avoid this difficulty is to obtain the relationship between G and $\beta_i$ by the method discussed in Chapter 4, using precisely the same radial lattice arrangement as in the lifting surface case. This also happens to be convenient since the Fourier coefficients of the circulation distribution $c_{il}$ are obtained directly in the lattice solution of the lifting line problem.

This procedure was incorporated in the computation scheme which is outlined in Appendix ( A ). The resulting camber correction factors are shown in Chapter 7, together with the results for asymmetrical blades using the results of Chapter 5.

# CHAPTER 7

# RESULTS AND CONCLUSIONS

## Analysis of Lifting Surface Results

There are two principal questions which need to be answered in determining the effectiveness of the vortex lattice method. First of all, it is important to determine how fine a lattice spacing is necessary to produce results with the desired accuracy. Obviously, the method would be of little practical value if the required spacing were so small that unreasonably long computation times were needed. In addition, extremely small spacings would require special measures to avoid the loss of significant figures which would also increase the computation time.

The second question is whether the formulation of the lifting-surface problem with the simplifying assumptions introduced in Chapter 1 is an adequate representation of the physical situation.

Considering the first question, the convergence of the lattice approximation in a typical case was studied by computing camber corrections using six different lattice spacings. The characteristics of the propeller and the lattice parameters are given in Table 7.1. The blade outline, in this case, was symmetrical and corresponded to the Troost B-Series (35).

Table 7.1

Data for Test Calculations

Propeller Data

Number of blades, $g = 3$
Expanded Area Ratio $A_E/A_o = 0.65$
Mean line type - Parabolic
Inflow velocity - constant (open water)
Circulation distribution - optimum

Lattice Parameters

| Test | 1 | 2 | 3 | 4 | 5 | 6 |
|---|---|---|---|---|---|---|
| Radial lattice spaces, M | 8 | 8 | 8 | 24 | 24 | 24 |
| Chordwise lattice spaces, 2N | 4 | 6 | 8 | 4 | 6 | 8 |
| Radial control points, P | 3 | 3 | 3 | 4 | 4 | 4 |
| Chordwise control points, Q | 1 | 2 | 3 | 1 | 2 | 3 |
| Computation time (minutes) - IBM 709 | 2 | 3 | 5 | 5 | 11 | 17 |

The initial results of this test were fairly erratic, particularly near the tip of the blade. The reason for this was that too many terms in the Fourier series for the circulation distribution were retained, as can be seen from the following considerations.

The numerical results indicated that the normal velocity component induced by the known part of the circulation distribution

$$\sum_{i=1}^{I} c_{i1} \sin i\rho \sin\sigma \qquad (7.1)$$

was almost a linear function of the chordwise distance s. It was also noted that the induced velocity fields obtained from each of the lattice arrangements were in good agreement, the only noticeable differences occurring with the largest spacing used. Consequently, the erratic results could only be due to the way in which the higher coefficients in the circulation distribution were determined.

Since a parabolic mean line was used in these examples, the higher terms in the Fourier series would be zero if the velocity induced by (7.1) were exactly a linear function of s, at which point the chordwise load distribution would be the same as in two-dimensional flow. However, in this case additional terms are required since the velocity induced by (7.1) is not exactly a linear function of s. These higher terms induce velocity fields which vary more or less simusoidally over the chord. Since the coefficients of these terms are determined only by

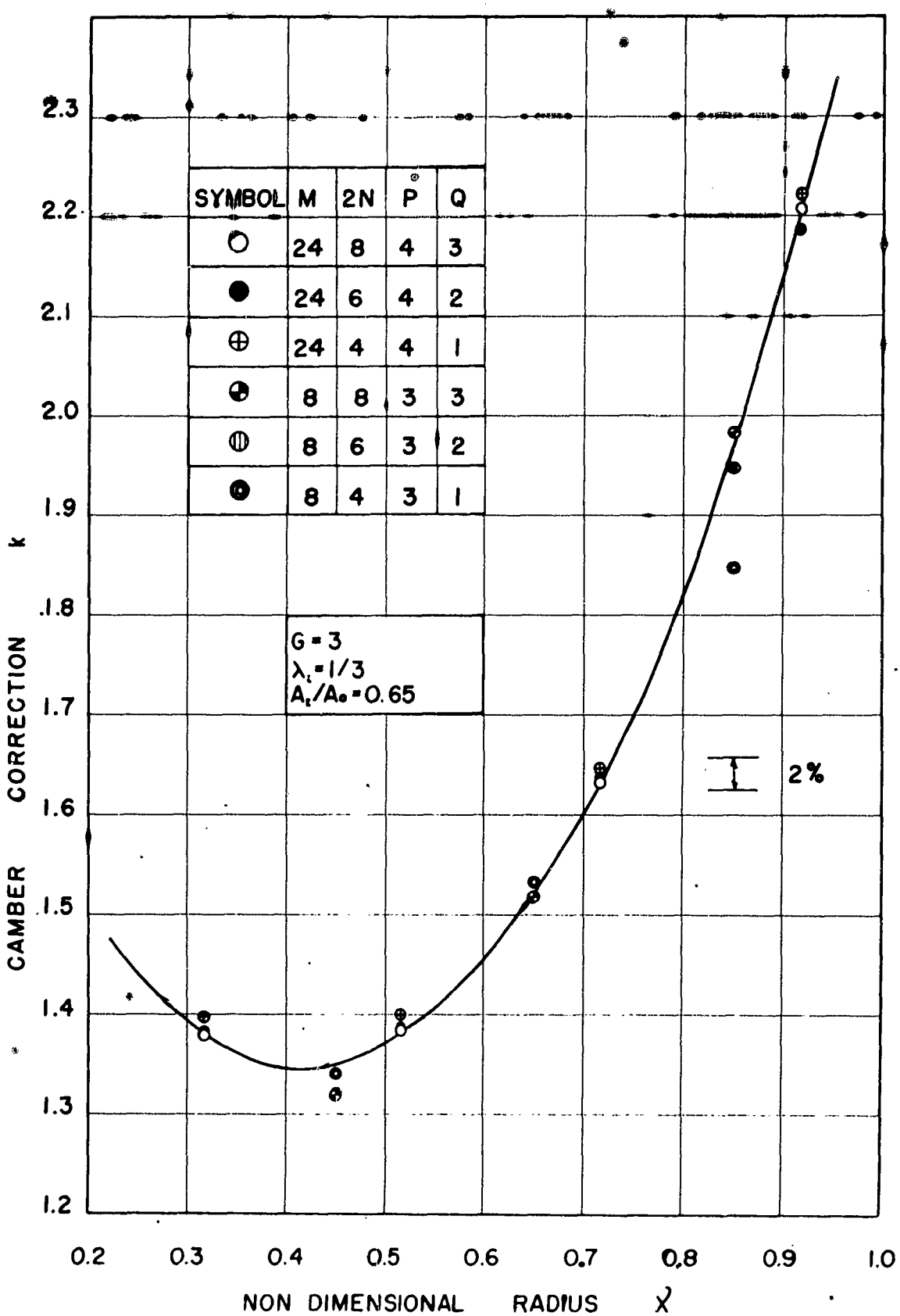


FIG. 7.1 . COMPARISON OF CAMBER CORRECTIONS . OBTAINED WITH SEVERAL DIFFERENT LATTICE ARRANGEMENTS

the boundary conditions at a few distinct points, completely erroneous results are obtained unless a sufficient number of chordwise control points are used. In this case the number was insufficient, so that the higher terms, while satisfying the boundary conditions at the control points, made matters considerably worse everywhere else.

Consequently, in the six test runs listed in Table 7.1, the camber corrections were re-computed simply by deleting all of the terms in the circulation distribution except (7.1), and obtaining the camber from the average value of $\partial u_n/\partial s$ at each radius.

The camber factors obtained in this way are shown in Fig. 7.1. It can be seen that the results obtained from three smallest spacings (24 x 8, 24 x 6, 24 x 4) all agree to within $\pm$ 2%, and that the only large error occurs with the coarsest spacing (8 x 4) at $\chi = 0.85$.

While the characteristics of this propeller are fairly typical, this one set of tests cannot be considered as establishing the convergence of the lattice method under all conditions. However, from these results it is tentatively concluded that the 24 x 8 spacing should give camber corrections which are within $\pm$ 2% of the values which would be obtained from a continuous vortex sheet.

The second question, namely, whether the formulation of the lifting-surface problem with the simplifying assumptions introduced in Chapter 1 is an adequate representation of the physical problem, is something which is very difficult to answer due to the large number of variables involved. While a comparison between theory and experiment might be successful in one or two particular cases, this is no assurance that agreement will exist in general.

Another difficulty results from the fact that existing experimental data include only overall measurements of thrust and torque, so that it is

impossible to determine whether the desired radial load distribution has been obtained. The first successful pressure measurements on a rotating propeller blade were made recently by Auslaender[36] at the David Taylor Model Basin with fairly elaborate instrumentation, however, even these results contain some experimental scatter. Evidently, it is very difficult to locate enough pressure taps on the blade to determine the lift coefficient accurately. The transmission of pressure readings from a rotating shaft also presents a difficult instrumentation problem.

In the present work camber corrections are given for eight propellers showing the effect of a few of the many possible variables. These propellers all have symmetrical B-Series blade outlines and a hub radius of 0.2. The lattice arrangement is the same as in test 6 described previously, i.e., the finest spacing possible with the current program. As in the test runs, the higher terms in the circulation distribution were deleted.

The first six results, shown in Figs. 7.2 - 7.7, are for optimum, open water propellers with parabolic mean lines. These results include a limited number of variations in expanded area ratio $A_E/A_o$, hydrodynamic advance coefficient, $\lambda_1$, and number of blades. Camber corrections given by Van Manen[3] and Eckhardt and Morgan[5] are shown on the same plots for comparis

It is evident that the lattice results have the same general shape as those given by Van Manen, both camber corrections becoming larger near the tip of the blade. The Eckhardt and Morgan results, on the other hand, become more or less constant on the outer regions of the blade. As mentioned in Chapter 1, the latter corrections are derived from Ludwieg and Ginzel results for circulation distributions with reduced loading at the tip. Consequently, the lattice results seem to substantiate the fact that a large camber correction is necessary at the tip in order to achieve an optimum radial load distribution with normal blade shapes. However, this increase near the tip is somewhat less than the results given in Reference (3).

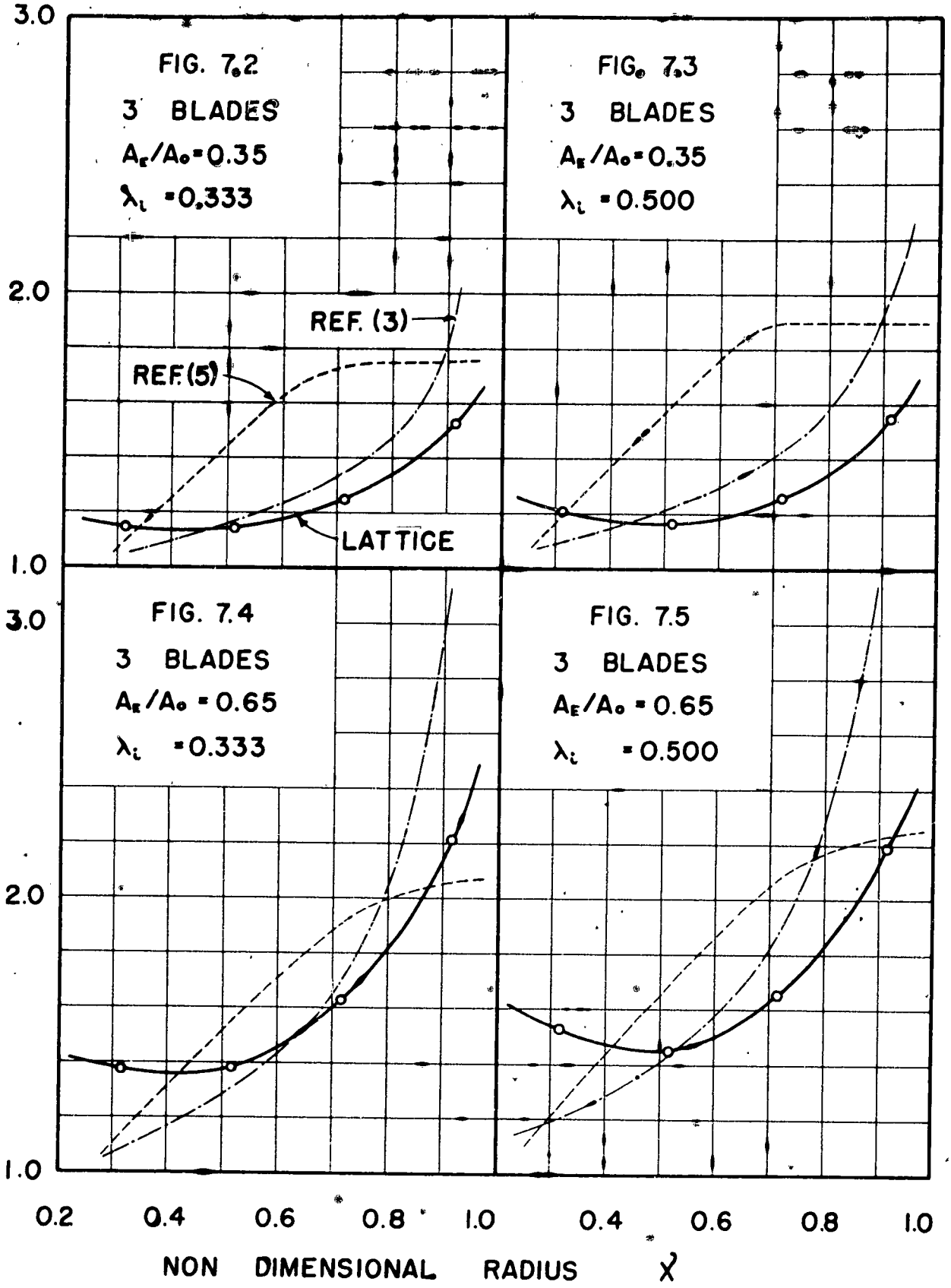


FIGS. 7.2 - 7.5 CAMBER CORRECTION K VS. NON DIMENSIONAL RADIUS $\chi$

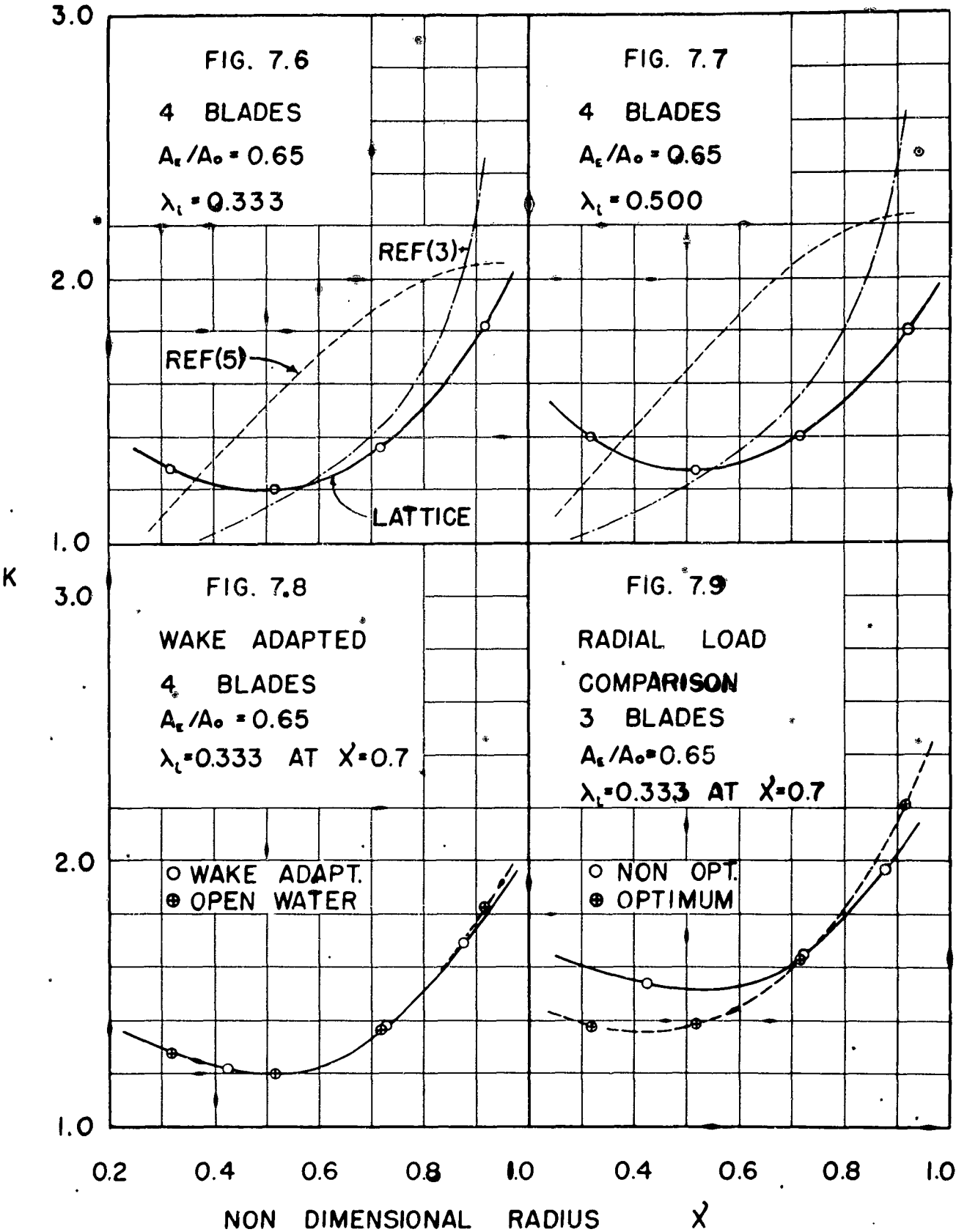


FIGS. 7.6-7.9 CAMBER CORRECTION K VS. NON DIMENSIONAL RADIUS X

Fig. 7.8 shows a comparison of a wake-adapted and an open-water propeller, both having the same advance coefficient at $\chi = 0.7$. The wake distribution is taken from the numerical example given by Hecker[32]. The two results are practically identical. However, the wake variation in this example is fairly small, and the radial load distribution is almost the same as in the open-water case. Consequently, it is possible that more extreme wake variations such as would occur with low speed cargo ships might affect the camber correction.

Finally, the effect of radial load distribution is shown in Fig. 7.9 for two open-water propellers. One propeller has a reduced circulation at the tip, following the pitch distribution recommended by Eckhardt and Morgan[5]. The other is an optimum propeller with the same advance coefficient at $\chi = 0.7$. The results show that a reduction in local propeller loading tends to reduce the camber correction, and vice versa.

The results given in Figs. 7.8 and 7.9 were obtained with a slightly different lattice arrangement consisting of sixteen radial lattice spaces with additional half spaces at the ends. This arrangement was found to give the same results as with twenty-four equal spaces, but with somewhat less computation time.

To test the program for asymmetrical blades, two propellers were run, one with a symmetrical and the other with a skewed blade. All other characteristics were the same. The results showed that the camber corrections for the two propellers were practically identical. However, the propeller with skewed blades required an additional pitch correction of about 2.5 degrees/unit lift coefficient near the tip. While this correction is not very large, it indicates that a pitch correction might be incorporated in the design of propellers with a large amount of skew.

## Conclusions

On the basis of the limited number of numerical results described in the preceding section, it appears that the vortex lattice method is a feasible way of obtaining lifting surface corrections for marine propellers. The method has the advantage that variations in blade shape, wake, and circulation distribution can be taken into account. The numerical examples given illustrate the fact that the latter, which is not taken into account in current design methods, can effect the lifting surface correction.

It is therefore recommended that a systematic series of calculations of camber and pitch corrections be made covering a wide variation in such parameters as number of blades, pitch, blade shape, and radial load distribution. These results may be of use both for design applications, and to determine which parameters cause significant differences in the lifting surface correction.

At the same time, these results will permit an evaluation of the effectiveness of the vortex lattice method by comparison with existing experimental results. However, it would also be desirable to build and test a number of model propellers designed according to these results. These tests, if possible, should include pressure distribution measurements.

However, before this is done, it is recommended that a more accurate treatment of the hub boundary condition be included in the lattice method. As indicated in Chapter 4, the lattice method developed in the present work takes the hub into account in a fairly crude way simply by requiring that the circulation at the hub be zero while neglecting the condition that the radial velocity must be zero. It is believed that the presence of the hub can be taken into account by a discrete source distribution within the hub cylinder. The strength of the source distribution

and the value of the circulation at the hub could be determined by including control points on the hub cylinder in addition to those on the blade surface. This added refinement should not greatly increase the complexity of the computations, and should produce more accurate results in the inner part of the blade.

It is also recommended that the lifting surface programs be modified to accommodate finer lattice spacings with an increase in the number of chordwise control points in order to obtain additional terms in the Fourier Series for the circulation distribution. This would also provide an additional check on the accuracy of the camber corrections obtained with the present programs.

## REFERENCES


(1) Lerbs, H. W., "Moderately Loaded Propellers with a Finite Number of Blades and an Arbitrary Distribution of Circulation", TRANSACTIONS S.N.A.M.E., Vol. 60, 1952, pp 73-117

(2) Lerbs, H. W., "Ergebnisse der Angewandten Theorie des Schiffspropellors", Jahrbuch der Schiffbautechnischen Gesellschaft 49, 1955.

(3) van Manen, J. D., "Fundamentals of Ship Resistance and Propulsion - Part B", Netherlands Ship Model Basin, 1957.

(4) van Manen, J. D., "Wake-Adapted Screw Series Designed by Induction-Factor Method", JOURNAL OF SHIP RESEARCH, Vol. 2, No. 2, October 1958.

(5) Eckhardt, M. K., and Morgan, W. B., "A Propeller Design Method", TRANSACTIONS, S.N.A.M.E., Vol. 63, 1955.

(6) Goldstein, S., "On the Vortex Theory of Screw Propellers", Proceedings of the Royal Society of London, Series A., Vol. 63, 1929.

(7) Lerbs, H. W., "Propeller Pitch Correction Arising From Lifting Surface Effect", D.T.M.B., Washington, D. C., Report #942, 1955.

(8) Ludwieg, H., and Ginzel, I., "On the Theory of Screws With Wide Blades", Aerodynamische Versuchsanstalt, Goettingen, Rep. 44/A/08, 1944.

(9) Ginzel, J. I., "Influence of Blade Shape and of Circulation Distribution on the Camber Correction Factor", Admiralty Research Laboratory, Teddington, Middlesex, Report A.R.L./R2/G/HY/7/1.

(10) Ginzel, J. I., "Theory of the Broad-Bladed Propeller", Admiralty Research Laboratory, Teddington, Middlesex, Report A.R.L./R3/G/HY/7/1, 1952.

(11) van Manen, J. D., and Crowley, J. D., "Some Aspects of Circulation Theory Design of Screw Propellers", INTERNATIONAL SHIPBUILDING PROGRESS Vol. 6, October 1959, No. 62.

(12) Morgan, W. B., "The Design of Counterrotating Propellers Using Lerbs' Theory", TRANSACTIONS, S.N.A.M.E., 1960.

(13) Cox, G. G., "Corrections to the Camber of Constant Pitch Propellers", Quarterly Transactions of the Royal Institution of Naval Architects, January 1961.

(14) Alef, W. E., "An Application of J. Weissinger's 3/4-Point Method to Free Running Ship Screws", Hamburg Model Basin Report No. 1124, 1958.

(15) Sparenberg, J. A., "Application of Lifting Surface Theory to Ship Screws", Proceedings of the Koninkl. Nederl. Akademie van Wetenschappen - Amsterdam, Series B, 62, No. 5, 1959.

(16) Falkner, V. M., "The Calculation of Aerodynamic Loading on Surfaces of any Shape", Aeronautical Research Committee R & M 1910, 1943.

(17) Falkner, V. M., "The Solution of Lifting-Plane Problems by Vortex-Lattice Theory", Aeronautical Research Council, R & M No. 2591, 1947.

(18) Falkner, V. M., "The Scope and Accuracy of Vortex Lattice Theory", Aeronautical Research Council R & M No. 2740, 1952.

(19) Robinson, A., and Laurmann, J. A., "Wing Theory", Cambridge University Press, 1956.

(20) Prandtl, L., and Tietjens, O. G., "Fundamentals of Hydro & Aeromechanics", Dover Publications, Inc., New York, 1957.

(21) Guilloton, R., "Applications de la Courbure Induite aux Calculs des Helices Marines", Association Technique Maritime et Aeronautique, 1955.

(22) Strscheletzky, M., "Hydrodynamische Grundlagen zur Berechnung der Schiffsschrauben", Verlag G. Braun, Karlsruhe, 1950.

(23) Betz, A., "Schraubenpropeller mit geringstem Energieverlust", Kgl. Ges. d. Wies. Nachrichten Math. - phys. Klasse - 1919, Heft 2.

(24) Hildebrand, F. B., "Introduction to Numerical Analysis", McGraw-Hill Book Co., Inc., New York, 1956.

(25) Wrench, J. W., Jr., "The Calculation of Propeller Induction Factors", David Taylor Model Basin, Washington, D. C., Report 1116, 1957.

(26) Morgan, W. B., "Propeller Induction Factors", David Taylor Model Basin, Washington, D. C., Report No. 1183, November 1957.

(27) Kramer, K. N., "The Induced Efficiency of Optimum Propellers Having a Finite Number of Blades", NACA Technical Memorandum No. 884, 1939.

(28) Lock, C. N. H., and Yeatman, D. M., "Tables for Use in an Improved Method of Airscrew Strip Theory Calculation", Admiralty Research Council, R & M No. 1674, 1935.

(29) "The Calculation of Goldstein Factors for Three, Four, Five and Six-Bladed Propellers", David Taylor Model Basin, Washington, D. C., Report No. 1034, 1956.

(30) Tachmindji, A. J., and Milam, A. B., "The Calculation of the Circulation Distribution for Propellers with Finite Hub Having Three, Four, Five, and Six-Blades", David Taylor Model Basin, Washington, D. C., Report No. 1141, 1957.

(31) McCormick, B. W., "The Effect of a Finite Hub on the Optimum Propeller", JOURNAL OF AERONAUTICAL SCIENCE, 1955.

(32) Hecker, R., "Manual for Preparing and Interpreting Data of Propeller Problems Which are Programmed for the High-Speed Computers at the David Taylor Model Basin", David Taylor Model Basin, Washington, D. C., Report No. 1244, 1959.

(33) Abbott, I. H., and Von Doenhoff, A. E., "Theory of Wing Sections", Dover Publications Inc., New York, 1959.

(34) Van Dorn, N. H., and De Young, J., "A Comparison of Three Theoretical Methods of Calculating Span Load Distribution on Swept Wings", NACA Technical Note No. 1476, 1947.

(35) Troost, L., "Open Water Test Series with Modern Propeller Forms", TRANSACTIONS OF NORTHEAST COAST INSTITUTION OF ENGINEERS AND SHIPBUILDERS, Vol. 67, 1952.

(36) Auslaender, J., "Measurement of Pressure Distribution on Blades of Marine Propellers", Proceedings of the American Towing Tank Conference, Berkeley, California, 31 August 1959.

(37) "Reference Manual - 709-7090 Data Processing System", IBM Corporation, 1959

(38) "Reference Manual - 709 Fortran-Automatic Coding System for the IBM 709 Data Processing System", IBM Corporation, 1959.

(39) "Fortran Assembly Program (FAP) for the IBM 709/7090", 709/7090 Data Processing System Bulletin, IBM Corporation, 1960.

(40) Merwin, M. L., and Corbato, F. J., "Description of the Fortran-Fap Monitor System for the 709 Computer", M. I. T. Computation Center Memorandum, CC-160, June 1960.

# APPENDICES

# APPENDIX A

## PROGRAM DESCRIPTIONS

### Introduction

Digital computer programs were prepared to obtain numerical solutions of the following three problems

a) Determine the non-dimensional radial circulation distribution for a lifting-line propeller with a prescribed distribution of $\tan \beta$ and $\tan \beta_i$.

b) Determine the camber and pitch correction for a propeller with an arbitrary blade outline, $\tan \beta$ and $\tan \beta_i$ and mean-line type.

c) Determine the camber correction under the same conditions as (b), but for the special case of a symmetrical blade and a mean-line which is symmetrical about the mid-chord.

A number of other programs were prepared to test various features of the vortex lattice method, however, these are not of sufficient general interest to be reported.

The above programs were prepared for use with the IBM 709 Data Processing System at the M. I. T. Computation Center, and were run using the Fortran Monitor System. The principal source program language was FORTRAN, however, some of the programs were written in FAP in order to perform certain operations not within the scope of the FORTRAN language. Descriptions of these systems appear in References (37), (38), (39), and (40).

Programs (b) and (c) were also modified for use with the IBM 7090 installed at the David Taylor Model Basin, and some of the results shown in Chapter 7 were obtained there.

Each of the three programs consists of a number of specially prepared subroutines as well as standard library routines. In some cases the same subroutine can be used in all three programs.

Brief descriptions of the principal subroutines will be given in the following sections. However, these sections are intended only to indicate the general mode of operation and references to computer language will be avoided. Liastings of the source programs are given in Appendix B

Helical Vortex Integration

The helical vortices are divided into two parts; the part on the blade which extends between the bound vortex elements closest to the leading and trailing edges, and a downstream part which starts at the bound vortex nearest the trailing edge and extends an infinite distance downstream. As indicated in Chapter 2, the velocity induced by the helical vortices on the blade is obtained entirely by numerical integration, while the integration of the downstream helices is performed by numerical integration up to a sufficiently large value of $\varphi$, and the remaining contribution estimated.

It is assumed that the numerical integration can be truncated within the first six revolutions downstream, i.e., $\varphi_t \leq 12\pi$. Consequently, it will be sufficient to divide the interval from the bound vortex nearest the leading edge to a point six revolutions downstream into a sequence of 5-point Gauss ordinates. At each ordinate, the functions $F_n(\varphi_i)$ and the weights $W(\varphi_i)$ defined in (2.19) and (2.21) are to be computed. Each integration may then be performed by computing the constants $c_n$ and $d_n$ defined in (2.18) and applying (2.21).

For the downstream integration it has been found empirically that the angular intervals shown in Table A-1 when subdivided into 5-point Gauss ordinates result in total accumulated integration errors of less than .0005 in the non-dimensional induced velocities defined in (2.10) - (2.12)

## Table A-1 Angular Spacing For Numerical Integration

(In Degrees)

1st Revolution - Coarse Spacing - $.25 \leq |1 - \eta|$

0, 20, 50, 90, 180, 270, 360

1st Revolution - Medium Spacing - $.10 < |1 - \eta| \leq .25$

0, 5, 10, 20, 40, 60, 100, 150, 200, 270, 360

1st Revolution - Fine Spacing - $.02 \leq |1 - \eta| \leq .10$

0, 1, 2, 4, 7, 10, 20, 30, 50, 75, 100, 150, 200, 250, 300, 360

2nd - 6th Revolution - $.02 \leq |1 - \eta|$

120 Degree Spacing

## Table A-2

### Weights and Ordinates for Legendre-Gauss Integration Formulas

| K | Weight, $W_k$ | Ordinate, $X_k$ | |
|---|---|---|---|
| 1 | .118464 | .046910 | 5 point rule |
| 2 | .239314 | .230765 | |
| 3 | .284444 | .500000 | |
| 4 | .239314 | .769235 | |
| 5 | .118464 | .953090 | |
| 1 | .5 | .288675 | 2 point rule |
| 2 | .5 | .711325 | |

The weights and ordinates for an interval of unit length is given in Table A-2.

From these two tables, a set of values of $\varphi_i$ may be obtained. For each $\varphi_i$ there will be seven elements of $F_{ni}$ and one weight $W_i$, so that there will be a total of forty numbers associated with each five-point Gauss interval. The total downstream integration table consists of 1,840 elements.

The portion of the helical vortex on the blade is subdivided into a number of elements lying between bound vortex elements. These, together with the six downstream revolutions, are shown schematically in Fig. A.1. The maximum number of chordwise bound vortex elements is assumed to be eight, so that a total of fifteen intervals on the blade is possible.

The angular intervals on the blade depend on the geometry of the blade and will in general be different at each radius. Consequently, it is impossible to subdivide these intervals into a fixed number of Gauss ordinates. In this case, the minimum number of Gauss intervals is determined such that the spacing will not exceed the initial spacing necessary for the downstream integration for each of the three ranges of $|1 - \eta|$ . Since it is possible that many of the intervals on the blade will be very small (such as 11 and 13 in Fig. A-1), provision is made for using a 2-point Gauss Rule if the interval is less than 40% of one 5-point Gauss interval. Finally, if the interval is less than .5% of a 5-point interval, the integral is approximated by its mean value.

It is obvious from geometrical considerations that the parameter $|1 - \eta|$ used in selecting the integration spacing is applicable only to the index blade. It has been found that the integration of the helices

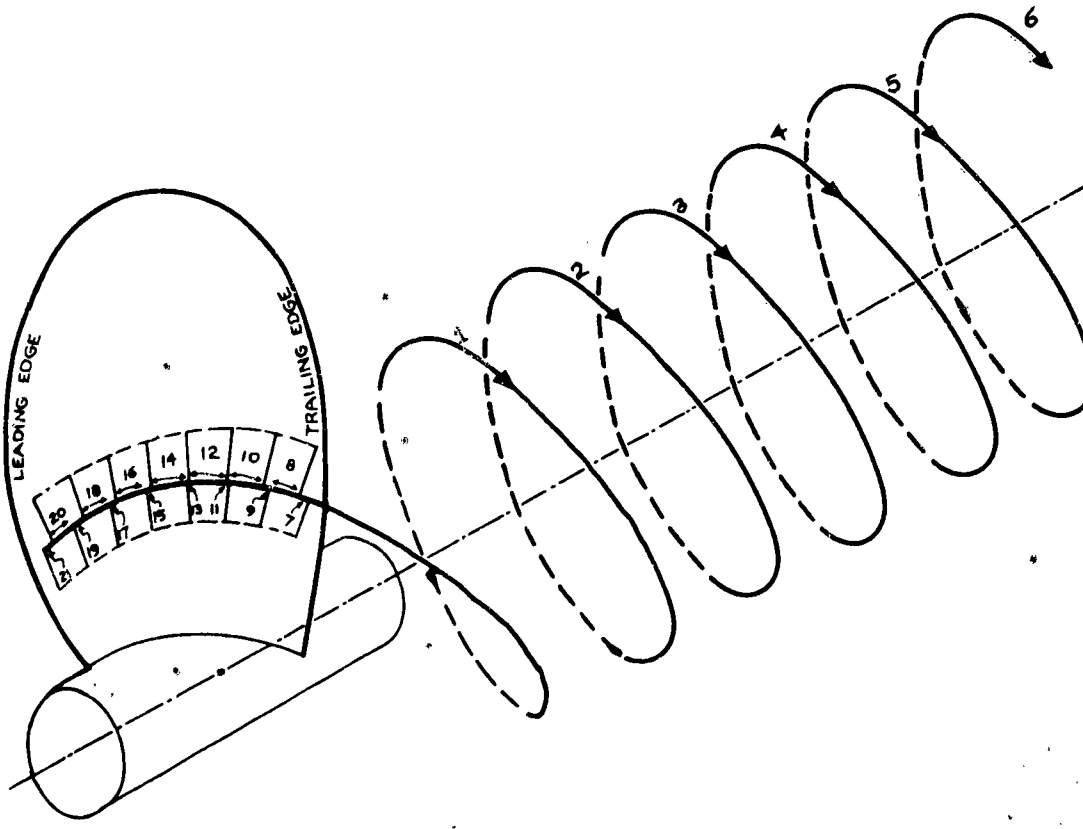


FIG. A.1 SKETCH SHOWING MAXIMUM OF 21 HELICAL INTEGRATION INTERVALS

on the other blades may be done with the coarse spacing for all values of $|1 - \eta|$ without altering the final result.

The integration of the helical vortices requires three subroutines. The downstream integration table is generated by a subroutine called HUMBUG, and this needs to be called only once at the beginning of each run. The instruction CALL HUMBUG (P, L) causes the 1840 elements of the table to be computed and stored in increasing memory locations starting at P. Location L is the first element of an "address directory" which requires sixty-three storage locations in decreasing numerical order starting at L. The "Address directory" is a (21 x 3) array corresponding to the twenty-one possible integration intervals shown in Fig. A-1 and the three possible spacings. Each element of the array contains the starting address of the integration table for that interval as well as the number of angles $\varphi_i$ in the interval. Subroutine HUMBUG fills in only the first (6 x 3) elements, which correspond to the downstream part of the integration.

Subroutine LIST does more or less the same thing for the intervals on the blade. The calling sequence is

CALL LIST (NSPACE, ANGLES, L)

where NSPACE is the number of spaces on the blade (which cannot exceed 15), ANGLES is the first element of a list of angles defining the limits of each interval, and L is the "address directory" which is the same as in the calling sequence for HUMBUG. The list of angles starts at the bound vortex element nearest the leading edge, and is stored in decreasing memory locations. These are all angles in radians relative to the angle of the trailing edge element, and will consequently all be $\leq 0$. Subroutine LIST determines the number of integration spaces in each interval, computes the functions $F_{ni}$ and $W_i$ and stores them immediately following the functions

generated by NUMBUG and completes the sixty-three element address directory. If the function table being generated begins to exceed the size of core storage, an error stop results. This subroutine is called once at each lattice radius.

The actual integration is performed in subroutine HELIX which is called as follows:

CALL HELIX (ETA, TANBIO, TANBI, COSBI, PHIZ, NG, NSPACE, L, UN)

where the following arguments are as defined in Chapter 2:

ETA = $\eta$ TANBIO = $\tan \beta_{io}$ TANBI = $\tan \beta_i$

COSBI = $\cos \beta_i$ PHIZ = $\varphi_o$ NG = g UN = $\bar{u}_n$

The arguments NSPACE and L are the same as in LIST. The angle $\varphi_o$ is measured from the particular control point to the start of the downstream helix, in accordance with the notation of Fig. 2.1. The symbol UN denotes the first of a sixteen-element array stored in decreasing memory locations.

HELIX starts by computing the constants $c_n$ and $d_n$. The integration is then performed according to (2.21) using the "address directory" to locate the pre-computed functions and to determine the number of points in each interval. The first downstream interval, designated by 1 in Fig. A-1 is computed first. If $|1 - \eta| > .25$ all g blades are integrated simultaneously. If $|1 - \eta| \leq .25$ all but the index blade are integrated using the coarse spacing, and the index blade is then computed using the medium or fine spacing. After each downstream revolution has been completed, the integral to infinity is estimated from the relation

$$\delta\bar{u}_n \approx \frac{g \cos \beta_i \, (\tan \beta_{io} \tan \beta - \eta)}{2 \varphi_b^2 \eta^2 \tan^3 \beta_{io}} \qquad (A.1)$$

which is obtained from (2.35), (2.36) and (2.23). When two successive estimates agree to within .0005, the downstream integral is assumed to have converged. If the number of spaces on the blade is zero, as would be the case in lifting line theory, the integration is complete. Otherwise the interval closest to the trailing edge, designated by 7 in Fig. A-1 is integrated using the functions computed by LIST. This process is repeated for all the remaining intervals up to the bound vortex nearest to the leading edge. The result of the preceding interval is added to each new interval, so that the result is a table of the integral from $(ANGLE)_n$ to $\infty$. This is stored in decreasing memory locations starting at UN. The first element of UN contains the value of the integral from the leading edge bound vortex to infinity.

The time required to perform the helical integration depends on the pitch angle and the number of blades. For a three-bladed propeller, the downstream integration takes roughly 1 - 1.5 seconds on an IBM 709. The integration on the blade is much faster, and a typical average time including both downstream and on-blade intervals is 0.25 seconds per interval for a three-bladed propeller. This includes a prorated amount of the time spent in the data-generating subroutines HUMBUG and LIST. A six-bladed propeller would take a little less than twice as long. Listings of HUMBUG, LIST AND HELIX appear in Appendix B.

General Lifting Line Program

This program forms and solves the set of equations given in (4.20), using the helical integration subroutines previously described. The input data consists of a list of nine values of the non-dimensional radius $\chi$, with corresponding values of tan $\beta_i$ and tan $\beta$. The remaining

data consists of the number of blades, g, the number of lattice spaces M, the number of control points P and a list of the values of M containing control points. If the pitch of the free vortex system is constant, the first element in the list of tan $\beta_i$ may be replaced with the advance coefficient $\lambda_i$, and the remaining elements of tan $\beta_i$ and tan $\beta$ left blank. The result in either case is a table of the non-dimensional circulation G defined in (4.2) as well as the Fourier coefficients of G. In addition, if tan $\beta \neq 0$, the circulation is also expressed in the form

$$G' = \frac{\Gamma}{2\pi R V_a} = G\left[\frac{\tan \beta_i}{\tan \beta} - 1\right] \qquad (A.2)$$

in accordance with the definitions in (1) and (5). If $\lambda_i$ is given, the propeller is assumed to be optimum and the Goldstein factors $\kappa$ are computed from (4.14).

Since the input data is not necessarily at the same set of radii as required for the lattice, the required values of tan $\beta_i$ and tan $\beta$ are obtained by three-point Lagrangian interpolation. In addition, since the conversion from the actual radius r to the transformed radius $\rho$ according to (4.3) occurs very frequently in both the lifting line and lifting surface programs, the transformation is performed in a subroutine called MAP. Finally, the printed output from this program is controlled by a subroutine called WAITER.

The computation time in minutes on an IBM 709 can be approximated by the following relation

$$T = \frac{gMP}{178}(.7 + .2/\lambda_i) \qquad (A.3)$$

A listing of the programs and a sample set of results appear in Appendix B.

Lifting Surface Programs

Two lifting surface programs were prepared, one corresponding to the general case covered in Chapter 5, and the other for the special case of a symmetrical blade as discussed in Chapter 6. Since both programs are practically the same, the general discussion in this section will apply to both unless specifically indicated otherwise.

The input includes a list of nine values of $\chi$ together with corresponding values of tan $\beta_i$ and tan $\beta$ as in the lifting line case. In addition, the chord lengths $\ell/D$ at each value of $\chi$ is required as well as the chord load factors $\mu_{nj}$ defined in (5.19). In the general program, the mid-chord angles $\bar{\theta}$ shown in Fig. 5.1, and the radial load distribution must be given at each value of $\chi$. The latter may be given in the form of Goldstein factors $\kappa$, or either non-dimensional circulations G or G'.

In the symmetrical blade program, the mid-chord angles are zero by definition and need not be given. The other difference is that the Fourier coefficients of G are given, rather than G itself. This avoids the inaccuracies introduced by interpolation, since the total strength of the bound vortex elements at a particular radius will be exactly the same as in the lifting line case with the same radial lattice arrangement. Finally, the slopes of the mean line with unit camber ratio $h_q$ defined in (5.22), the camber ratio for unit lift coefficient in two-dimensional flow and the constants defining the lattice and control point arrangement must be given.

In either case a main program reads the data and computes the various geometrical properties associated with the lattice arrangement. Pitch angles and chord lengths at each of the lattice radii are obtained

by parabolic interpolation. In the general program a subroutine called AKL computes and solves the set of equations given in (5.32). In the symmetrical blade case a similar subroutine called CAMBER computes and solves the equations given in (6.18).

The only elements in (5.32) and (6.18) which require any significant amount of computation are the velocities induced by the horseshoe elements, $\bar{u}_{mnpq}$. As can be seen from Figs. 5.1 or 5.2, these consist of two semi-infinite helical vortex segments connected by a radial bound vortex. The velocity contribution of the bound vortex may be obtained explicitly by evaluating equations (3.9) and (3.10), and this may be done very easily in a subroutine called BOUND. The velocity induced by the helical segments may be obtained from the subroutine HELIX described previously. However, connecting the right helical segment to the right horseshoe requires a little bit of bookkeeping since the order in which the radial vortices intersect a particular helical vortex from above and below depends on the outline of the blade.

The computation time required in minutes on an IBM 709 can be estimated by the following relation*

$$T = .62 + .0033\ (PQM\ (9 + N)) \qquad (A.4)$$

where the symbols are as defined in Chapter 5. This equation holds for both the general and symmetrical blade programs provided N is interpreted as the total number of chordwise vortices. A listing of the programs for computing the symmetrical blade case, and a sample set of results appears in Appendix B. The programs for the general case are very similar, and will therefore not be included.

*An IBM 7090 is approximately five times as fast.

# APPENDIX B

## SOURCE PROGRAM LISTINGS

## AND

## SAMPLE PROGRAM OUTPUT

TABLE B.1 LIFTING LINE MAIN PROGRAM

```
      DIMENSION FILL(8000),X(9),XTBI(9),XTB(9)          ,DUMMY(9,3),RZ(25)
     1 ,TANBZ(25),R(24),RHO(25),TANBI(24),TBETA(24),COSBI(24),B(8)
     2 ,ZETA(8,25),U(8,25),A(8,8),E(16),GAMMA(9),GDTMB(9),ANS(9,5),
     3  MC(8),LZ(70)
      COMMON  FILL,PZ,LZ,ANS  ,RZ,TANBZ,R,RHO,TANBI,TBETA,COSBI,B,ZETA,
     1 U,A,E,G,PHIZ,ALAM,RH,ZT,TEMP,AMT,DELM,HDELM,Y,AI,SN1,SN2,TDEL
     2  ,TBI,CBI,TBZ,ETA,WN,DET,MC,NSTOP,MT,NPT,NG,NTM1,MOPT
      EQUIVALENCE (X,DUMMY,ANS),(XTBI,ANS(10)),(XTB,ANS(19)),(GAMMA,ANS(
     128)),(GDTMB,ANS(37))
      CALL OCTALS
      CALL STOMAP
      CALL HUMBUG(PZ,LZ)
1     CALL CLOCK(2)
      READ INPUT TAPE 4,101,NSTOP
101   FORMAT(I1)
      IF(NSTOP)  14,24,14
24    READ INPUT TAPE 4,100,(X(N),N=1,9),(XTBI(N),N=1,9),(XTB(N),N=1,9),
     1   MT,NPT,NG,(MC(N),N=1,8)
100   FORMAT(3(9F8.6/)1114)
      MAX=MT+1
      G=NG
      NTM1=0
      PHIZ=0.0
      ALAM=X(6)*XTBI(6)
      RH=X(1)
      MOPT=0
      IF(XTBI(2))  7,2,7
2     ALAM=XTBI(1)
      MOPT=1
      IF(RH)  3,4,3
4     X(1)=.01
3     DO 5        N=1,9
      XTBI(N)=ALAM/X(N)
5     CONTINUE
      DO 36      M=1,MAX
      DO 36      I=1,NPT
      ZETA(I,M)=1.0
36    CONTINUE
7     DO 15       N=1,9
      XTBI(N)=XTBI(N)*X(N)
      XTB(N)=XTB(N)*X(N)
15    CONTINUE
      DO 16       M=1,3
      DO 16       N=1,4
      K=10-N
      TEMP=DUMMY(N,M)
      DUMMY(N,M)=DUMMY(K,M)
      DUMMY(K,M)=TEMP
16    CONTINUE
      AMT=MT
      DELM=(1.-RH)/AMT
      HDELM=.5*DELM
      AM=RH-HDELM
```

```
      RZ(1)=RH+.25*HDELM
      TEMP=RZ(1)
      CALL INTERP(TEMP,Y,X,XTBI,3,9)
      TANBZ(1)=Y/RZ(1)
      DO 9        M=1,MT
      R(M)=AM+DELM
      AM=R(M)
      TEMP=AM
      CALL MAP(TEMP,RH)
      RHO(M)=TEMP
      RZ(M+1)=R(M)+HDELM
      IF(M-MT)  19,10,19
10    RZ(M+1)=RZ(M+1)-.25*HDELM
19    TEMP=RZ(M+1)
      CALL INTERP(TEMP,Y,X,XTBI,3,9)
      TANBZ(M+1)=Y/RZ(M+1)
      TEMP=R(M)
      CALL INTERP(TEMP,Y,X,XTBI,3,9)
      TANBI(M)=Y/R(M)
      CALL INTERP(TEMP,Y,X,XTBI,3,9)
      TBETA(M)=Y/R(M)
      COSBI(M)=1./SQRTF(1.+TANBI(M)**2)
9     CONTINUE
      DO 6        I=1,NPT
      MS=MC(I)
      TDEL=R(MS)*(TANBI(MS)-TBETA(MS))
      TBI=TANBI(MS)
      CBI=COSBI(MS)
      B(I)=2.*R(MS)*CBI
      DO 6        M=1,MAX
      IF(MOPT)  18,18,17
18    ZETA(I,M)=R(M)*(TANBI(M)-TBETA(M))/TDEL
17    TBZ=TANBZ(M)
      ETA=RZ(M)/R(MS)
      CALL HELIX(ETA,TBZ,TBI,CBI,PHIZ,NG,NTM1,LZ,WN)
      U(I,M)=WN
6     CONTINUE
      DO 8        I=1,NPT
      DO 8        K=1,NPT
      A(I,K)=0.0
8     CONTINUE
      RHO(MAX)=0.0
      DO 34       I=1,NPT
      AI=I
      SN1=0.
      DO 34       M=1,MAX
      IF(M-1)   31,31,32
31    J=M
      GO TO 33
32    J=M-1
33    SN2=SINF(AI*RHO(M))
      DO 30       K=1,NPT
      A(K,I)=A(K,I)+U(K,M)*(SN2*ZETA(K,M)-SN1*ZETA(K,J))
30    CONTINUE
      SN1=SN2
34    CONTINUE
      WRITE OUTPUT TAPE 2,102,((A(K,I),I=1,NPT),K=1,NPT)
102   FORMAT(4E15.8)
```

```
      DET=1.0
      ME=XSIMEQF(8,NPT,1,A,B,DET,E)
      GO TO(12,11,11),ME
11    CALL ERROR(20H     ERROR IN XSIMFQF)
14    CALL EXIT
12    DO 13        M=1,9
      GAMMA(M)=0.0
      TEMP=X(M)
      XTBI(M)=XTBI(M)/TEMP
      XTB(M)=XTB(M)/TEMP
      CALL MAP(TEMP,RH)
      DO 20        I=1,NPT
      AI=I
      GAMMA(M)=GAMMA(M)+SINF(AI*TEMP)*A(I,1)
20    CONTINUE
      IF(MOPT)  14,22,21
22    GDTMB(M)=((XTBI(M)/XTB(M))-1.0)*GAMMA(M)
      GO TO 13
21    GDTMB(M)=((X(M)**2+ALAM**2)/(2.*X(M)**2*ALAM))*GAMMA(M)*G
13    CONTINUE
      CALL WAITER
      GO TO 1
      END
```

TABLE B.2 MAIN PROGRAM- LIFTING SURFACE- SYMMETRICAL BLADE

```
      DIMENSION FILL(8000),A(56,56),ANS(24),B(56),BUG(8),CHORD(24),
     1  COSBI(24),COEFZ(8,7),D(24),E(56),F(56),HMU(8,7),H(7),
     2  PSI(16),P(16),PSIB(8),RZ(25),R(24),RHO(24),SNRHO(8),TANBZ(25),
     3  TANBI(24),TBETA(24),TIL(24),THETA(8,7),U(24,8,7),WN(16),X(9),
     4  XCORD(9),XTBI(9),XTB(9),XGAM(8),XRHO(9),MC(8),NFLIP(16),
     5  LZ(63),DUMMY(9,5)
      COMMON  FILL,PZ,LZ,A,ANS,B,BUG,COEFZ,COSBI,CHORD,D,E,F,H,HMU
     2  ,P,PSI,PSIB,R,RHO,RZ,SNRHO,TANBI,TANBZ,TBAR,THETA,TIL,U,WN,XGAM
     3  ,ALAM,ANT,AMT,AM,AI,ANGLE,CBI,DELM,DET,ETA,G,GNZL,HDELM,PHIZ,
     4  RH,RB1,RB2,TBI,TBZ,TEMP,UB,W,Y,ZETA,MC,NFLIP,JIN,JOUT,JT,KTEST,
     5  K101,MS,NBOTH,MT,NT,NPT,NZ1,NZ2,NG,NQT,NTT,NTM1,NIP,NF,TBETA
      EQUIVALENCE(X,FILL,DUMMY),(XCORD,E,DUMMY(10)),(XTBI,DUMMY(19)),
     1 (XTB,DUMMY(28)),(XRHO,DUMMY(37))
      CALL OCTALS
      CALL STOMAP
      CALL HUMBUG(PZ,LZ)
      CALL CLOCK(2)
      JIN=4
      JOUT=2
20    READ INPUT TAPE JIN,100,(X(N),N=1,9),(XCORD(N),N=1,9),(XTBI(N),
     1  N=1,9),(XTB(N),N=1,9)
      READ INPUT TAPE JIN,101,KTEST,MT,NT,NPT,NZ1,NZ2,NG,(MC(N),N=1,8),
     1 GNZL
      NQT=(NT+NZ1-NZ2-2)/NZ1
      G=NG
      JT=NQT
      NBOTH=NT+NT
      NTT=NBOTH + NBOTH
      ZETA=0.
      ALAM=0.
      NTM1=NTT-1
      RH=X(1)
      READ INPUT TAPE JIN,102,((HMU(N,J),N=1,NT),J=1,JT),(H(N),N=1,NQT),
     1  (XGAM(N),N=1,8)
      DO 51       N=1,8
      COEFZ(N,1)=XGAM(N)
      DO 51       J=2,7
      COEFZ(N,J)=0.
51    CONTINUE
      IF(XTBI(2))  7,2,7
   2  ALAM=XTBI(1)
      IF(RH) 3,4,3
   4  X(1)=.01
3     DO 5       N=1,9
      XTBI(N)=ALAM/X(N)
   5  CONTINUE
      ZETA=-1.0
   7  DO 15 N=1,9
      TEMP=X(N)
      CALL MAP(TEMP,RH)
      XRHO(N)=TEMP
      XTBI(N)=XTBI(N)*X(N)
      XTB(N)=XTB(N)*X(N)
  15  CONTINUE
      DO 16       M=1,5
```

```
      DO 16 N=1,4
      K=10-N
      TEMP=DUMMY(N,M)
      DUMMY(N,M)=DUMMY(K,M)
      DUMMY(K,M)=TEMP
   16 CONTINUE
      ANT=NT
      AMT=MT
      DELM=(1.-RH)/AMT
      HDELM=.5*DELM
      AM=RH-HDELM
      RZ(1)=RH+.25*HDELM
      TEMP=RZ(1)
      CALL INTERP(TEMP,Y,X,XTBI,3,9)
      TANBZ(1)=Y/RZ(1)
      DO 9 M=1,MT
      R(M)=AM+DELM
      AM=R(M)
      TEMP=AM
      CALL MAP(TEMP,RH)
      RHO(M)=TEMP
      RZ(M+1)=R(M)+HDELM
      IF(M-MT) 19,10,19
   10 RZ(M+1)=RZ(M+1)-.25*HDELM
   19 TEMP=RZ(M+1)
      CALL INTERP(TEMP,Y,X,XTBI,3,9)
      TANBZ(M+1)=Y/RZ(M+1)
      TEMP=R(M)
      CALL INTERP(TEMP,Y,X,XTBI,3,9)
      TANBI(M)=Y/R(M)
      CALL INTERP(TEMP,Y,X,XTB,3,9)
      TBETA(M)=Y
      TEMP=RHO(M)
      CALL INTERP(TEMP,Y,XRHO,XCORD,3,9)
      CHORD(M)=Y
      COSBI(M)=1./SQRTF(1.+TANBI(M)**2)
    9 CONTINUE
      DO 6       N=1,NPT
      M=MC(N)
      D(N)=0.
      DO 6      I=1,NPT
      AI=I
      D(N)=D(N)+XGAM(I)*SINF(AI*RHO(M))
    6 CONTINUE
      DO 30      N=1,NT
      K=NBOTH-N+1
      DO 30       J=1,JT
      HMU(K,J)=HMU(N,J)
   30 CONTINUE
      WRITE OUTPUT TAPE JOUT,103,NT,MT,NPT,NZ1,NZ2,(MC(N),N=1,8),NG,
     1  ALAM,RH,GNZL
      WRITE OUTPUT TAPE JOUT,104,(CHORD(N),N=1,MT)
      WRITE OUTPUT TAPE JOUT,105,(TANBI(N),N=1,MT)
      WRITE OUTPUT TAPE JOUT,106,(TBETA(N),N=1,MT)
      WRITE OUTPUT TAPE JOUT,107,(D(N),N=1,NPT)
      WRITE OUTPUT TAPE JOUT,108,((HMU(N,J),N=1,NT),J=1,JT)
      WRITE OUTPUT TAPE JOUT,109,(H(N),N=1,NQT)
```

```
      CALL CAMBER
      CALL CLOCK(2)
      GO TO 20
  100 FORMAT(9F8.8)
  101 FORMAT(15I4,F8.6)
  102 FORMAT(7F10.7)
  103 FORMAT(6H0  NT=I1,5H  MT=I2,6H  NPT=I1,6H  NZ1=I1,6H  NZ2=I1,5H  M
     1C=8I4,5H  NG=I1,7H  ALAM=F6.4,5H  RH=F9.3,7H  GNZL=F6.4)
  104 FORMAT(8H0 CHORD=10F10.6)
  105 FORMAT(8H0 TANBI=10F10.6)
  106 FORMAT(8H0 TBETA=10F10.6)
  107 FORMAT(8H0 GAMMA=10F10.6)
  108 FORMAT(8H0 HMU  =10F10.6)
  109 FORMAT(8H0 H    =10F10.6)
      END
```

TABLE B.3 WAITER SUBROUTINE

```
      SUBROUTINE WAITER
      DIMENSION FILL(8000),X(9),XTBI(9),XTB(9),        DUMMY(9,3),RZ(25)
     1 ,TANBZ(25),R(24),RHO(25),TANBI(24),TBETA(24),COSBI(24),B(8)
       ,S(8,25),U(8,25),A(8,8),F(16),GAMMA(9),GDTMB(9),ANS(9,5),MC(8)
     3  ,LZ(70)
      COMMON FILL,PZ,LZ,ANS  ,RZ,TANBZ,R,RHO,TANBI,TBETA,COSBI,B,S,U,A,
       E,G,PHIZ,ALAM,RH,ZETA,TEMP,AMT,DELM,HDELM,Y,AI,SN1,SN2,TDEL
     2  ,TBI,CBI,TBZ,ETA,WN,DET,MC,NSTOP,MT,NPT,NG,NTM1,MOPT
      EQUIVALENCE (X,DUMMY,ANS),(XTBI,ANS(10)),(XTB,ANS(19)),(GAMMA,ANS(
      28)),(GDTMB,ANS(37))
      WRITE OUTPUT TAPE 2,100,NG,X(4),ALAM,MT,NPT,(MC(N),N=1,NPT)
      WRITE OUTPUT TAPE 2,101
      WRITE OUTPUT TAPE 2,102,(A(N,1),N=1,NPT)
      WRITE OUTPUT TAPE 2,103
      IF(MOPT)  1,1,2
1     WRITE OUTPUT TAPE 2,104
      WRITE OUTPUT TAPE 2,105
      GO TO 3
2     WRITE OUTPUT TAPE 2,106
      WRITE OUTPUT TAPE 2,107
3     DO 4        M=1,9
      K=10-M
      WRITE OUTPUT TAPE 2,108,(ANS(K,N),N=1,5)
4     CONTINUE
      RETURN
100   FORMAT(25H1     NUMBER OF BLADES  G=I1,17H    LAMDA I AT X=F4.2,4H
     1IS F6.4/22H0    LATTICE SPACES M=I2,6H       I1,21H CONTROL POINTS
     2AT M=8I3)
101   FORMAT(40H0     FOURIER COEFFICIENTS OF G     A(I) )
102   FORMAT(5H0     4F10.6)
103   FORMAT(25H0     G=GAMMA/TWO PI R U* )
104   FORMAT(27H0     GBAR=GAMMA/TWO PI R VA)
105   FORMAT(51H0       X     TAN BETA I  TAN BETA      G          GBAR/)
106   FORMAT(27H0     KAPPA=GOLDSTEIN FACTOR)
107   FORMAT(51H0       X     TAN BETA I  TAN BETA      G         KAPPA/)
108   FORMAT(F9.2,F10.3,F11.3,F10.4,F12.4)
      END
```

TABLE B.4 MAP SUBROUTINE

```
      SUBROUTINE MAP (TEMP,RH)
      IF(TEMP-.999)  1,1,2
2     TEMP=3.1415926
      GO TO 19
1     CN=(1.+RH-2.*TEMP)/(1.-RH)
      IF(ABSF(CN)-.00001) 17,17,18
17    TEMP=1.5707963
      GO TO 19
18    CTN=SQRTF(1.+CN**2)/CN
      TEMP=ATANF(CTN)
      IF(CTN) 20,19,19
20    TEMP=TEMP+3.1415926
19    RETURN
      END
```

TABLE B.5 CAMBER SUBROUTINE

```
      SUBROUTINE CAMBER
      DIMENSION FILL(8000),A(56,56),ANS(24),B(56),BUG(8),CHORD(24),
     1  COSBI(24),COEFZ(8,7),D(24),E(56),F(56),HMU(8,7),H(7),
     2  PSI(16),P(16),PSIB(8),RZ(25),R(24),RHO(24),SNRHO(8),TANBZ(25),
     3  TANBI(24),TBETA(24),TIL(24),THETA(8,7),U(24,8,7),WN(16),X(9),
     4  XCORD(9),XTBI(9),XTB(9),XGAM(8),XRHO(9),MC(8),NFLIP(16),
     5  LZ(63),DUMMY(9,5),GAMMA(24)
      COMMON  FILL,PZ,LZ,A,ANS,B,BUG,COEFZ,COSBI,CHORD,D,E,F,H,HMU
        ,P,PSI,PSIB,R,RHO,RZ,SNRHO,TANBI,TANBZ,TBAR,THETA,TIL,U,WN,XGAM,
     3  ,ALAM,ANT,AMT,AM,AI,ANGLE,CBI,DELM,DET,ETA,G,GNZL,HDELM,PHIZ,
     4  RH,RB1,RB2,TBI,TBZ,TEMP,UB,W,Y,ZETA,MC,NFLIP,JIN,JOUT,JT,KTEST,
     5  K101,MS,NBOTH,MT,NT,NPT,NZ1,NZ2,NG,NQT,NTT,NTM1,NIP,NF,TBETA
     6  ,GAMMA
      EQUIVALENCE(X,FILL,DUMMY),(XCORD,E,DUMMY(10)),(XTBI,DUMMY(19)),
     1 (XTB,DUMMY(28)),(XRHO,DUMMY(37))
      NIP=2*(NZ1-NZ2-1)
      NP=1
      DO 1          M=1,MT
      TIL(M)=CHORD(M)*COSBI(M)/(2.*ANT*R(M))
      IF(M-MC(NP))  1,2,1
2     DO 3          NQ=1,NQT
      TEMP=2*NZ1*NQ-NIP
      THETA(NP,NQ)=TIL(M)*TEMP*
3     CONTINUE
      NP=NP+1
1     CONTINUE
      K101=NPT*NQW
      DO 4          K=1,K101
      B(K)=0.
      DO 4          L=1,K101
      A(K,L)=0.
4     CONTINUE
      DO 5          NU=1,NTM1,2
      TEMP=NU-NBOTH
      PSI(NU)=TIL(1)*TEMP
      PSI(NU+1)=PSI(NU)
5     CONTINUE
      TBZ=TANBZ(1)
      DO 6          N=1,NTT
      P(N)=PSI(N)-PSI(NTT)
6     CONTINUE
      CALL LIST(NTM1,P,LZ)
      DO 38         NP=1,NPT
      MS=MC(NP)
      ETA=RZ(1)/R(MS)
      TBI=TANBI(MS)
      CBI=COSBI(MS)
      DO 38         NQ=1,NQT
      PHIZ=PSI(NTT)-THETA(NP,NQ)
      CALL HELIX(ETA,TBZ,TBI,CBI,PHIZ,NG,NTM1,LZ,WN)
      IF (KTEST)  60,61,60
60    WRITE OUTPUT TAPE JOUT,101,(WN(N),N=1,NTT)
61    M=2
```

```
      DO 38       N=1,NBOTH
      U(N,NP,NQ)=WN(M)
      M=M+2
   38 CONTINUE
      DO 14       M=1,MT
      IF(KTEST)  72,73,72
   72 WRITE OUTPUT TAPE JOUT,104,M
   73 RB1=RZ(M)
      RB2=RZ(M+1)
      GAMMA(M)=0.0
   19 DO 21       I=1,NPT
      AI=I
      SNRHO(I)=SINF(AI*RHO(M))
      GAMMA(M)=GAMMA(M)+SNRHO(I)*XGAM(I)
   21 CONTINUE
      N=1
      DO 22       NU=1,NTM1,2
      TEMP=NU-NBOTH
      PSI(NU)=TIL(M)*TEMP
      PSIB(N)=PSI(NU)
      IF(M-MT)  23,24,23
   23 PSI(NU+1)=TIL(M+1)*TEMP
      GO TO 25
   24 PSI(NU+1)=PSI(NU)
   25 IF(PSI(NU+1)-PSI(NU)) 26,27,27
   26 NFLIP(NU)=0
      NFLIP(NU+1)=8
      AM=PSI(NU)
      PSI(NU)=PSI(NU+1)
      PSI(NU+1)=AM
      GO TO  84
   27 NFLIP(NU)=8
      NFLIP(NU+1)=0
   84 N=N+1
   22 CONTINUE
      DO 8        NU=2,NTM1,2
      IF(PSI(NU+1)-PSI(NU)) 9,8,8
    9 AM=PSI(NU)
      NF=NFLIP(NU)-1
      PSI(NU)=PSI(NU+1)
      NFLIP(NU)=NFLIP(NU+1)+1
      PSI(NU+1)=AM
      NFLIP(NU+1)=NF
    8 CONTINUE
      TBZ=TANBZ(M+1)
      DO 7        N=1,NTT
      P(N)=PSI(N)-PSI(NTT)
    7 CONTINUE
      CALL LIST(NTM1,P,LZ)
      DO 14       NP=1,NPT
      J1=(NP-1)*NQT
      MS=MC(NP)
      ETA=RZ(M+1)/R(MS)
      TBI=TANBI(MS)
      CBI=COSBI(MS)
      IF(ZETA)  50,51,51
   51 ZETA=+((TANBI(M)-TBETA(M))/(TBI-TBETA(MS)))*(R(M)/R(MS))
   50 ALAM=R(MS)*TBI
```

```
      IF(M-1)  80,80,81
80    BUG(NP)=2.*R(MS)*COSBI(MS)
81    DO 14      NQ=1,NQT
      K=J1+NQ
      IF(M-MS)  83,82,83
82    A(K,NP)=12.566375*GNZL*GAMMA(MS)*R(MS)*H(NQ)/CHORD(MS)
      B(K)=B(K)+BUG(NP)
      B(K1)=B(K1)+BUG(NP)
85    F(K)=0.
      DO 41      N=1,NBOTH
      U(N+16,NP,NQ)=U(N,NP,NQ)
41    CONTINUE
      PHIZ=PSI(NTT)-THETA(NP,NQ)
      CALL HELIX(ETA,TBZ,TBI,CBI,PHIZ,NG,NTM1,LZ,WN)
      IF (KTEST)  62,63,62
62    WRITE OUTPUT TAPE JOUT,101,(WN(N),N=1,NTT)
63    DO 36      NU=1,NTT
      N=NFLIP(NU)+(NU+1)/2
      U(N,NP,NQ)=WN(NU)
36    CONTINUE
      DO 37      N=1,NBOTH
      ANGLE=PSIB(N)-THETA(NP,NQ)
      CALL BOUND(RB1,RB2,ETA,ALAM,ANGLE,NG,UB)
      W=UB+U(N+8,NP,NQ)-U(N+16,NP,NQ)
      IF(KTEST) 64,65,64
64    WRITE OUTPUT TAPE JOUT,102,NP,NQ,N,UB,W
65    IF(JT-2)  99,40,40
40    DO 35      I=1,NPT
      DO 35      J=2,JT
      L=NPT+(I-1)*(JT-1)+J-1
      A(K,L)=A(K,L)-SNRHO(I)*W*HMU(N,J)*ABSF(ZETA)
35    CONTINUE
99    F(K)=F(K)+W*HMU(N,1)
37    CONTINUE
      B(K)=B(K)+F(K)*GAMMA(M)*ABSF(ZETA)
14    CONTINUE
      WRITE OUTPUT TAPE JOUT,107
      WRITE OUTPUT TAPE JOUT,103,((A(K,L),L=1,K101),K=1,K101)
      WRITE OUTPUT TAPE JOUT,108
      WRITE OUTPUT TAPE JOUT,103,(B(K),K=1,K101)
      DET=1.0
      ME=XSIMEQF(56,K101,1,A,B,DET,E)
      GO TO(68,69,69),ME
69    CALL ERROR(20H    ERROR IN XSIMEQF)
      CALL EXIT
68    N=1
      DO 90      K=1,NPT
      MS=MC(K)
      ANS(N)=R(MS)
      ANS(N+1)=A(K,1)
      ANS(N+2)=1./A(K,1)
      N=N+3
90    CONTINUE
      J=3*NPT
      WRITE OUTPUT TAPE JOUT,109
      WRITE OUTPUT TAPE JOUT,110,(ANS(N),N=1,J)
      K=NPT+1
```

```
      DO 92      I=1,NPT
      IF(JT-2)  92,93,93
   93 DO 94       J=2,JT
      COEFZ(I,J)=A(K,1)
      K=K+1
   94 CONTINUE
   92 CONTINUE
      WRITE OUTPUT TAPE JOUT,111
      WRITE OUTPUT TAPE JOUT,112,((COEFZ(I,J),J=1,7),I=1,8)
      RETURN
  101 FORMAT(8H      WN=8F8.3)
  102 FORMAT(5H   P=I3,5H   Q=I3,5H   N=I3,5H  UB=F8.3,5H   W=F8.3)
  104 FORMAT(15HO **********M=I2)
  107 FORMAT(33HO       COEFFICIENT MATRIX  A(K,L)//)
  103 FORMAT(8E15.5)
  108 FORMAT(28HO       RIGHT HAND SIDE  B(K)//)
  109 FORMAT(54HO       RADIUS      CAMBER FACTOR K     CAMBER FACTOR 1/K)
  110 FORMAT(7HO       F5.3,8H         F7.3,13H                F7.3)
  111 FORMAT(48HO  CIRCULATION DISTRIBUTION COEFFICIENTS  C(I,J))
  112 FORMAT(7E15.5)
      END
```

TABLE 8.6 BOUND SUBROUTINE

```
      SUBROUTINE BOUND(RB1,RB2,ETA,ALAM,ANGLE,NG,UB)
      G=NG
      DELBL=6.2831853/G
      S=0.
      R=RB2/ETA
      RLAM=R/SQRTF(R**2+ALAM**2)
      A=R**2+(ALAM*ANGLE)**2
      PHI=ANGLE
      DO 1        N=1,NG
      T=0.
      CP=COSF(PHI)
      SP=SINF(PHI)
      B=-2.*R*CP
      C=ALAM**2*ANGLE*CP+R**2*SP
      X=RB1
      D=B**2-4.*A
      DO 2        I=1,2
      IF(ABSF(D)-.0001) 3,3,4
    4 Y=-2.*(2.*X+B)/(D*SQRTF(A+B*X+X**2))
      GO TO 5
    3 Y=-1./(2.*(X+.5*B)**2)
    5 IF(I-1) 6,7,6
    7 T=T-Y
      X=RB2
      GO TO 2
    6 T=T+Y
    2 CONTINUE
      S=S+T*C
      PHI=PHI+DELBL
    1 CONTINUE
      UB=S*RLAM
      RETURN
      END
```

TABLE B.7 HUMBUG SUBROUTINE

```
*       FAP
        COUNT   176
        ENTRY   HUMBUG
        BSS     3
HUMBUG  SXD     *-3,1
        SXD     *-3,2
        SXD     *-3,4
        AXT     56,1
        CLA     M+8,1
        ADD     1,4
        STA     M+8,1
        TIX     *-3,1,1
        CLA     2,4
        ADD     ONE
        STA     *+3
        AXT     48,1
        CLA     L+1,1
        STO     0,1
        TIX     *-2,1,1
        CLA     ONE
        STD     XR1A
        AXT     8,2
NUREV   SXD     XR2A,2
        CLA     M+8,2
        PDX     0,1
        STA     *+1
        AXC     0,2
NILE    SXD     XR1B,1
        LXD     XR1A,1
        TXI     *+1,1,-1
        LDQ     PHI,1
        FMP     =.017453293
        STO     X
        LDQ     PHI+1,1
        FMP     =.017453293
        FSB     X
        STO     DEL
        SXD     XR1A,1
        AXT     5,1
PINTO   LDQ     DELTA+5,1
        FMP     DEL
        FAD     X
        STO     X
        STO     1,2
        XCA
        FMP     X
        STO     0,2
        CLA     =1.0
        STO     2,2
        CLA     X
        TSX     $COS,4
        NOP     *+2
        PZE     HUMBUG-1
        STO     3,2
```

```
          XCA
          FMP       X
          STO       5,2
          CLA       X
          TSX       $SIN,4
          NIR       *+2
          PZE       HUMBUG-1
          STO       4,2
          XCA
          FMP       X
          STO       6,2
          LDQ       GAUSS+5,1
          FMP       DEL
          STO       7,2
          TXI       *+1,2,-8
          TIX       PINTO,1,1
          LXD       XR1B,1
          TIX       NILE,1,1
          LXD       XR1A,1
          TXI       *+1,1,-1
          SXD       XR1A,1
          LXD       XR2A,2
          TIX       NUREV,2,1
          LXD       HUMBUG-3,1
          LXD       HUMBUG-2,2
          LXD       HUMBUG-1,4
          TRA       3,4
          PZE       1720,0,15
          PZE       1600,0,15
          PZE       1480,0,15
          PZE       1360,0,15
          PZE       1240,0,15
          PZE       0,0,75
          BSS       15
          PZE       1720,0,15
          PZE       1600,0,15
          PZE       1480,0,15
          PZE       1360,0,15
          PZE       1240,0,15
          PZE       600,0,50
          BSS       15
          PZE       1720,0,15
          PZE       1600,0,15
          PZE       1480,0,15
          PZE       1360,0,15
          PZE       1240,0,15
L         PZE       1000,0,30
M         PZE       0,0,15
          PZE       600,0,10
          PZE       1000,0,6
          PZE       1240,0,3
          PZE       1360,0,3
          PZE       1480,0,3
          PZE       1600,0,3
          PZE       1720,0,3
ONE       PZE       1,0,1
PHI       DEC       0.,1.,2.,4.,7.,10.,20.,30.,50.,75.,100.,150.,200.,250.
```

```
        DEC     300.,360.,0.,5.,10.,20.,40.,60.,100.,150.,200.,270.
        DEC     360.,0.,20.,50.,90.,180.,270.,360.,360.,480.,600.,720.
        DEC     720.,840.,960.,1080.,1080.,1200.,1320.,1440.,1440.,1560.
        DEC     1680.,1800.,1800.,1920.,2040.,2160.
DELTA   DEC     .046910,.183855,.269235,.269235,.183855
GAUSS   DEC     .118464,.239314,.284444,.239314,.118464
XR1A    PZE
XR1B    PZE
XR2A    PZE
DEL     PZE
X       PZE
        END
```

TABLE B.8 LIST SUBROUTINE

```
*       FAP
        COUNT   176
        ENTRY   LIST
        BSS     3
LIST    SXD     *-3,1
        SXD     *-3,2
        SXD     *-3,4
        CLA*    1,4
        STD     NUH
        CLA     2,4
        STA     A5+2
        ADD     =01
        STA     A5
        CLA     3,4
        ADD     =01
        STA     A9
        SUB     =06
        STA     *+1
        CLA     **
        STO     LAST
        STA     *+1
        AXC     **,4
        SXD     A7,4
        AXT     1,1
A8      SXD     M,1
        LXD     NUH,1
        CLA     =06000000
        STD     N
A4      SXD     NU,1
        LXD     N,2
        TXI     *+1,2,1
        SXD     N,2
A5      CLA     **,1
        STO     X
        CLA     **,1
        FSB     X
        STO     DFL
        LXD     M,1
        FDP     EPSLN+3,1*
        STO     D
        CLA     D
        FSB     =.4
        TPL     G5
        FAD     =.399
        TPL     G2
        CLA     =01000000
        STO     B
        STO     H
        CLA     =010000000
        STD     A2
        STD     KL
        TRA     A6
G2      CLA     =07000000
```

```
        STD     A2
        CLA     =06000000
        STD     KL
        CLA     =01000000
        STD     H
        CLA     =02000000
        STD     B
        TRA     A6
G5      CLA     D
        UFA     =0211001000000
        ANA     =0000777000000
        STD     H
        LDQ     H
        MPY     =05000000
        ALS     17
        STD     B
        CLA     =01000000
        STD     KL
        CLA     =05000000
        STD     A2
        CLA     H
        LRS     18
        ORA     =0233000000000
        FAD     =0233000000000
        STO     TEMP
        CLA     DEL
        FDP     TEMP
        STO     DEL
A6      CLA     M
        SUB     =01000000
        XCA
        MPY     =025000000
        ALS     17
        ADD     N
        PDX     **,1
        LDQ     LAST
        MPY     =010000000
        ARS     1
        ADD     LAST
        STA     LAST
        CLA     B
        STD     LAST
        CLA     LAST
A9      STO     **,1
        STA     *+1
        AXC     **,2
        TXL     ERROR,2,316
A7      TXH     ERROR,2,**
        LXD     H,1
A3      SXD     P,1
        LXD     KL,1
A1      LDQ     DELTA+1,1
        FMP     DEL
        FAD     X
        STO     1,2
        TSX     $COS,4
        NTR     *+2
        PZE     LIST-1
```

```
        STO     3,2
        XCA
        FMP     4,2
        STO     5,2
        CLA     1,2
        TSX     $SIN,4
        NTR     *+2
        PZE     LIST-1
        STO     6,2
        XCA
        FMP     1,2
        STO     6,2
        LDQ     1,2
        FMP     1,2
        STO     0,2
        CLA     =1.0
        STO     2,2
        LDQ     GAUSS+1,1
        FMP     DEL
        STO     7,2
        TXI     *+1,2,-8
        TXI     *+1,1,1
A2      TXL     A1,1
        CLA     X
        FAD     DEL
        STO     X
        LXD     P,1
        TIX     A3,1,1
        LXD     NU,1
        TIX     A4,1,1
        LXD     M,1
        TXI     *+1,1,1
        TXL     A8,1,3
        LXD     LIST-3,1
        LXD     LIST-2,2
        LXD     LIST-1,4
        TRA     4,4
ERROR   TSX     $MIST,4
NU      PZE
NUH     PZE
N       PZE
M       PZE
LAST    PZE
X       PZE
DEL     PZE
EPSLN   DEC     .01745,.08727,.34907
D       PZE
B       PZE
H       PZE
KL      PZE
TEMP    PZE
        DEC     .5,.866025,.288675,.953090,.769235,.5,.230765
DELTA   DEC     .046910
        DEC     1.0,.5,.5,.118464,.239314,.284444,.239314
GAUSS   DEC     .118464
P       PZE
        END
```

TABLE B.9 HELIX SUBROUTINE

```
*       FAP
        COUNT   469
        ENTRY   HELIX
HELIX   SXD     HELIX-2,4
        SXA     RESTO,1
        SXA     RESTO+1,2
        REM     THIS IS THE START OF  THE PARAM PART    GETS CONSTANTS
        LDQ*    5,4
        FMP*    1,4
        XCA
        FMP*    2,4
        STO     XZ
        CLA*    6,4
        ARS     18
        STA     BLADS
        ORA     =0233000000000
        FAD     =0233000000000
        STO     GFLO
        CLS*    4,4
        STO     CONST
        LDQ*    1,4
        FMP*    2,4
        STO     E4
        LDQ     E4
        FMP     E4
        STO     ETA
        LDQ*    1,4
        FMP*    1,4
        STO     E1
        LDQ*    2,4
        FMP*    3,4
        FSB*    1,4
        FDP     ETA
        FMP     =-.012665148            1/A*PI
        FDP*    2,4
        FMP     GFLO
        STO     TRUNK
        CLA     =01000000
        STO     TEMP
        CLA     =1.0
        FSB*    1,4
        SSP
        FSB     =.25
        TPL     ROUGH
        FAD     =.19
        TPL     MED
        CLA     TEMP
        ADD     =02000000
        TRA     *+3
MED     CLA     TEMP
        ADD     =01000000
        STO     TEMP
ROUGH   CLA     TEMP
```

```
        STD     M
        AXC     CBUG,2
        SXA     C,2
        AXC     DBUG,2
        SXA     D,2
BLADE   AXT     0,1
        CLA     =1.0
        STO     K
KLOOP   CLA     GFLO
        FSB     K
        FDP     GFLO
        FMP     =6.2831853
        FAD*    5,4
        STO     PHIK
        TSX     $COS,4
        NTR     *+2
        PZE     HELIX-2
        STO     CPK
        CLA     PHIK
        TSX     $SIN,4
        NTR     *+2
        PZE     HELIX-2
        STO     SPK
        LXD     HELIX-2,4
        LXA     C,2
        STZ     -6,2
        STZ     -5,2
        LDQ*    1,4
        FMP     CPK
        STO     E2
        LDQ*    1,4
        FMP     SPK
        STO     E3
        LDQ     E2
        FMP     E4
        STO     E5
        LDQ     E3
        FMP*    E4
        STO     E6
        LDQ     XZ
        FMP     E2
        CHS
        FAD     E6
        STO     E7
        LDQ     E3
        FMP     XZ
        FAD     E5
        STO     E8
        LDQ*    3,4
        FMP     E4
        CHS
        FAD     E1
        STO     -4,2
        LDQ*    2,4
        FMP     E6
        FSB     E2
        STO     -3,2
        LDQ*    3,4
```

```
          FMP     E7
          CHS
          FAD     E3
          STO     -2,2
          LDQ*    3,4
          FMP     E6
          STO     -1,2
          LDQ*    3,4
          FMP     E5
          STO     0,2
          LXA     D,2
          LDQ     ETB
          STQ     -6,2
          FMP*    5,4
          XCA
          STQ     TEMP
          FMP     =2.0
          STO     -5,2
          LDQ     TEMP
          FMP*    5,4
          STO     TEMP
          LDQ*    1,4
          FMP*    1,4
          FAD     =1.0
          FAD     TEMP
          STO     -4,2
          LDQ*    1,4
          FMP     =2.0
          XCA
          STQ     TEMP
          FMP     CPK
          CHS
          STO     -3,2
          LDQ     TEMP
          FMP     SPK
          STO     -2,2
          STZ     -1,2
          STZ     0,2
          TXI     *+1,2,7
          SXA     D,2
          LXA     C,2
          TXI     *+1,2,7
          SXA     C,2
          CLA     K
          FAD     =1.0
          STO     K
          TIX     KLOOP,1,1
          REM     START HELIX PART      PERFORMS INTEGRATION
          CLA*    7,4
          STD     NT                    NO OF ON BLADE INTERVALS
          CLA*    6,4
          STD     NG                    NO OF BLADES
          CLA     ADRC
          STA     A1
          CLA     ADRD
          STA     A2
          CLA     8,4
```

```
         ADD     =01
         STA     A14                 L+1
         STA     A15
         CLA     9,4
         STA     A11
         ADD     =01
         STA     A11+1
         CLA     NT
         ARS     18
         SSM
         ADD     9,4
         STA     A13
         CLA     =01000000
         STD     N
         STZ     XNEW                USED TO CHECK CONVERGENCE
NUBLD    CLA     M                   INTEGRATION SPACING FACTOR
         STO     MBUG                SAVE ORIGINAL M
         STZ     X
         SXD     NTBUG,4
NUREV    CLA     MBUG
         SUB     =01000000
         XCA
         MPY     =025000000          SELECT DATA TABLE
         ALS     17
         ADD     N
         PDX     0,1                 21(M-1)+N
A14      CLA     **,1                L+1  BEING BACKWARDS STORAGE
         STO     LNM                 ADDR OF  P,0,NO OF POINTS
         CLA     N
         PDX     0,1
A15      CLA     **,1                L+1    SELECT DATA TABLE
         STO     LN1                 FOR M=1 SPACING
         CLA     LN1                 SET UP
         ADD     =07                 ADDRESSES
         STA     A3                  FOR FIRST
         STA     A5                  POINT IN
         SUB     =02                 INTERVAL
         STA     A4
         CLA     MBUG                GET NO OF BLADES
         ARS     1                   IN FIRST GROUP
         ANA     =01000000
         SSM                         NGBUG=NG IF M=1
         ADD     NG                  NGBUG=NG-1 IF M NOT 1
         STD     NGBUG
         LXD     LN1,1               POINTS PER INTERVAL   COARSE
         CLA     A9
         STA     A10                 TIX A7,1,1
A7       LXD     NGBUG,2             NO OF BLADES IN FIRST GROUP
         SXD     XRBUG,2
         CLA     *+3
         STA     *+1
A6       AXT     0,2                 7*K-2  FINDS C AND D
         AXT     5,4                 5 TERMS FOR ONE POINT
         STZ     T1                  SUM NUMERATOR HERE
         STZ     T2                  SUM DENOMINATOR HERE
A1       LDQ     **,2                C+7*NG
A3       FMP     **,4                P(N,M)+8*J-1
         FAD     T1
```

```
         STO     T1
A2       LDQ     **,2            D+7*NG-7
A4       FMP     **,4            P(N,M)+8*J-3
         FAD     T2
         STO     T2
         TXI     *+1,2,-1
         TIX     A1,4,1          DOING 1 POINT FOR 1 BLADE
         LDQ     T2              DONE  1 POINT FOR 1 BLADE
         FMP     T2
         XCA
         FMP     T2
         TSX     $SQRT,4
         NTR     *+2
         PZE     HELIX-2
         STO     T2              DENOM**3/2
         CLA     T1
         FDP     T2
A5       FMP     **              P(N,M)+8*J-1=WEIGHT
         FAD     X
         STO     X
         LXD     XRBUG,2
         TNX     PIANO,2,1
         SXD     XRBUG,2         SET UP FOR SAME POINT
A8       CLA     A6              NEXT BLADE
         ADD     =07
         STA     A6
         TRA     A6
PIANO    CLA     A3              NEXT POINT    1ST BLADE GROUP
         ADD     =010
         STA     A3              SET UP
         STA     A5              ADDRESSES
         SUB     =02             FOR NEXT POINT
         STA     A4              IN INTERVAL
A10      TIX     **,1,1          A6 OR A7
         CLA     MBUG            1ST GROUP DONE
         SUB     =01000000
         TZE     NUINT           IF M=1 ALL BLADES HAVE BEEN DONE
         CLA     A8
         STA     A10             TIX A6,1,1
         CLA     LNM
         ADD     =07             SET UP FOR
         STA     A3              MEDIUM OR FINE
         STA     A5              SPACING ON
         SUB     =02             INDEX BLADE
         STA     A4
         CLA     A6              PICK UP
         ADD     =07             INDEX BLADE
         STA     A6
         CLA     =01000000
         STO     MBUG            FAKE M
         LXD     LNM,1           NON-COARSE SPACING
         TRA     A6              BACK TO DO INDEX BLADE
NUINO    CLA     N               NEXT INTERVAL
         SUB     =07000000
         TMI     *+2
         TRA     BLADE
         CLA     XNEW
```

```
        STO     XOLD
        LDQ     N
        MPY     N
        ARS     1
        ORA     =0233000000000
        FAD     =0233000000000
        STO     T1                      TEMP STORAGE
        CLA     TRUNK
        FDP     T1
        XCA
        FAD     X
        STO     XNEW
        FSB     XOLD
        SSP
        FSB     =.0005                  ALLOWABLE TRUNCATION ERROR
        TMI     CONVR
        CLA     A9
        STA     A10                     TIX A7,1,1
        LXD     N,1
        TXI     *+1,1,1
        SXD     N,1
        TXL     NUREV,1,6               DO MAX 6 REVS DOWNSTREAM
CONVR   LDQ     XNEW
        FMP     CONST
A13     STO     **                      WN    DOWNSTREAM HELIX DONE
        CLA     NT                      NO OF INTERVALS ON BLADE
        TZE     RESTO                   NO INTEGRATION ON BLADE   RETURN
        CLA     =07000000
        STD     N
        LXD     NT,4
        SXD     NTBUG,4
        TRA     NUBLD
BLADE   LXD     NTBUG,4
        LDQ     X
        FMP     CONST
A11     FAD     **,4                    WN
        STO     **,4                    WN+1
        LXD     N,1
        TXI     *+1,1,1
        SXD     N,1
        TIX     NUBLD,4,1
RESTO   AXT     **,1
        AXT     **,2
        LXD     HELIX-2,4
        TRA     10,4
A9      PZE     A7
N       PZE
NT      PZE
NG      PZE
NTBUG   PZE
NGBUG   PZE
M       PZE
MBUG    PZE
XRBUG   PZE
LNM     PZE
LN1     PZE
C       PZE
D       PZE
```

```
ADRC   PZE      CBUG+1
ADRD   PZE      DBUG-1
TRUNK  PZE
CONST  PZE
SPK    PZE
CPK    PZE
K      PZE
PHIK   PZE
GFLO   PZE
TEMP   PZE
ETB    PZE
X      PZE
XOLD   PZE
XNEW   PZE
T1     PZE
T2     PZE
       BSS      41
CBUG   PZE
       BSS      41
DBUG   PZE
E1     PZE
E2     PZE
E3     PZE
E4     PZE
E5     PZE
E6     PZE
E7     PZE
E8     PZE
XZ     PZE
       END
```

**TABLE B.10 - LIFTING-LINE PROGRAM SAMPLE OUTPUT**

**OPTIMUM OPEN-WATER PROPELLER**

NUMBER OF BLADES G=3 LAMDA I AT X=0.70 IS 0.3333

LATTICE SPACES M=24 4 CONTROL POINTS AT M= 4 10 16 22

FOURIER COEFFICIENTS OF G ACI>

0.139690 -0.008823 -0.000841 -0.000429

G=GAMMA/TWO PI R U*

KAPPA=GOLDSTEIN FACTOR

| X | TAN BETA I | TAN BETA | G | KAPPA |
|---|---|---|---|---|
| 0.20 | 1.667 | -0. | -0. | -0. |
| 0.30 | 1.111 | -0. | 0.0828 | 0.8330 |
| 0.40 | 0.833 | -0. | 0.1137 | 0.8670 |
| 0.50 | 0.667 | -0. | 0.1320 | 0.8577 |
| 0.60 | 0.556 | -0. | 0.1405 | 0.8276 |
| 0.70 | 0.476 | -0. | 0.1398 | 0.7716 |
| 0.80 | 0.417 | -0. | 0.1282 | 0.6773 |
| 0.90 | 0.370 | -0. | 0.1006 | 0.5146 |
| 1.00 | 0.333 | -0. | 0.0000 | 0.0000 |

THE DATE IS MAY 4, 1961.
THE TIME IS 1319.5

**WAKE-ADAPTED PROPELLER**

NUMBER OF BLADES G=3 LAMDA I AT X=0.70 IS 0.3332

LATTICE SPACES M=24 4 CONTROL POINTS AT M= 4 10 16 22

FOURIER COEFFICIENTS OF G ACI>

0.142769 -0.009572 -0.000906 0.000090

G=GAMMA/TWO PI R U*

GBAR=GAMMA/TWO PI R VA

| X | TAN BETA I | TAN BETA | G | GBAR |
|---|---|---|---|---|
| 0.20 | 1.415 | 0.910 | 0. | 0. |
| 0.30 | 1.006 | 0.691 | 0.0842 | 0.0324 |
| 0.40 | 0.787 | 0.563 | 0.1153 | 0.0459 |
| 0.50 | 0.646 | 0.475 | 0.1342 | 0.0485 |
| 0.60 | 0.548 | 0.410 | 0.1437 | 0.0483 |
| 0.70 | 0.476 | 0.361 | 0.1436 | 0.0457 |
| 0.80 | 0.421 | 0.323 | 0.1320 | 0.0406 |
| 0.90 | 0.377 | 0.290 | 0.1032 | 0.0301 |
| 1.00 | 0.342 | 0.265 | 0.0000 | 0.0004 |

THE DATE IS MAY 4, 1961.
THE TIME IS 2341.8

TABLE B.11 - LIFTING SUBROUTINE - SUBSONICAL BLANK SAMPLE OUTPUT

SUBPROGRAM STORAGE MAP

| NAME | ORIGIN | ENTRY | NAME | ORIGIN | ENTRY | NAME | ORIGIN | ENTRY | NAME | ORIGIN | ENTRY | NAME | ORIGIN | ENTRY |
|---|---|---|---|---|---|---|---|---|---|---|---|---|---|---|
| (MAIN) | 00144 | 00163 | MAP | 01374 | 01402 | OCTALS | 01522 | 01531 | HUMBUG | 02130 | 02137 | LIST | 02454 | 02464 |
| MIST | 02764 | 02773 | HELIX | 03032 | 03037 | INTERP | 03754 | 03757 | BOUND | 04221 | 04230 | AKL | 04573 | 04610 |
| (FPT) | 07013 | 07021 | EXIT | 07435 | 07463 | EXITM | 07435 | 07441 | (TSHM) | 07475 | 07520 | (TSH) | 07475 | 07531 |
| (CSH) | 07475 | 07511 | (F2EF) | 07761 | 10156 | FTNPM | 07761 | 10023 | (F2PM) | 07761 | 10017 | (PCUP) | 14236 | 14341 |
| (STPC) | 14236 | 14240 | (PRLT) | 14616 | 15032 | (RSLT) | 14616 | 14753 | (SVLT) | 14616 | 14633 | (BCD)) | 16005 | 16010 |
| (CMPR) | 16027 | 16031 | (DCDR) | 16114 | 16116 | (FLO)) | 16175 | 16204 | (FIX)) | 16175 | 16202 | (ILSC) | 16262 | 16264 |
| (MOVE) | 16324 | 16326 | (NBLK) | 16404 | 16407 | (OCT)) | 16467 | 16471 | (OCTD) | 16520 | 16522 | (OPCD) | 16575 | 16577 |
| (PRNT) | 17153 | 17156 | (PSTN) | 17353 | 17357 | (EXIB) | 17474 | 17556 | (SETX) | 17474 | 17477 | (SPOT) | 17701 | 17703 |
| STOMAP | 17732 | 17737 | (CSHM) | 20161 | 20164 | (SPH) | 20165 | 20201 | (STHM) | 20165 | 20211 | (STH) | 20165 | 20236 |
| (SPHM) | 20636 | 20641 | (WTC) | 20642 | 20705 | (WER) | 20642 | 20654 | (FDC) | 20733 | 20764 | (RER) | 20739 | 20742 |
| (RTN) | 21000 | 22450 | (FIL) | 21000 | 22437 | (IOH) | 21000 | 21002 | (TCO) | 22601 | 22675 | (TEF) | 22601 | 22674 |
| (RCH) | 22601 | 22673 | (ETT) | 22601 | 22672 | (REW) | 22601 | 22671 | (WEF) | 22601 | 22670 | (BSR) | 22601 | 22667 |
| (WRS) | 22601 | 22666 | (RDS) | 22601 | 22665 | (IOS) | 22601 | 22606 | (TRC) | 22601 | 22676 | (IOU) | 22732 | 22735 |
| ATN | 22750 | 22752 | ATAN | 22750 | 22752 | SIN | 23067 | 23072 | COS | 23067 | 23071 | SQR | 23242 | 23246 |
| SQRT | 23242 | 23246 | (TES) | 23337 | 23337 | (EXE) | 23340 | 23344 | RECOUP | 24317 | 24322 | ERROR | 24325 | 24331 |
| LDUMP | 24501 | 24504 | TIME | 24510 | 24562 | CLOCK | 24510 | 24515 | GETTM | 24644 | 24646 | XDETRM | 25005 | 25526 |
| XSIMEQ | 25005 | 25376 | MOVIE) | 25627 | 25627 | | | | | | | | | |

THE DATE IS APRIL 17, 1961.
THE TIME IS 1508.4

NT=3 MT= 8 NPT=3 NZ1=1 NZ2=0 MC= 3 5 7 0 0 0 0 0 NG=3 ALAM=0.2423 RH=0.200 GNZL=0.0800

CHORD= 0.233404 0.259304 0.282426 0.300560 0.311472 0.313185 0.298909 0.228218

TANBI= 0.969200 0.692286 0.538444 0.440545 0.372769 0.323067 0.285059 0.255053

TBETA= 0. 0. 0. 0. 0. 0. 0. 0.

GAMMA= 0.114489 0.126195 0.106211

HMU = 0.109375 0.182292 0.208333 0.189887 -0.002532 -0.187355

H = -1.333333 -2.666666

COEFFICIENT MATRIX A(K,L)

| | | | | | | | |
|---|---|---|---|---|---|---|---|
| -0.24452E-00 | 0. | 0. | -0.52090E 01 | -0.43664E 01 | 0.25272E 01 | -0.48904E-00 | 0. |
| 0. | -0.51862E 01 | -0.41693E 01 | 0.28334E 01 | 0. | -0.35300E-00 | 0. | -0.74322E 01 |
| 0.17587E 01 | 0.84853E 01 | 0. | -0.70600E 00 | 0. | -0.74031E 01 | 0.22122F 01 | 0.83255F 01 |
| 0. | 0. | -0.40484E-00 | -0.85590E 01 | 0.11601E 02 | -0.57495E 01 | 0. | 0. |
| -0.80969E 00 | -0.86532E 01 | 0.12562E 02 | -0.77153E 01 | | | | |

RIGHT HAND SIDE B(K)

| | | | | | |
|---|---|---|---|---|---|
| -0.27468E-00 | -0.56039E 00 | -0.44718E-00 | -0.90505E 00 | -0.69949E 00 | -0.13839E 01 |

| RADIUS | CAMBER FACTOR K | CAMBER FACTOR 1/K |
|---|---|---|
| 0.450 | 1.169 | 0.856 |
| 0.650 | 1.295 | 0.772 |
| 0.850 | 1.682 | 0.594 |

CIRCULATION DISTRIBUTION COEFFICIENTS C(I,J)

| | | | | | | |
|---|---|---|---|---|---|---|
| 0.12837E-00 | -0.44394E-03 | 0. | 0. | 0. | 0. | 0. |
| -0.49850E-02 | -0.13892E-02 | 0. | 0. | 0. | 0. | 0. |
| 0.25870E-02 | 0.10633E-02 | 0. | 0. | 0. | 0. | 0. |
| -0. | 0. | 0. | 0. | 0. | 0. | 0. |
| -0. | 0. | 0. | 0. | 0. | 0. | 0. |
| -0. | 0. | 0. | 0. | 0. | 0. | 0. |
| -0. | 0. | 0. | 0. | 0. | 0. | 0. |
| -0. | 0. | 0. | 0. | 0. | 0. | 0. |

THE DATE IS APRIL 17, 1961.
THE TIME IS 1511.3

## APPENDIX C

### TABLE OF CHORD-LOAD FACTORS $\mu_{nJ}$ DEFINED IN (5.20)

| | n | J = 1 | J = 2 | J = 3 | J = 4 | J = 5 | J = 6 | J = 7 |
|---|---|---|---|---|---|---|---|---|
| N=2 | 1 | .5 | | | | | | |
| | 2 | .5 | | | | | | |
| N=4 | 1 | .195312 | .292969 | | | | | |
| | 2 | .304688 | .152344 | | | | | |
| | 3 | .304688 | -.152344 | | | | | |
| | 4 | .195312 | -.292969 | | | | | |
| N=6 | 1 | .109375 | .182292 | .189887 | .134187 | | | |
| | 2 | .182292 | .182292 | -.002532 | -.184823 | | | |
| | 3 | .208333 | .069444 | -.187355 | -.131896 | | | |
| | 4 | .208333 | -.069444 | -.187355 | .131896 | | | |
| | 5 | .182292 | -.182292 | -.002532 | .184823 | | | |
| | 6 | .109375 | -.182292 | .189887 | -.134187 | | | |
| N=8 | 1 | .072007 | .126010 | .146058 | .129591 | .080010 | .010426 | -.052892 |
| | 2 | .123367 | .154209 | .068072 | -.069119 | -.154856 | -.124451 | .004068 |
| | 3 | .147079 | .110310 | -.065429 | -.153981 | -.054423 | .118564 | .147254 |
| | 4 | .157547 | .039387 | -.148701 | -.076562 | .129269 | .108879 | -.098430 |
| | 5 | .157547 | -.039387 | -.148701 | +.076562 | .129269 | -.108879 | -.098430 |
| | 6 | .147079 | -.110310 | -.065429 | +.153981 | -.154423 | -.118564 | .147254 |
| | 7 | .123367 | -.154209 | .068072 | +.069119 | -.154856 | +.124451 | .004068 |
| | 8 | .072007 | -.126010 | .146058 | -.129591 | -.129591 | .080010 | -.052892 |

## INITIAL DISTRIBUTION

| Copies | |
|---|---|
| 1 | Chief, Bureau of Ships, Department of the Navy, Washington 25, D. C. |
| 10 | Chief, Bureau of Ships, Department of the Navy, Washington 25, D. C.<br>Technical Information Branch, Code 335 (3)<br>Ship Design, Code 410 (1)<br>Preliminary Design, Code 420 (1)<br>Hull Design, Code 440 (1)<br>Hull Scientific, Code 442 (1)<br>Applied Science Division, Code 340 (1)<br>Preliminary Design Section, Code 421 (1)<br>Propellers Shafting (Code 644) (1) |
| 6 | Commanding Officer and Director, David Taylor Model Basin, Washington 7, D. C., Attention Code 513 |
| 3 | Chief, Naval Research, Department of the Navy, Washington 25, D. C.<br>Mathematics, Code 432 (1)<br>Mechanics, Code 438 (1)<br>Undersea Warfare, Code 466 (1) |
| 1 | Chief, Bureau of Naval Weapons, Department of the Navy, Washington 25, D. C., Att.: Asst. Chief, Research and Development Division |
| 1 | Director, Naval Research Laboratory, Washington 20, D. C., Att.: Code 2021 |
| 1 | Director, Naval Ordnance Research Laboratory, Pennsylvania State University, University Park, Pennsylvania |
| 1 | Commander, Naval Ordnance Test Station, Pasadena Annex, 3202 East Foothill Blvd., Pasadena, California |
| 1 | Commander, Naval Ordnance Laboratory, White Oak, Silver Spring, Maryland, Att.: Library |
| 4 | National Aeronautics and Space Administration, 1512 H St., N.W., Washington 25, D. C.<br>Langley Research Center (1)<br>Ames Research Center (1)<br>Lewis Research Center (1) |
| 2 | Armed Services Technical Information Agency, Arlington Hall Station, Arlington 12, Virginia |
| 1 | Dr. A. S. Peters, Institute for Mathematics and Mechanics, New York University, 45 Fourth Avenue, New York, New York |
| 1 | Technical Research Group, 2 Aerial Way, Syosset, New York, Att.: Dr. Paul Kaplan |
| 1 | The Society of Naval Architects and Marine Engineers, 74 Trinity Place, New York 6, New York |
| 2 | Superintendent, U. S. Naval Post Graduate School, Monterey, California |
| 1 | Dr. M. S. Plesset, Division of Engineering, California Institute of Technology, Los Angeles 15, California |
| 1 | Mr. Hollinshead deLuce, Bethlehem Steel Company, Shipbuilding Division, Quincy 69, Massachusetts |
| 1 | Gibbs anc Cox, Inc., 21 West Street, New York 6, New York |
| 1 | Mr. C. H. Hancock, Hydraulic Laboratory, Newport News Shipbuilding and Dry Dock Company, Newport News, Virginia |
| 1 | Prof. C. Ridgely-Nevitt, Webb Institute of Naval Architecture, Glen Cove, New York |
| 1 | Mr. Andrew I. McKee, Director of Research and Design, Electric Boat Div., General Dynamics Corporation, Groton, Connecticut |

## INITIAL DISTRIBUTION (Cont.)

| Copies | |
|---|---|
| 1 | Mr. V. L. Russo, Chief, Division of Preliminary Design, Maritime Administration, U. S. Dept. of Commerce, Washington 25, D. C. |
| 1 | Reed Research Inc., 1048 Potomac St., N. W., Washington 7, D. C., Att.: Mr. Stanley Reed |
| 1 | Prof. H. A. Schade, Chairman, Dept. of Naval Architecture, College of Engineering, University of California, Berkeley 4, California |
| 1 | Dr. A. G. Strandhagen, Head, Dept. of Engineering Mechanics, University of Notre Dame, Notre Dame, Indiana |
| 1 | Prof. R. B. Couch, Chairman, Dept. of Naval Architecture and Marine Engineering, University of Michigan, Ann Arbor, Michigan |
| 1 | Mr. E. P. Worthen, Chief Engineer, Bethlehem Steel Company, Shipbuilding Division, Quincy 69, Massachusetts |
| 1 | Dr. J. Breslin, Director, Davidson Laboratory, Stevens Institute of Technology, Hoboken, New Jersey |
| 1 | Hydronautics Inc., 200 Monroe Street, Rockville, Maryland |
| 1 | Dr. H. W. Lerbs, Director, Hamburg Ship Model Basin, Bramfelder Strasse 164, Hamburg 33, Germany |
| 1 | Superintendent, Admiralty Experiment Works, Haslar, Gosport, Hants, England |
| 1 | Superintendent, Ship Division, National Physics Laboratory, Teddington, Middlesex, England |
| 1 | Dr. J. D. van Manen, Ned. Scheepsbouwkundig Proefstation, Haagsteeg 2, Postbox 28, Wageningen, The Netherlands |
| 1 | Director, Basin d'Essais les Carenes, Paris XVe, France |
| 1 | Director, Skippsmodeltanken, Trondheim, Norway |
| 1 | Director, Institut fur Shiffbau, Berliner Tor 21, Hamburg, Germany |
| 1 | Professor L. C. Burrill, Department of Naval Architecture, Kings College, University of Durham, Newcastle-upon-Tyne, England |
| 1 | Director, Statens Skipsmodeltanken, Goteborg, Sweden |
| 1 | Ir. J. Gerritsma, Shipbuilding Dept., Delft Technical University, Delft, Netherlands |